Fabrication of vertically aligned silicon nanowire arrays and its application in hybrid heterojunction solar cells

by

Debika BANERJEE

MANUSCRIPT-BASED THESIS PRESENTED TO ÉCOLE DE TECHNOLOGIE SUPÉRIEURE IN PARTIAL FULFILLMENT FORTHE DEGREE OF DOCTOR OF PHILOSOPHY
Ph.D.

MONTREAL, AUGUST 29, 2018

ÉCOLE DE TECHNOLOGIE SUPÉRIEURE
UNIVERSITÉ DU QUÉBEC

BOARD OF EXAMINERS (THESIS PH.D.)

THIS THESIS HAS BEEN EVALUATED

BY THE FOLLOWING BOARD OF EXAMINERS

Mr. Sylvain G. Cloutier, Thesis Supervisor
Department of Electrical Engineering, École de technologie supérieure

Mr. Mohammad Jahazi, President of the Board of Examiners
Department of Mechanical Engineering, École de technologie supérieure

Mr. Vahé Nerguizian, Member of the jury
Department of Electrical Engineering, École de technologie supérieure

Mrs. Claudine Allen, External Independant Member
Department of Physics, Engineering Physics and Optics, Laval University

THIS THESIS WAS PRENSENTED AND DEFENDED

IN THE PRESENCE OF A BOARD OF EXAMINERS AND PUBLIC

JUNE 12, 2018

AT ÉCOLE DE TECHNOLOGIE SUPÉRIEURE

ACKNOWLEDGEMENTS

I am thankful to Professor Sylvain G. Cloutier for his constant support, encouragement, constructive feedbacks and focused guidance over the past five years. I am thankful to him for influencing me into doing silicon photovoltaics and thus opening an entirely new world for me. I am grateful to him for making my graduate life in ETS very enjoyable and rewarding. He has given me enough freedom to design research projects independently and help me to grow as an independent researcher.

I am thankful to my co-supervisor Professor Véronique François for guiding me through the optics with the nanowire system.

I had the good fortune of collaborating with many talented researchers. I would like to thank Felipe, Jaime, Charles and Xiaohang for collaborating on various parts of this thesis. I would like to acknowledge the technical assistance received from Dr Riad Nechache, Mr. Nelson Landry, Mr. Normand Gravel and Mr. Christian Talbot from our ETS laboratories.

I would also like to thank past and future students in our research group for their support and all the invigorating discussions. Thank you Felipe, Jaime, Charles, FX, Xiaohang, Ivy, Ibtihel, Suchismita, Soraya, Arooba, Sumana and Sayani for their friendship and for making me feel at home.

Special thanks to Charles and FX for helping me to write the thesis abstract in French.

Finally, I would like to thank my father (Mr. Dibakar Banerjee) and my mother (Mrs. Reba Banerjee) for their unconditional support, love and sacrifices.

FABRICATION OF VERTICALLY ALIGNED SILICON NANOWIRE ARRAYS AND ITS APPLICATION IN HYBRID HETEROJUNCTION SOLAR CELLS

Debika BANERJEE

RÉSUMÉ

Partout dans le monde, de nombreuses approches pour réduire la sévérité du changement climatique émergent chaque jour. L'énergie photovoltaïque est l'une des avenues attrayantes et efficaces pour la génération d'énergie renouvelable sans carbone. Régnant sur l'industrie photovoltaïque, les cellules solaires à base de silicium cristallin sont efficaces mais coûteuses, en raison de leur complexité de fabrication. Cela amène la motivation à la recherche fondamentale afin de trouver des moyens plus simples et moins coûteux de récolter la lumière et produire de l'électricité. Les plateformes hybrides, à l'aide de la nanotechnologie, s'abordent d'inclure divers matériaux polymères inorganiques et organiques, combinés avec du silicium cristallin, pour fabriquer des cellules solaires hybrides à hétérojonction. L'objectif principal de cette thèse est de développer une méthode rentable pour fabriquer des cellules solaires hybrides à hétérojonction, à base de nanofils de silicium. En raison de leur rapport surface/volume intrinsèquement grand, l'emploi de nanofils de silicium aide à réduire l'utilisation de matériaux et donc le coût de fabrication. Nous avons trouvé la méthode de déplacement galvanique comme étant la technique la plus rentable par rapport aux autres méthodes de synthèse de nanofils de silicium. Les propriétés optiques et électriques de ces nanofils ont été mesurées afin d'évaluer leurs potentiel pour leurs utilisation dans des dispositifs photovoltaïque. Nous avons étudié l'effet de confinement de phonons sur les nanofils de silicium. Le silicium, étant un matériau à bande interdite indirecte; Le confinement de phonons aide à la transition bande à bande des électrons et des trous, ce qui augmente encore l'efficacité photovoltaïque des dispositifs construits autour des nanofils de silicium.

Dans cette thèse, nous introduisons d'abord une architecture de dispositif qui combine des nanofils de silicium et du TiO_2 anatase, démontrant la fabrication de cellules solaires à hétérojonction en utilisant une modification d'interface avec HBr. Cette approche aboutit à des dispositifs PV avec jusqu'à 6,2% d'efficacité de conversion de puissance (PCE) qui représente une amélioration de 3 fois par rapport à des architectures similaires avec une modification d'interface utilisant d'autres voies. Cette thèse offre une voie prometteuse pour l'ingénierie d'interface de dispositifs optoélectroniques hybrides à base d'hétérojonction.

La deuxième architecture de dispositif décrite dans cette thèse démontre la fabrication de cellules solaires hybrides à hétérojonction composées de nanofils de silicium et de PEDOT :PSS sensibilisés au plasmon. L'amélioration significative induite grâce aux plasmon est démontrée en contrôlant le processus de nettoyage pendant l'étape de fabrication de nanofils. Ceci permet de laisser une quantité infime de nanoparticules d'argent attachées aux nanofils de silicium avant de les enrober de PEDOT: PSS traité au solvant. Les dispositifs

cellules solaires produites démontrent un PCE allant jusqu'à 8,4% sous AM 1,5G comparer à 5,5% pour les dispositifs sans nanoparticules d'argent. Cette thèse offre un moyen favorable de réaliser des cellules solaires à base de silicium.

Mots-clés : Nanofils de silicium, GDM, cellules solaires, hétérojonction hybride.

FABRICATION OF VERTICALLY ALIGNED SILICON NANOWIRE ARRAYS AND ITS APPLICATION IN HYBRID HETEROJUNCTION SOLAR CELLS

Debika BANERJEE

ABSTRACT

Worldwide, numerous approaches to reduce climate change emerge every day. Photovoltaic is one of the attractive and efficient methods to generate carbon free renewable power. Reigning over the photovoltaics industry, crystalline silicon-based solar cells are efficient but expensive due to their complexity in processing. This brings the motivation for fundamental research in a quest to find of simpler and less expensive ways to harvest light in order to generate electricity. Hybrid platforms, with the help of nanotechnology, strive to include various inorganic, organic, polymer materials combined with crystalline silicon to fabricate hybrid heterojunction solar cells. The main objective of this thesis is to develop a cost-effective method to fabricate silicon nanowire-based hybrid heterojunction solar cells. Employing silicon nanowires help to reduce the material usage and thus the cost by their inherently large surface to volume ratio. We found galvanic displacement method as the most cost-effective technique compared to other methods used for the synthesis of silicon nanowires. Optical and electrical properties of these nanowires have been measured to evaluate the potential of these materials for their usage in photovoltaics. We have investigated phonon confinement effect on the silicon nanowires. Being silicon an indirect band gap material; phonon confinement helps in band to band transition of electrons and holes which further increases the photovoltaic efficiency of devices built around silicon nanowires.

In this thesis, we first introduce a device architecture that combines silicon nanowires and anatase TiO_2, demonstrating the fabrication of bulk heterojunction solar cells using interface modification with HBr. This approach results in PV devices with up to 6.2% of power conversion efficiency (PCE) that represents 3 times enhancement compared to similar architectures with interface modification using other routes. This thesis provides a promising route for interface engineering of hybrid heterojunction based optoelectronic devices.

The second device architecture described in this thesis shows the fabrication of hybrid heterojunction solar cells comprised of plasmon sensitized silicon nanowires and PEDOT:PSS. Significant plasmon induced enhancement is demonstrated by controlling the cleaning protocol during the nanowire fabrication step. This allows to leave minute amount of silver nanoparticles attached to the silicon nanowires before coating with solvent treated PEDOT:PSS. The solar cell devices produced show a PCE up to 8.4% under AM 1.5G compared to 5.5% without silver nanoparticles. This thesis yields a favorable way to achieve better performing ultra-low-cost silicon-based solar cells.

Keywords : Silicon nanowires, GDM, solar cells, hybrid heterojunction.

TABLE OF CONTENTS

LIST OF TABLES

LIST OF FIGURES

LIST OF ABREVIATIONS

GDM	Galvanic displacement method
MAWCE	Metal assisted wet chemical etching
NPs	Nanoparticles
NWs	Nanowires
PCE	Power conversion efficiency
RCWA	Rigorous coupled wave analysis
SPR	Surface plasmon resonance
UV	Ultra violet

LIST OF SYMBOLS

Ag	Silver
H	Hydrogen
HBr	Hydro bromic acid
HNO_3	Nitric acid
FF	Fill factor
I_{sc}	Short-circuit current
J_{sc}	Short-circuit current density
N_2	Nitrogen
O_2	Oxygen
Si	Silicon
TiO_2	Titanium di oxide

INTRODUCTION

I have selected the option of writing the experimental part in original paper-based research works according to the ETS thesis preparation and submission policies. These manuscripts consist of chapter 5-7 of this thesis. Each chapter comprises of an abstract, introduction, results and discussions and experimental methods. Additionally, this thesis consists of an overall abstract, introduction, research outline, literature review, conclusions, and statement of original contributions and future works.

Chapter 1 explains the fundamental technologies of solar cells including different techniques to increase the efficiency of SiNWs-based hybrid solar cells.

Chapter 2 describes the overall research outline of this thesis.

Chapter 3 comprises of an extensive literature review for this thesis work.

Chapter 4 consists of the simulation works to determine the optical properties of the silicon nanowires.

The chapters 5-7 demonstrate the studies performed to accomplish the research goals. Chapter 5 investigates the phonon confinement effect on vertically aligned SiNWs. Phonon confinement effect can increase the band-to-band transitions in Si to potentially increase the conversion efficiencies in SiNWs based photovoltaic devices. Unfortunately, producing nanowires exploiting nanoscale confinement to achieve the phonon localization effect can be a costly process. Here we report on the observation of such phonon-localization effect in SiNWs fabricated at very low-cost without chemically altering Si using an all-solution based metal assisted wet chemical etching (MAWCE) method.

Chapter 6 illustrates the photovoltaic performance of HBr treated SiNWs/TiO_2 n^+-n bulk heterojunction solar cells. TiO_2 is a large bandgap, widely used material as an electrode in

dye-sensitized solar cells as well as a transparent front contact in heterojunction solar cells. Unfortunately, few reports are available where TiO_2 is used as the main component for single heterojunction fabrication with Si. It is because previously works are focused on fabricating devices using narrow bandgap semiconductors. Here we report a feasible route for low cost, all solution based, easily available n-SiNW/n-TiO_2 isotype heterojunction for photovoltaic device by interface-modification using HBr.

Chapter 7 demonstrates about significant plasmon-induced enhancement to achieve better ultra-low-cost solar cell devices. Recently, hybrid silicon nanowire based heterojunction solar cells attracted attention in the photovoltaic market due to their high photovoltaic potential and low processing costs. Here we report how strong localized surface plasmon modes induced using silver (Ag) nanoparticles can be used to achieve significant improvement in a simple hybrid organic inorganic photovoltaic device between n-type silicon nanowires (SiNWs) and poly(3,4-ethylenedioxythiophene):poly-(styrenesulfonate) (PEDOT:PSS).

In this research duration, I was able to contribute to 8 peer-reviewed journal articles (published/in press/submitted/to be submitted) with 5 as first author and 3 as a co-author. From this, I have picked up 3 articles pertaining to the thesis research goal, in which I am the first author.

CHAPTER 1

STATE OF THE ART

1.1 The Importance of Solar Energy:

Solar energy is important for humans, animals and plants. Humans and animals use sunlight for synthesis of vitamin D (Dincer, 2000). Solar energy is used as a source of clean energy since it does not harm the ecosystem. Most importantly, solar energy is versatile. It can be used to produce power for many appliances (cooking, cars, watches, calculators etc.) as well as it can produce electricity to run the entire world. It is a source of renewable energy which will become the only source of energy in the future since fossils fuels will come to an end (Höök et Tang, 2013). This is because, we have consumed an improbable amount of fossil fuels since the ancient times. The rate of consuming the fossil fuels is increasing with world's population. Hence it will run out faster in near future. Fossil fuels also affect the atmosphere. It is responsible for global warming and climate change due to growing levels of certain toxic gases in the environment. Therefore it is necessary to switch to green energy to avoid these fossil-fueled problems.

The energy in light is converted into electrical power in a solar cell (Heeger, 2014). Sunlight contains photons that hit the solar panel and get absorbed by the semiconducting materials of the panel. It helps to knock the electrons to loose from their atoms and flow as electric current (Kim et al., 2013).

1.2 Materials Used for Fabricating Solar Cells:

Solar cells can be made from various materials- inorganic or organic (Noh et al., 2013). Direct band gap materials such as GaAs, InP, CdTe give more energy conversion efficiency than indirect ones e.g. Ge, Si (Shah et al., 1999). Metals like Ag, Al, Au, Cu, Zn can be used to fabricate solar cells and insulators like glass is also a very good substrate to design a solar cell (Kluth et al., 1999). For this thesis research, we will fabricate solar cells using silicon (Si) wafer since in the crystalline form, Si has lot of special chemical properties (Wenham et Green, 1996). Moreover, Si is not toxic and is found in nature in abundance.

1.3 Sources of Losses in Solar Cells:

There are four important loss mechanisms (Kaushika et Rai, 2007) that need to be analyzed in solar cells namely a) photon absorption, b) exciton generation, c) exciton separation into free carriers, and d) carrier collection by electrodes.

Photon absorption is the ability of a solar cell to capture and preserve as many photons reaching its surface. Photons in the sunlight hit the solar cell and are absorbed by the semiconducting solar cell material. However, material surface defects, angle of incidence and difference in index of refraction make this task a tough one to achieve (Trupke, Green et Würfel, 2002a).

There are two main sources of loss in photon absorption: i) reflection, for which certain portion of the incident light manages to enter the active region of the device and the rest is reflected (Zhao et al., 1995), and ii) transmission, which strongly depends on the material and active region thickness (Trupke, Green et Würfel, 2002b). An active region too thin, in the order of 100 nm or less will not take full advantage of the photon collection, and one too thick, on the order of 1 um or more presents difficulties for fabrication with desired precision. Thickness in the active region affect directly operation parameters such as short circuit current density, filling factor and efficiency, as can be seen in figure 1.1 (Moulé, Bonekamp et Meerholz, 2006).

Reflection loss can be significantly reduced by the addition of antireflection coatings and micro grooving the cell surface (Zhao et Green, 1991). These modifications make the surface an appropriate interface for light to go through at different wavelengths at normal incidence. To maximize this wavelength range, several layers of antireflection coating are used in which is each layer is more sensitive to a certain wavelength value. In comparison, a Si solar cell without any antireflection coating loses 30% or more of the incident light to reflection (Zhao et Green, 1991).

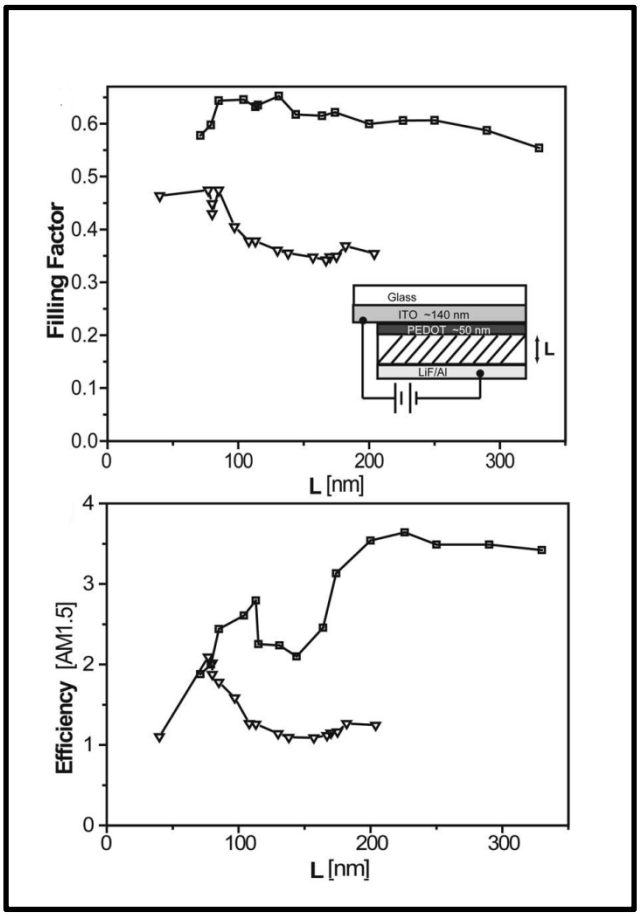

Figure 1.1 Thickness dependence of (upper image) Filling Factor (FF) and (lower image) efficiency for (1:1) P3HT:PCBM (squares) and (1:4) OC1C10PPV: PCBM (triangles) PV Taken from (Moulé, Bonekamp et Meerholz, 2006)

The second loss mechanism is exciton formation inside the cell. A clear confirmation of a photon being absorbed is the creation of an exciton, which is an electron-hole pair bound by Coulomb potential. If this binding energy is smaller than the device's thermal energy at room

temperature, the exciton will break and the carriers will relax to the band edges as free charge carriers that can be further extracted. If the binding energy is strong, a bound exciton state will be formed by the carriers, as is the case for organic semiconductors (Knupfer, 2003), and the carriers will be relaxed due to carrier phonon coupling. As a result, the energy will be dissipated by heat transfer. This loss mechanism accounts for 30-40% of the incident solar radiation (Garnett et al., 2011). Additionally, carrier relaxation losses are related to the charge separation processes that are due to the potential gradient in the active region. In the end, it facilitates the carrier collection by the contact interfaces.

On the other hand, carrier relaxation losses are controlled by using alloys of materials with different bandgaps in order to reduce the heat losses, but materials such as indium gallium nitride show a miscibility gap at intermediate concentrations due to large lattice mismatch strains. Figure 1.2 presents a general schematic of a multilayer solar cell. Another approach to improve this condition is by using high purity single crystalline substrates with a large minority carrier diffusion length that will greatly enhance carrier separation for further collection (Ellingson et al., 2005).

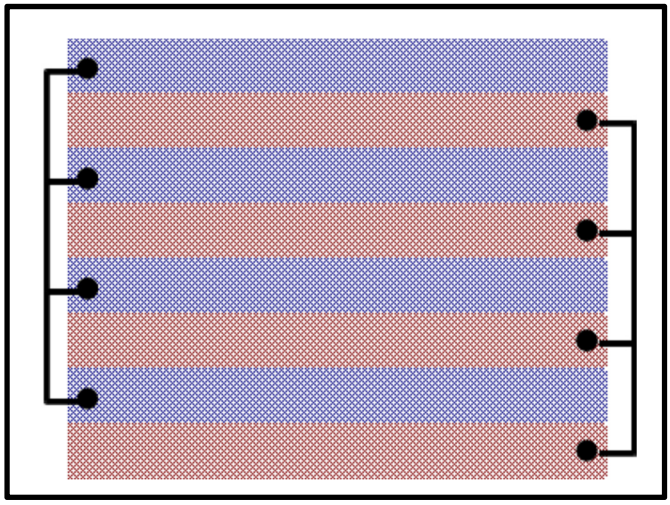

Figure 1.2 Heterojunction morphology aimed to improve carrier collection
The image shows a multilayer heterojunction that requires multiple deposition steps and post growth processing to contact individual layers
Adapted from (Ellingson et al., 2005)

1.4 Efficiency Enhancement Techniques of Solar cells using Vertically Aligned Silicon Nanowires:

A significant amount of research has gone into understanding the unique electrical, mechanical and thermal properties of nanowires (NWs) (Thelander et al., 2006). The Si based NWs have become popular since adequate industrial infrastructure can help to fabricate SiNWs at low manufacturing costs. Typically diameters of nanowires tune on the order of nanometres. The motivation for research on NWs arises from the fact that electrons in nanowires are restricted in the lateral direction occupying energy levels different from the energy levels found in bulk materials. For this reason, SiNWs show luminescence. On the other hand, indirect band gap SiNWs can barely be used in functional optoelectronics. These two qualities together and the formation of SiNWs which are electrically and optically porous can steer new generation of Si based nanoscale devices. The other advantage of using NWs is that these tiny architectures can be assembled without complex and costly fabrication facilities making device fabrication a cheap endeavor. Applications of NWs are investigated in different fields such as field-effect transistors (FETs) (Goldberger et al., 2006), flexible large area electronics, thermoelectric, photovoltaics (Garnett et Yang, 2008), battery electrodes (Peng et al., 2008), and electronic biosensors (Zheng et al., 2005).

While there are various routes available to obtain uniform NW arrays, doping concentration in the substrate material remains to be one of the key issues in the fabrication and performance of NW-based devices (Hochbaum et al., 2008). As it stands, the popular doping methods are thermal diffusion, ion implantation and *in-situ* doping during growth of the nanowires (Lauhon et al., 2002). However these methods still suffer from the disadvantages of increased crystallographic defects and doping fluctuations at high doping levels. Additionally, most of these methods have the need of either high temperatures processing or prolonged fabrication times attributed to the limitations of the growth mechanisms. Therefore, obtaining accurate doping concentrations in large-area aligned NWs remains to be a challenging problem.

Till date, different methods have been developed to manufacture SiNWs such as chemical vapor deposition using the VLS (Vapor Liquid Solid) technique, laser ablation, thermal evaporation decomposition, molecular beam epitaxy, chemical etching, and solution growth (Holmes et al., 2000; Ryan et Barrett, 2012; Westwater et al., 1997; Zhang et al., 2008). Among these methods, metal assisted wet electroless chemical etching (MAWCE) (Ng et al., 2011; Zhang et al., 2008) of Si substrates is an attractive method for the fabrication of these tiny systems. This is because of the following reasons (a) the fabrication route involved is a low-cost approach (b) the NWs produced using this technique show very small values of reflectance which is why these systems have the potential for usage in photovoltaic applications (c) the resulting NWs have the potential for effective use in self-powered functional nanoelectronic systems. The key feature of this technique is selective electrochemical etching of Si using metal catalysts which results in well organized and highly dense arrays of SiNWs with identical crystallographic orientations. In addition, ordered SiNWs with structural dimensions on the orders of hundreds of nanometres can be fabricated using this technique.

1.5 Efficiency Enhancement Techniques using Modelling/Simulations:

With recent developments in materials processing technology, there is a growing need for optimization of device performance by careful selection of materials, device design. Currently, silicon nanowire based solar cells have been shown to reach an ultimate efficiency of 20 % which is still far from the maximum theoretical efficiency of 34% predicted. This gap between theoretical and experimental efficiencies can be minimized by understanding the loss mechanisms. This objective can be realized in two ways. The first choice is to understand the effect of materials, sizes on the loss mechanisms by performing careful experiments which is a costly endeavour. The other way is to perform simulations to understand these different mechanisms. The advantage of simulation techniques is that they are cost effective and less time consuming. The simulation techniques adopted till date can be categorized in two classes : i) continuum based analytical techniques, e.g analytical slovers for Rigorous coupled wave analysis (RCWA) (Xie, Oh et Shen, 2011) ii) finite element techniques to solve for based on Maxwell's equation of electromagnetic waves (Gao, Yu et Huang, 2006).

1.6 Efficiency Enhancement Techniques using Phonon Confinement Mechanism:

Phonon confinement effect plays an important role to increase the conversion of energy in solar cells based on SiNWs (Richter, Wang et Ley, 1981). Crystalline Si has an indirect band gap of 1.1 eV which is not good for efficient light emission. Exciton binding energy for crystalline Si is also very small ≈ 15 meV. Phonon confinement mechanism changes the indirect nature of band structure for crystalline Si. This effect can be measured using Raman spectroscopy (Adu et al., 2006). SiNWs with very small diameters (<20nm) can show phonon confinement effect which helps to increase the optical transition of SiNWs based solar cells (Piscanec et al., 2003). In this thesis, we have investigated phonon confinement process in vertically aligned SiNWs.

1.7 Efficiency Enhancement Techniques by interface modifications:

Surface recombination (Tiedje et al., 1984) plays an important role to reduce the performance of solar cells. Researchers used different techniques of surface passivation (Aberle, 2000) to limit the surface recombination. Thin film layer depositions of SiO_2, Al_2O_3 etc. are very popular techniques to passivate the device surface (Jan, Mark et Andrés, 2001; Schmidt et al., 2008). For, SiNWs based devices, cleaning the native oxide layer from the nanowire surface before the junction formation helps to enhance the photovoltaic performance (McAlpine et al., 2007). HF treatment (Ma et al., 2003) is the most well-known for removing native oxide layer from the nanowire surface. In this thesis we have explored a new route for surface passivation using HBr which boosts the efficiency of SiNWs/TiO_2 bulk heterojunction solar cells by 3 folds compared to the similar devices treated with HF.

1.8 Efficiency enhancement techniques by incorporating silver plasmons:

Silver (Ag) plasmons help to absorb the UV light from the solar spectrum (Wang et al., 2009). In this thesis, we have explained significant plasmon induced efficiency increment in low-cost hybrid solar cells comprised of plasmon sensitized SiNWs and PEDOT:PSS. We observed reduced reflectance in UV/VIS region for plasmonic SiNWs. A significant efficiency enhancement of 52% has been noticed when minute amounts of Ag plasmons are incorporated with SiNWs/PEDOT:PSS solar cells compared to the similar structure without Ag plasmons.

CHAPTER 2

OVERALL RESEARCH OUTLINE

2.1 Research outline for low-cost solar cells :

2.1.1 Objectives for probing phonon processes in vertically aligned SiNWs :

The primary objective of this part of the thesis is to probe the phonon localization process in vertically aligned SiNWs to improve the band to band transition in SiNWs-based optoelectronic devices. The specific objectives of this part are:

- To investigate the phonon confinement effect using high resolution Raman spectroscopy;
- To establish a cost-effective route to achieve phonon localization effect in SiNWs since fabricating nanowires to exploit nanoscale confinement can be a costly method;
- To eliminate the other possibilities like surface enhanced Raman effect, laser-induced heating etc. that can cause the change in contrast of the results from Raman spectroscopy.

2.1.2 Objectives for fabricating SiNWs-based heterojunction solar cells :

The primary objective of this part is to develop new routes to fabricate cheap and efficient SiNWs-based heterojunction solar cells. The specific research objectives are:

- To establish a new path to fabricate SiNWs/TiO_2 bulk heterojunction solar cells;
- To develop a new process to passivate the dangling bonds from the SiNWs surface which will help in enhancing the optoelectronic properties of the solar cells;
- To study the plasmonic effect in SiNWs and implement it in fabricating hybrid heterojunction solar cells;
- To process the solution of organic materials (PEDOT:PSS) to increase its conductivity and use it to fabricate hybrid heterojunction solar cells in conjunction with plasmon sensitized SiNWs;

- To increase the overall efficiency of existing solar cells by employing different materials;
- To reduce the cost of solar cells by all solution based fabrication process.

2.2 Outline of thesis chapters :

This thesis is divided into 8 chapters. Chapter 1 depicts the background and research objectives of this thesis. Chapter 2 demonstrates the research outline followed by an extensive literature survey in chapter 3. Chapter 4 consists of the simulation works carried out to determine the optical properties of the nanowires. Chapters 5-7 are original research articles published. These articles include the main studies performed to achieve the thesis objectives. Figure 2.1 demonstrates an overall outline of the areas covered to achieve the objectives. Chapter 8 describes the overall conclusion from this thesis. Statement of original contributions from this research and future works are included in chapter 9.

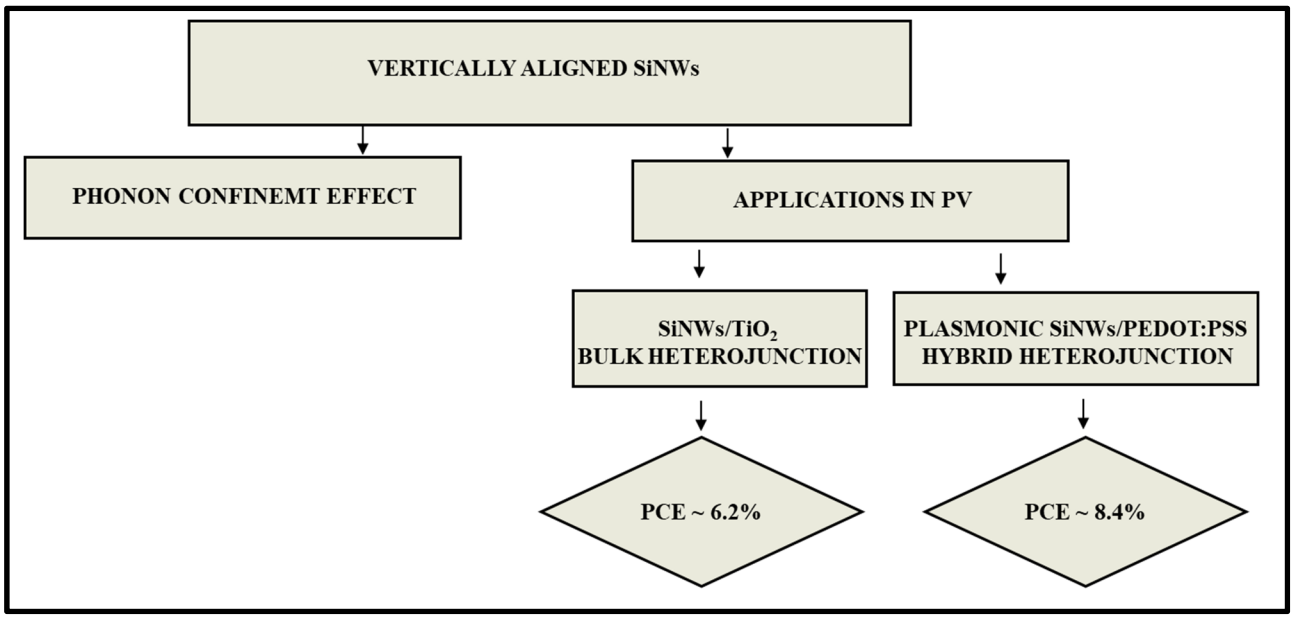

Figure 2.1 Schematic outline of the overall thesis research

CHAPTER 3

LITERATURE REVIEW

3.1 Silicon Nanowires:

In general silicon nanowire synthesis techniques can be broadly classified into the following categories. :

Bottom-up approach: nanowires nucleation and growth takes place at the substrate surface from molecular precursors using nanoparticles as catalyst.

Top-down approach: nanowires growth starts at the substrate surface and continues through the bulk through the patterned areas.

The most popular bottom-up approach for the synthesis of SiNWs is vapor-liquid-solid (VLS) technique (Westwater et al., 1997). It is one of the most attractive techniques used for the growth of silicon nanowires structures using Chemical Vapor Deposition (CVD) (Hofmann et al., 2003). In this method, first silicon forms vapor phase which then passes all the way through a liquid droplet becoming a solid. Usually, the growth of a crystal from a gas against a solid surface by means of adsorption is a sluggish process. In VLS technique this problem is taken care of by using a liquid alloy to rapidly adsorb silicon from a supersaturated vapor. Afterwards crystal growth takes place from these sites at the liquid–solid interface. The physical nature of SiNWs grown using this technique can be controlled by the physical properties of the liquid alloy(Hofmann et al., 2003).

Other than CVD some other methods can be combined with VLS to fabricate SiNWs. These techniques are Molecular beam epitaxy (MBE) (Fuhrmann et al., 2005), Laser ablation (Zhang et al., 1998), Evaporation of silicon (Niu, Sha et Yang, 2004). MBE uses high-purity silicon source which is heated at high temperatures to make it evaporate. MBE is carried out

at ultra-high vacuum levels to reduce contamination and allow monitoring of the growth, surface structure while fabrication. Gaseous beam of evaporated silicon atoms or molecules is directed onto the substrate so that the atoms gets absorbed leading to crystallization.
In addition to VLS the other methods which belong to the bottom-up approach are, (i) Oxide assisted growth technique, (ii) Solution-liquid-solid (SLS) method and (iii) Template-directed synthesis method.

In the oxide-assisted growth (OAG) method (Lee et al., 2013), oxides are used for facilitating the formation of nanowires. The major advantage of this approach is that no metal catalysts are needed in the process. This eliminates the risk of contamination in the material, thus the performance of nanowires are better.

Compared to VLS technique, SLS method employs an organic solvent for the growth of NWs at atmospheric pressure. This technique was first implemented by Korgel *et al.* by effectively producing SiNWs with diameters of few nanometres and lengths up to few micrometers. They used a supercritical fluid as the solvent (Holmes et al., 2000).

In template-directed method the template acts as a platform to generate the raw material in situ. In addition to it the sample formed into a nanostructure with its morphology matching to that of the template (Q. Peng, P. Huang et Zhu, 2004; Xia et al., 2003). The advantages of this technique can be summarized as e.g., easy fabrication, controllable compositions and distribution, uniform size of nanostructures compared to fabrication methods.

Primary challenges for bottom-up approach based NW fabrication methods are controlling diameter and orientation of the nanowires. These problems affect the efficiency of the fabrication of NW arrays.

On the other hand, top-down approach is much more attractive for batch production of ordered nanowires. Top-down methods have gained popularity for the fabrication of ordered SiNWs arrays in terms of crystallographic orientation, diameter, length and position. These

techniques can be broadly categorized into two classes based on the orientation of the NWs. The first category belongs to horizontal nanowires lying on the substrate plane which is most often associated with lithography and dry or wet etching steps. The second category belongs to vertical nanowires which are oriented in normal to the surface of the substrate. These NWs are fabricated using reactive-ion etching or wet chemical etching.

Metal-assisted wet-chemical etching of silicon substrates for fabricating SiNWs is one of the top-down techniques. It is considered as a potential route for mass production of ordered vertically aligned nanowires because of the following reasons. Using this technique one can have exercise exact control over the geometry of the structure i.e. diameter, length, spacing. The most important fact is that all of these can be achieved avoiding high-cost and low-output usual lithographic processes. This technique is based on the principles of galvanic displacement (Carraro, Maboudian et Magagnin, 2007) reaction, details of which are discussed below:

3.2 Galvanic Displacement Method (GDM):

Galvanic displacement is defined by the process of natural reduction of a metal by another metal above it in the electromotive series (Peng et al., 2002). This technique is frequently used for metal depositions with nanoscale control. To do this, the desired metal ions are dissolved in aqueous solutions and which are then readily reduced to atoms during the oxidation of the substrate material. Generally, metals whose redox potentials are higher than hydrogen are deposited using this method. However, for this technique to be successful the substrate material should be oxidizeable.

In general, metal assisted wet electroless etching is categorized into two classes, which are processes involving one-step and two-step chemical reactions. In this technique SiNWs are fabricated by selective chemical etching of silicon substrates in aqueous acid solutions. Nanoparticles of metals which act as catalysts are deposited on the substrate surface (Peng et al., 2005).

The processes in the one-step reaction involve concurrent reduction of metal ions, and oxidation, dissolution of silicon. The etching mechanism in an aqueous solution of hydrofluoric acid (HF) containing silver nitrate ($AgNO_3$) has been studied in details (Q. Peng, P. Huang et Zhu, 2004). As is described in Equation 1, the first step in this process is the formation of an Ag+ ion close to the silicon substrate. These Ag+ ions absorb electrons resulting deposition of Ag nanoparticles on the substrate. This step is followed by the oxidation of silicon below the Ag nanoparticles to form SiO_2 (eq. 2). This SiO_2 is then dissolved in HF creating cavities on the substrate. Subsequently the Ag nuclei get dragged into these cavities. However, due to prolonged oxidation of SiO_2 electrons get accumulated on the Ag surface. As a result Ag^+ in the solution gets attracted to the neighborhood of the nuclei, and the resulting reduction entails to the accumulation of Ag nanoparticles trapped in the aforementioned substrate cavities.

$$Ag^+ + e^- \rightarrow Ag \tag{3.1}$$

$$Si\ (solid) + 2H_2O - 4e^- \rightarrow SiO_2(solid) + 4H^+ \tag{3.2}$$

$$SiO_2(solid) + 6HF \rightarrow H_2SiF_6 + H_2O \tag{3.3}$$

High concentration of Ag^+ in the etching solution and Si in the substrate helps these reactions run over and over again. This result in the formation of dendrite layers of Ag covering the Si substrate creating vertically aligned SiNWs on the silicon substrate. Most importantly, the lateral etching perpendicular to the walls of the developed cavities in the substrate does not voluntarily take place. This happens because the length of the diffusion path from the wall of the cavity to Ag particle is longer compared to that from the bottom of the cavity below the particle. Figure 3.1 represents the schematics of the etching procedure of silicon substrate in an aqueous solution composed of 5 M HF and 0.02 M $AgNO_3$ (1:1 ratio by volume) (Peng et al., 2006).

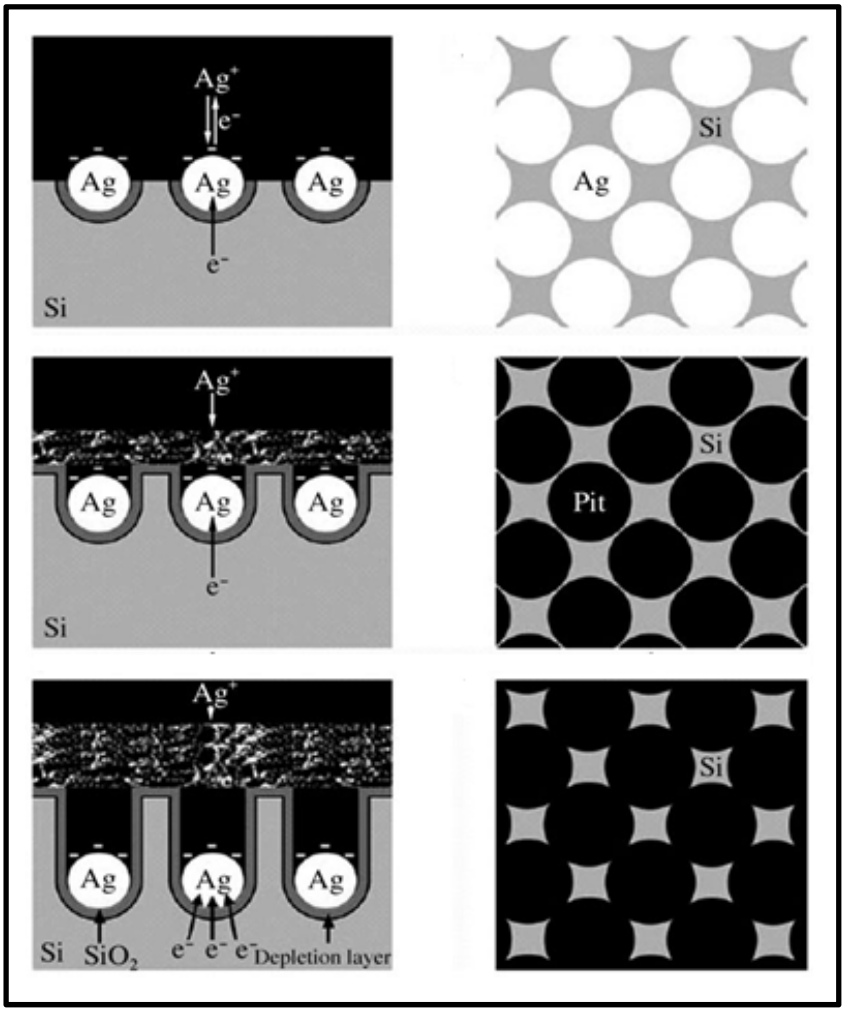

Figure 3.1 Left column indicates the lateral view of the typical one step etching process and right column indicates the top view of the same etching process
Taken from (Peng et al., 2006)

For highly doped Si wafers, rate of vertical etching is less compared to lateral etching, hence etching predominantly occurs parallel to the wafer surface. The preliminary nucleation of Ag nanoparticles occurs selectively near the dopants. At these locations the energy barrier for the redox reaction is usually low compared to the bulk. However, since highly doped wafers have high density of Ag nanoparticles which are close to each other, nanoparticles do not remain restrained to their own cavity. This is why lateral etching also takes place along with vertical etching.

To deal with this problem a two-step method is used (Qu et al., 2009). Similar to the one-step reaction, in this method also HF and $AgNO_3$ solution is used for the etching. As explained earlier, the Si below Ag particles get dissolved in HF. No dendritic layer of Ag can be formed due to the absence of excess Ag^+ in the solution. Electroless etching can also be performed using a mixture of HF and H_2O_2. The cathode and anode reactions for the etching process are given below:

Cathode reaction:

$$H_2O_2 + 2H^+ + 2e^- \rightarrow 2H_2O \tag{3.4}$$

Anode reaction:

$$Si + 2H_2O \rightarrow SiO_2 + 4H^+ + 4e^- \tag{3.5}$$

$$SiO_2 + 6HF \rightarrow [SiF_6]^{2-} + 2H_2O + 2H^+ \tag{3.6}$$

The total reaction :

$$Si^0 + 2H_2O_2 + 6F^- + 4H^+ \rightarrow [SiF_6]^{2-} + 4H_2O \tag{3.7}$$

Below discussed are the role of different chemical reagents used for Galvanic Displacement method based chemical etching.

Role of $AgNO_3$:

- The most important role of $AgNO_3$ is to form silver particles which later ionize to form Ag^+. The Ag^+ ions act as the catalyst to facilitate the etching process;
- Ag nanoparticles reduce H_2O_2 by absorbing electrons.

Role of H_2O_2:

- Increases the driving force for the etching process thus making the etching process faster;
- Oxidation of silver particles to form a localized Ag+ ion cloud in the vicinity of the silver nanoparticles. Increases the amount of free Ag+ in the solution thus increasing the porosity in the NWs.

Role of HF:

- Fluoride ions in the etchant help sustain the reaction by facilitating the dissolution of silicon or silicon oxide in the form of H_2SiF_6 (or SiF_2), exposing new silicon surface.

3.3 Rigorous Coupled Wave Analysis (RCWA):

The Rigorous Coupled Wave Analysis (RCWA) (Moharam et al., 1995) is used for analyzing the diffraction mechanisms for plane electromagnetive waves. In this method, the electromagnetic wave is incident on a diffraction grating bounded by dielectric mediums. When electromagnetic wave propagates through a dielectric media, the propagation of the wave can be analyzed by solving Maxwell's laws of electromagnetism.

The optical properties of nanowires i.e. transmittance, reflectance, and absorbance can be calculated by implementing the RCWA technique by idealizing the nanowire network as a stratified dielectric medium. However, solutions of Maxwell's equations for these systems are not a trivial task. The complexity arises while solving Maxwell's equation for the diffraction grating boundary conditions, several analytical, numerical mathematical methods have been proposed for solving this problem. Rigorous Coupled Wave Analysis (RCWA) is perhaps the most powerful tool amongst others. Using this tool one can calculate all the

optical properties for a series of nanowire system. This way nanowire parameters such as length, width, spacing can be optimised to extract maximum efficiencies from the solar cells. M. G. Moharam and T. K. Gaylord in their seminal paper (Moharam et al., 1995) used the RCWA method to analyse the reflection and transmission effect for general slanting gratings. Furthermore, they used this technique to solve for different gratings *e.g.*, surface-relief gratings (Peng et Morris, 1995), binary gratings (Grann, Moharam et Pommet, 1994), holographic gratings (Samuel et al., 2000), accousto-optic gratings (Wu et al., 2005) etc.

Alaeian *et. Al* (Hadiseh, Ashwin et Jennifer, 2012) extended this technique to find out the optimal geometry for maximum light absorption in radial junction silicon nanowire arrays. The scattering spectra of arrays of SiNWs were calculated by varying wire radii, length and lattice filling factors. They found, a silicon nanowire array of 300 nm of radii and 40% fill factor can reach an ultimate efficiency of 34% (not including black body radiation) which is very close to the theoretical maximum efficiency for a single-junction solar cell known as Shockley-Queisser limit. Hence in terms of cost-efficiency balance, their wire geometry seemed to provide optimal efficiency with the minimum cost for materials.

The RCWA technique has also been adapted for calculating optical properties of a silicon square nanohole array (Fang, Zhao et Bao, 2014). It was found that between solar cells comprising of silicon square nanohole arrays and hybrid silicon square nanowire hole arrays with varying the width of the nanoholes, the first is energetically effecient.

3.4 Phonon Confinement Effect in Silicon Nanowires:

The phonon confinement effect was first demonstrated by H. Richter and his group in 1981 (Richter, Wang et Ley, 1981). He measured the Raman peak broadening for microcrystalline silicon films.

Phonons are vibrational states of lattice. As we can see in figure 3.2 (a), the valence band maxima and the conduction band minima are aligned in the same straight line in case of direct bandgap materials. Hence, band to band transition is easy to take place in this type of materials. However, in case of indirect bandgap materials, the valence band maxima and the conduction band minima are not aligned in the same line. So, band to band transition will be difficult as we show in figure 3.2 (b). Phonon can supply the extra momentum in the favour of band to band transition for indirect bandgap materials. From the uncertainty principle, when we have spatial confinement, it increases the probability of finding a phonon with the right momentum to induce band to band transition from indirect bandgap materials.

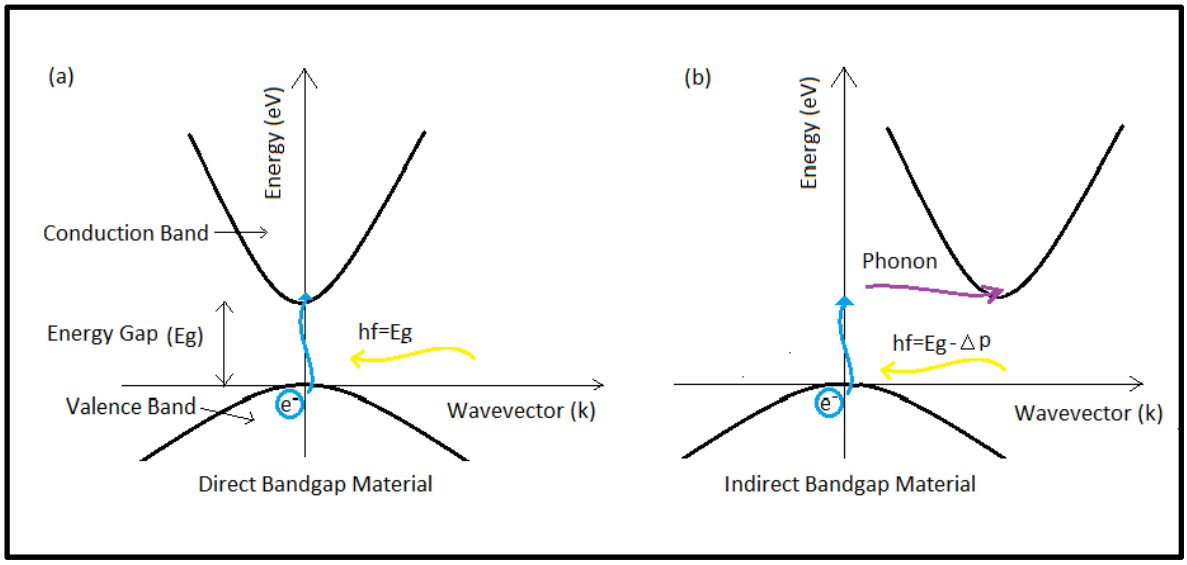

Figure 3.2 (a) E-k diagram for direct bandgap material
(b) E-k diagram for indirect bandgap material
Adapted from (L., 1971)

Phonon confinement effect in silicon nanowires fabricated with diameters less than 20 nm has been observed (Piscanec et al., 2003). Nanowires made using laser ablation method (Wang et al., 2000), vapor-liquid-solid growth mechanism, oxide assisted growth method, template assisted growth method have been shown to have phonon confinement effect.

Phonon confinement effect leads to the downshift and asymmetric broadening of the Raman peaks in silicon nanowires. However, it is not true in every case. Sometimes peak downshift

and broadening can come from inhomogeneous laser heating or from excess carries or from high power (Wang et al., 2000). S. Piscanec. *et. al.* found the pure contribution due to phonon confinement effect in silicon nanowires by varying the laser power, temperatures and excitation energy (Piscanec et al., 2003).

In 2000, Rong-ping Wang and his group noticed the phonon confinement effect in silicon nanowires with diameters less than 22nm (Wang et al., 2000). Then, K. W. Adu and his group in 2004 optimized that phonon confinement takes place in those silicon nanowires only whose diameters lies in the range between 4-25nm (Adu et al., 2006).

Sylvain G. Cloutier *et. al.* in 2005 (Cloutier, Guico et Xu, 2005) observed phonon localization effect in silicon nanostructures having diameter $\approx$70nm. This phonon localization effect is almost same as phonon confinement effect, described earlier. Though previously reported by the researchers that phonon confinement effect can be seen only in nanostructures with diameters less than 20nm, Sylvain G. Cloutier found the same effect in relatively large nanostructures. He explained it as introduction of defect centres at silicon interfaces which create nanosize crystellites. These nanocrystallites influence the phonon localization process. Phonon localization or phonon confinement effect is very useful for enhancement of the light emission ability in solar cells made of indirect band gap materials. Sylvain G. Cloutier *et. al.* in 2006 (Cloutier et al., 2006) showed that the presence of structural defects in the periodically nanopatterened c-Si employ the phonon-localization effect by getting rid of the long-range crystal symmetry which further enhances the radiative recombination.

3.5 Silicon nanowires-based heterojunction for PV applications:

There are three generations in solar cells productions. The first generation uses bulk planar silicon which is till dominating the photovoltaic market because of high efficiencies (Conibeer et al., 2006). However these cells are costly. The second generation cells uses thin film layer to produce the photovoltaic effect only on that part (Shah et al., 2004). These devices do not give very good efficiencies but it can be developed on flexible and cheap

substrates. The third generation solar cells use various nanostructures and materials to produce for efficient as well as cost effective production of photovoltaic cells (Green, 2002). Silicon nanowire based solar cell is a potential candidate for the fabrication of third generation solar cells. Silicon nanowires have unique physical and optical properties which make the mass production of silicon nanowire based solar cells feasible at comparatively low cost (Green, 2001; Richards, 2006).

SiNW arrays are used for manufacturing large area of SiNWs-solar cells (Garnett et Yang, 2010).Increased absorption of light has been observed with these arrays of nanowires as compared to planer silicon solar cells (Tsakalakos et al., 2007). Lieber et al. (Tian et al., 2007) fabricated single SiNWs solar cell using similar structure to run devices that need very small amount of power, obtaining a maximum power output of 200 pW for single nanowire device that leads to an energy efficiency of 3.4%.

Junction formation is carried out to separate the photo generated electrons and holes after the synthesis of nanowires. Junction in a solar cell can be of two types: homojunction and heterojunction. Homojunction solar cells have similar semiconducting materials with equal band gaps but different doping concentrations. These types of solar cells can have single pn junction or pin junction or pnn+ or npp+ or any other junction combination consisting of different doping concentrations (Tawada, Okamoto et Hamakawa, 1981). Figure 3.3 (left) illustrates traditional single junction solar cell (Yu et al., 2012). On the other hand, heterojunction solar cells are composed of semiconductors of different band gaps. These kinds of solar cells have some advantages over homojunction solar cells. Since, these cells consist of different semiconducting materials, tuning into different bandgaps can enhance the wavelength response of the solar cell. However, it is hard to find semiconductors which have good lattice matching to obtain heterojunction solar cells. Three dimensional nanowire solar cells have been proposed by Fan et. al. (Fan et al., 2009) as shown in figure 3.3 (right), where the pn junction interface and light absorption direction are parallel to each other so that carrier collection takes place at perpendicular direction to the absorption of light. Using these nanowire structures, the pn junction interface area is increased compared with the planar

solar cells. Hence, minority carrier diffusion length is shortened which reduces the recombination loss of electrons.

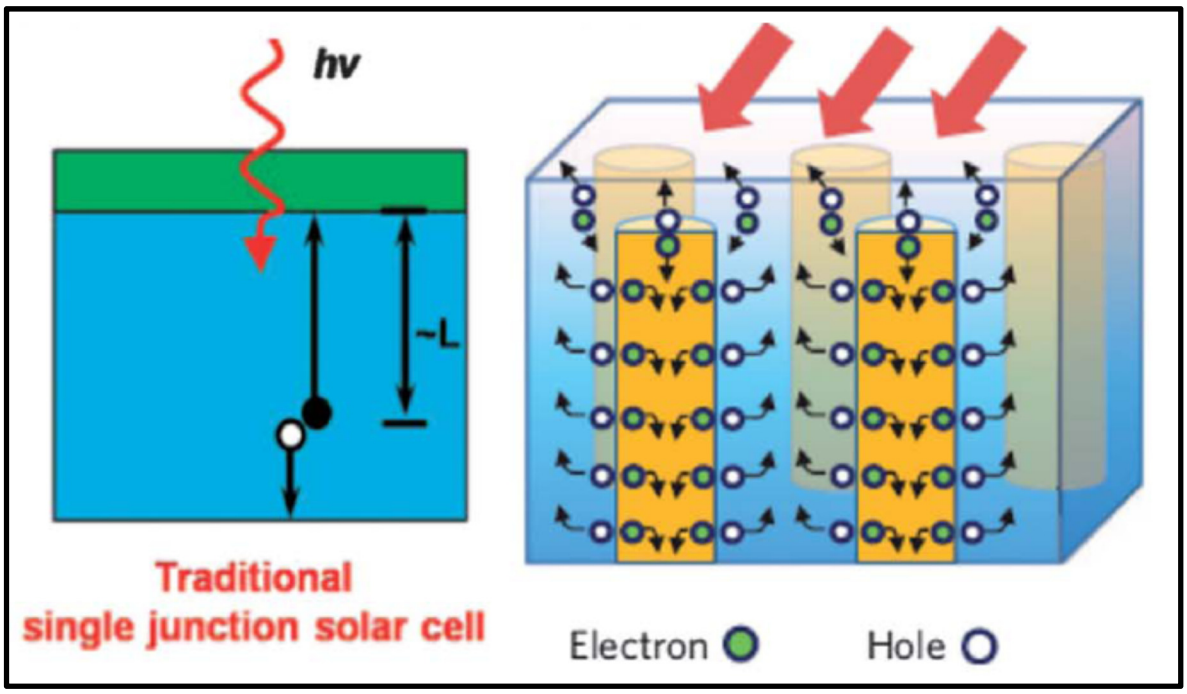

Figure 3.3 Traditional single junction solar cell (left)
Taken from (Yu et al., 2012)
3D nanowire solar cell (right)
Taken from (Fan et al., 2009)

Electron hole pairs can be separated either in the radial direction or in the axial direction. Figure 3.4 depicts radial pn junction Si nanowire array solar cell geometry (Kelzenberg et al., 2009). Junction can be formed by epitaxial growth, diffusion and ion implantation. Among them, diffusion of impurities is a popular method used for doping in semiconductors. Nanowire heterojunctions can be fabricated using a thin film layer deposition on the top of the nanowire array by thermal evaporation, chemical vapor deposition, and pulsed laser deposition for inorganic materials. In case of organic materials and dye sensitized solar cells (Law et al., 2006), spin coating, dip coating, solution dye absorption is used.

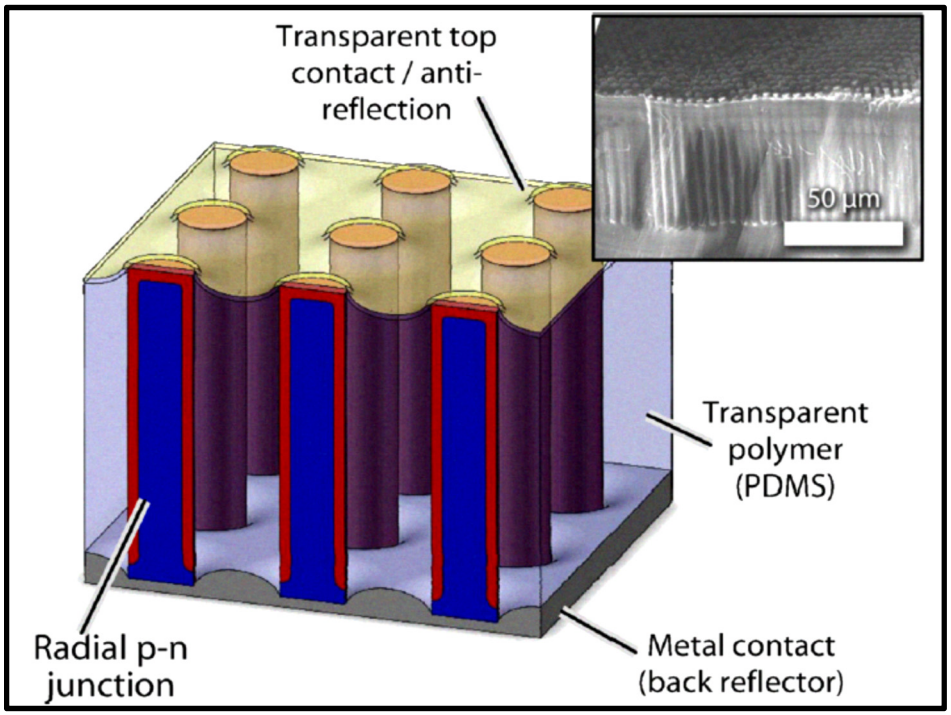

Figure 3.4 Radial pn junction Si wire array solar cell geometry
Inset SEM image of polymer embodied Si NW array
Taken from (Kelzenberg et al., 2009)

TiO_2 is a wide bandgap, n-type semiconducting material in its anatase crystalline form (Forro et al., 1994). Amorphous TiO_2 can easily be synthesized using sol-gel technique by all solution based method (Antonelli et Ying, 1995). Sintering at high temperature is used to prepare anatase crystalline TiO_2 (Campostrini et al., 1994). Anatase TiO_2 can be a potential element to fabricate heterojunction with Si [ref]. It is useful to improve the optical and electrical characteristics of Si-based devices (Hwang, Boukai et Yang, 2009). Anatase TiO_2 layer can be deposited on Si substrates via spin coating or dip coating processes (Wang, Helmersson et Käll, 2002).

Si-based hybrid heterojunction can also be formed using organic materials (Avasthi et al., 2011). Poly (3,4-ethelenedioxythiophene): poly (styrenesulfonate) (PEDOT:PSS) is an organic material that attracts a lot of attention now-a-days to fabricate efficient hybrid heterojunction with crystalline Si (Shen et al., 2011). Efficiency up to 16% has been reported by researchers for these types of hybrid heterojunction solar cells (Um et al., 2017). The

PEDOT:PSS layer can be employed as the hole transporting material for hybrid heterojunction solar cells (Sheng et al., 2016). PEDOT:PSS can be deposited on Si substrates using spin coating or dip coating methods (Subramani et al., 2016).

Implementing surface plasmon resonance (SPR) effect into silicon nanowire based solar cells helps to suppress the reflection in their resonance wavelength region (Anatoly et Igor, 2003). Adding minute amounts of silver nanoparticles in the silicon nanowires helps to achieve the plasmonic effect. These metallic nanoparticles interact with the incident light and scattered them in many directions. This phenomenon allows the solar cells to absorb more light since the scattered light travel along the solar cells.

Contacts are made to collect electrons and holes after formation of junctions in solar cells (Garnett et al., 2011). One of the contacts either top or bottom must be transparent for passing the light through it and the other one is made highly reflective for trapping and directing the light. The open circuit voltage, fill factor, short circuit current density and overall energy conversion efficiency are maximized if the contacts are ohmic (He et al., 2012) in nature. If the junction is Schottky type (Li et al., 2010), then one of the contacts has to be ohmic in nature and the other is Schottky. There are various ways of making the contacts, for instance in planar solar cells, ohmic contact is made by heavy doping of the nanowire system (Tress et al., 2011). The contact patterns are formed by either metal evaporation using mask or by writing the pattern using e-beam and photolithography (Garnett et al., 2011). These methods are generally employed for planar solar cells. Multiple lithography and etch step are required in case of radial junction based solar cells (Lu et Lal, 2010). For backside contact generally Ni/Al or Au is used and for the top contact grid Ag or Au is used(Garnett et al., 2011).

To conclude, this literature review section tried to give an overview of the synthesis of vertically aligned SiNWs and its potential applications in fabricating heterojunction solar cells, to develop a cost-effective way to produce third generation PV devices.

CHAPTER 4

SIMULATION WORKS TO DETERMINE THE OPTICAL PROPERTIES OF THE SILICON NANOWIRES

4.1 Introduction:

The maximum theoretical efficiency of a single p-n junction solar cell was first theoretically calculated by William Shockley and Hans Queisser in 1961 (Shockley et Queisser, 1961). This limit also called detailed balance limit. According to this limit, the maximum theoretical efficiency is 33.7%. The main objective of the simulation part of this thesis is to check whether an ideal p-n junction that made using silicon nanowires could approach to the Shockley-Queisser limit. Hence, the loss mechanisms of light incident on the nanowire surface have to be understood properly.

4.2 Design of the modelling:

First, optical properties of silicon nanowires such as reflectance, transmittance and absorbance will be simulated using the Photonics SHA 2D tool (Ni et al., 2009). Photonics SHA 2D tool is used for modelling the optical parameters such as reflectance, transmittance, and absorbance using 2D spatial harmonic analysis method which is similar to RCWA of single period multilayer grating. In this tool the incident wave can be any plane electromagnetic wave with any incident angle. The incident wave can be TE or TM polarized wave. The solver of this tool was made of C with LAPACK. Then the ultimate photovoltaic efficiency of the nanowire solar cell will be calculated using this relation:

$$\eta = \frac{\int_0^{\lambda_g} \boldsymbol{I}(\lambda)\boldsymbol{A}(\lambda)\frac{\lambda}{\lambda_g}\boldsymbol{d}\lambda}{\int_0^{\infty} \boldsymbol{I}(\lambda)\boldsymbol{d}\lambda} \tag{4.1}$$

η is the ultimate photovoltaic efficiency, $\boldsymbol{A}(\lambda)$ is the absorbance given by the equation

$$\boldsymbol{A}(\lambda) = 1 - \boldsymbol{R}(\lambda) - \boldsymbol{T}(\lambda) \tag{4.2}$$

$R(\lambda)$ is the reflectance and $\boldsymbol{T}(\lambda)$ is the transmittance.

$\int_0^\infty \boldsymbol{I}(\lambda)\boldsymbol{d}\lambda$ is the solar irradiance spectra.

We have simulated the optical properties of the silicon nanowires having a fixed diameter of 100nm and verying the length of the nanowires from 300 nm to 1 μm. The simulation results have been shown in the next section.

4.3 Results:

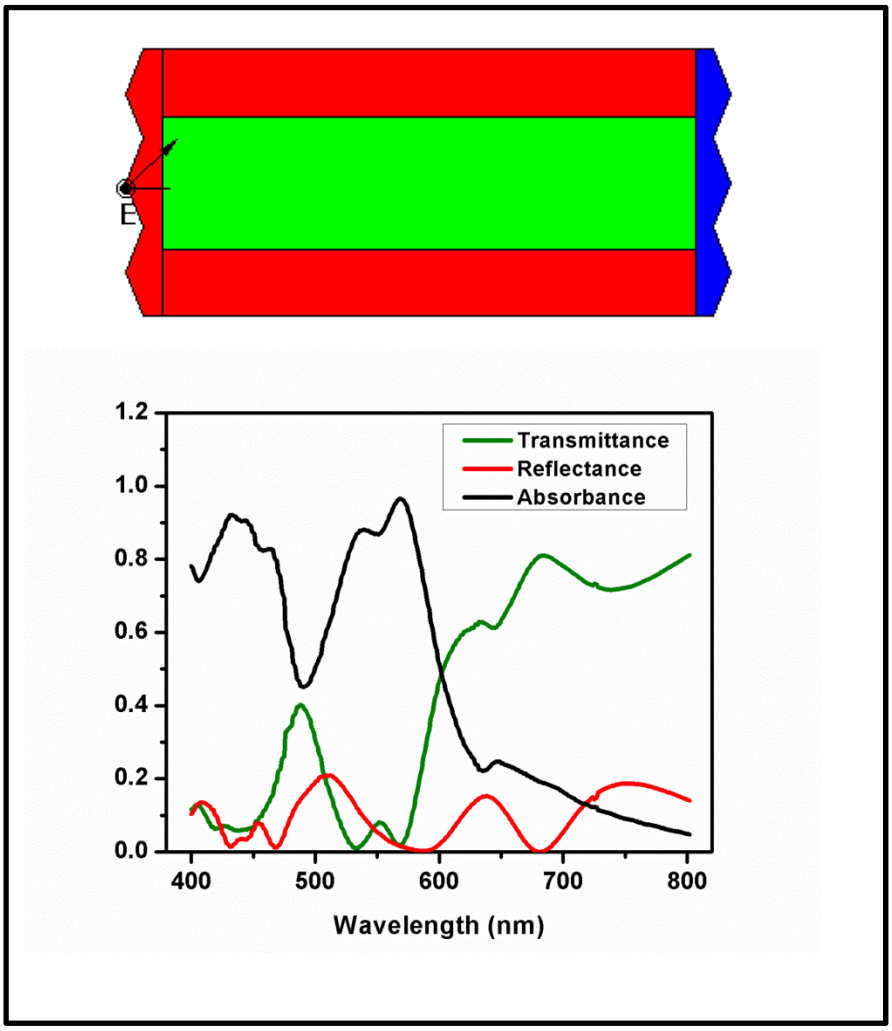

Figure 4.1 Upper Image: Model geometry uses for SHA 2D tool (region in red color is air, green colored region is silicon nanowire and blue region is the silicon substrate)
Lower Image: Optical properties vs. wavelength plot in 3 nm spacing (length of the nanowire 400nm and diameter 100nm)

Figure 4.1 and 4.2 represents the optical properties vs. wavelength plot for nanowires with lengths 400nm and 1 μm respectively.

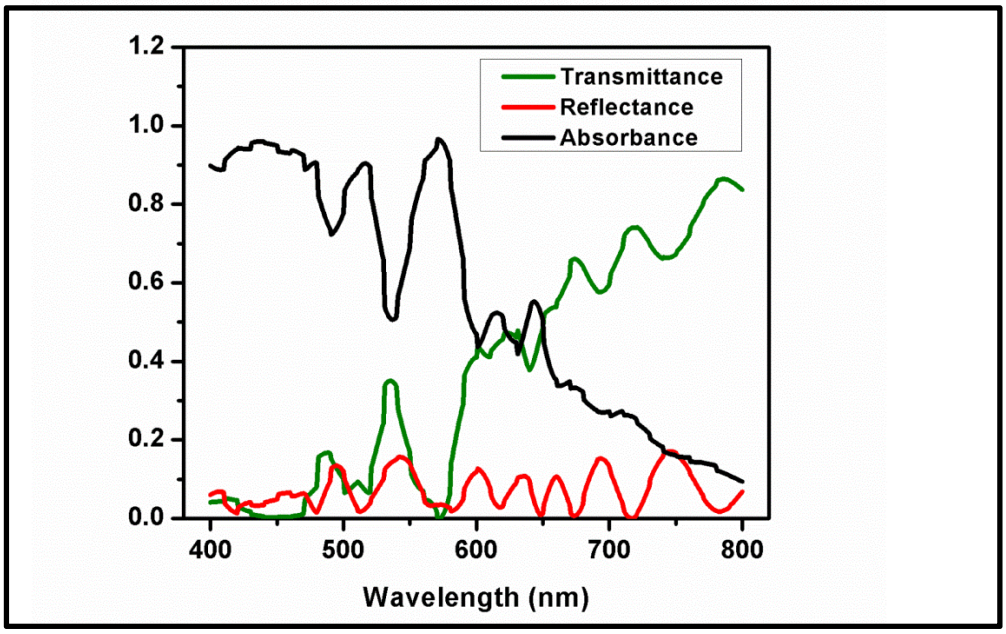

Figure 4.2 Optical properties vs. wavelength plot in 3 nm spacing (length of the nanowire 1μm and diameter 100nm)

Table 4.1 Calculated solar cells efficiencies

Nanowire Length in nm	**Simulation spacing in nm**	**Ultimate Photovoltaic Efficiency in %**
400	3	24.6626
1000	3	29.25

4.4 Conclusion:

Longer nanowires are able to supress the reflection better than the shorter nanowires. Nanowire based solar cells have the ability to approach to the Shockley-Queisser limit if we can find the proper geometry (length, diameter, filling factor etc.) for these silicon nanowires.

CHAPTER 5

PHONON PROCESSES IN VERTICALLY-ALIGNED SILICON NANOWIRE ARRAYS PRODUCED BY LOW-COST ALL-SOLUTION GALVANIC DISPLACEMENT METHOD

D. Banerjee [a], S. Cloutier [b], C. Trudeau [c] and F. Gerlein [d],
[a, b, c and d] Department of Electrical Engineering, École de Technologie Supérieure,
1100 Notre-Dame West, Montreal, Quebec, Canada H3C 1K3

Paper published in *Applied Physics Letters,* March 2016

Abstract: The nanoscale engineering of silicon can change significantly its bulk optoelectronic properties to make it more favorable for device integration. Phonon process engineering is one way to enhance inter-band transitions in silicon's indirect band structure alignment. This paper demonstrates phonon localization at the tip of silicon nanowires fabricated by galvanic displacement using wet electroless chemical etching of a bulk silicon wafer. High-resolution Raman micro-spectroscopy reveals that such arrayed structures of silicon nanowires display phonon localization behaviors, which could help their integration into the future generations of nano-engineered silicon nanowire-based devices such as photodetectors and solar cells.

5.1 Introduction :

In recent years, significant efforts have provided a much better understanding of the unique electrical, mechanical and thermal properties of 1-dimensional nanostructures (Schmidt et al., 2009). Typically, nanowires have diameters on the order of few nanometers and lengths of hundreds of nanometers or more, favoring charge carrier transport along a single dimension. Silicon-based nanowires have become popular given the raw material's availability, biocompatibility and low processing costs using current microelectronic standards. To fully exploit these advantageous material properties, the industry requires processes to fabricate silicon nanowire-based devices at low costs.

To date, different fabrication methods have produced silicon nanowires, including chemical vapor deposition using the vapor-liquid-solid technique (Westwater et al., 1997), laser

ablation (Morales et Lieber, 1998), thermal evaporation decomposition (Pan et al., 2001), molecular beam epitaxy (Schubert et al., 2004), chemical etching (Zhang et al., 2008), and solution growth (Holmes et al., 2000). Among these different methods, metal-assisted wet electroless chemical etching (MAWCE) of silicon substrates offers an attractive alternative for low-cost top-down fabrication over a large surface area. A few key reasons for MAWCE popularity (Huang et al., 2011) include: (a) being a low-cost, all solution-based fabrication route (Huang et al., 2012b), (b) the ability to yield nanowire-structured surfaces with very low reflectance for potential application in photovoltaic devices (Hung et al., 2011), (c) its potential for effective deployment in self-powered functional low-consumption systems (Hwang, Boukai et Yang, 2009). This emerging fabrication technique relies on the selective electrochemical etching of silicon using metal catalysts. It yields well-organized and highly-dense arrays of silicon nanowires of identical crystallographic orientations with lengths on the order of few microns and diameters in the tens of nanometers (Zhang et al., 2008).

Photovoltaic platforms based on nanowire systems such as dye-sensitized nanowire-based solar cells have been shown to suffer from poor light conversion efficiencies (Law et al., 2005). Partly, this is due to silicon's indirect band gap of 1.12 eV, which is ill-suited, for efficient sunlight absorption. However, the exciton binding energy for crystalline silicon is also very small (14.7 ± 0.4 meV), which is desirable for light harvesting applications. Moreover, phonon-enhancement effects could also provide another roadway towards improving the conversion efficiencies in photovoltaic silicon nanowire-based devices; because it increases the probability of phonon-assisted band-to-band transitions in bulk crystalline silicon's indirect band structure (Alfaro et al., 2006; Hybertsen, 1994). Previous studies have shown that phonon confinement in group IV elements (like silicon) can be helpful in improving their optical properties (Takagahara et Takeda, 1992), while phonon confinement in nanowires has been shown to take place in the radial direction (Adu et al., 2006; Barbagiovanni et al., 2014; Ingale et Rustagi, 1998; Rao et al., 1997). The existence of phonon confinement effect was first demonstrated by measuring the Raman peak broadening in microcrystalline silicon films (Richter, Wang et Ley, 1981). Later, an extended model was proposed to include nanowires (Campbell et Fauchet, 1986), demonstrating that phonons can

be spatially-confined in space to increase their momentum distribution. As a result, this directly improves the statistics to favor phonon-assisted band-to-band transition in indirect bandgap semiconductors (Landsberg, 1967). In general, this effect translates into a down-shift and asymmetric broadening of the Raman peaks in silicon nanowires (Adu et al., 2006; Duan, Kong et Shen, 2012). However, peak downshift and broadening can also arise from inhomogeneous laser-source heating and from an excess of carriers or Fano resonances. Previous studies have shown the possibility of discriminating the phonon confinement from other such effects by varying the laser power, temperatures and excitation energy (Piscanec et al., 2003). As such, the phonon confinement effect was first noticed in silicon nanowires with diameters less than 22 nm (Adu et al., 2005; Wang et al., 2000). The phonon localization effect was also observed in larger silicon nanostructures with the introduction of defect centers at silicon interfaces creating local confinement within nanoscale-sized crystallites (Cloutier et al., 2006; Cloutier, Guico et Xu, 2005).

In this paper, we report phonon-enhancement effect in vertically-aligned Si nanowire structures produced over large surface area at low-cost using all solution-based metal-assisted wet electroless chemical-etching (MAWCE) method. Since the nanowires are relatively large in diameter, our results clearly show that this phenomenon occurs exclusively at the apex of the nanowires, where spatial confinement can occur. As this effect can prove highly beneficial for power conversion efficiencies, we believe this can be an important incentive to explore the use of such vertical silicon nanowire arrays to significantly improve photovoltaic devices at low costs.

5.2 Experimental methods :

5.2.1 Synthesis of the vertically-aligned silicon nanowire arrays :

To fabricate silicon (Si) nanowire arrays from monolithic Si wafers, we used a Galvanic Displacement Method (GDM) (Ng et al., 2011; Peng et al., 2006). In this technique, Si nanowires are fabricated by selective chemical etching of Si substrates in aqueous acid solutions using metallic nanoparticles deposited on the substrate to act as catalysts (Ng et al.,

2011; Peng et al., 2002). The process then involves concurrent reduction of metal ions, oxidation and dissolution.

The etching mechanism presented here results from an aqueous solution of hydrofluoric acid (HF) containing silver nitrate ($AgNO_3$) (Peng et al., 2003; Peng et al., 2006; Peng et al., 2005). The first step in this process is the formation of Ag^+ ions close to the Si surface. The Ag^+ ions effectively absorb electrons when the deposition of Ag nanoparticles takes place on the substrate, followed by the oxidation of Si below the Ag nanoparticles to form silicon dioxide (SiO_2). This SiO_2 is finally dissolved by the HF contained in the aqueous solution, creating cavities on the substrate. Subsequently, the Ag catalyst seed sinks into these cavities. With the prolonged oxidation of SiO_2, electrons begin to accumulate on the Ag surface. As a result, Ag^+ present in the solution gets attracted to the vicinity of the nuclei. The resulting reduction leads to the growth of more Ag particles trapped in the aforementioned substrate cavities (Qu et al., 2009).

High concentrations of Ag^+ in the etching solution and the Si substrate help the reaction to run repeatedly, resulting in the formation of dendrite layers of Ag covering the Si substrate and creating vertically-aligned Si nanowires on the Si surface. Most importantly, the lateral etching perpendicular to the walls of the etched channels is not favorable because the diffusion path from the wall of the channels to the particle is longer compared to directly underneath (Qu et al., 2009).

For this work, we have used n-type Si wafers with 1-10 ohm-cm resistivity. Composition of the etchant used for the work is 0.02M $AgNO_3$ plus 5M HF. The reaction takes place during 1 hour at room temperature, in which the Si nanowire arrays are completely formed. The excess of Ag is removed by cleaning the wafers at room temperature using concentrated (70%) nitric acid (HNO_3) solution for 1 hour. The resulting nanowire arrays are shown in Figure 5.1(a). The nanowires have lengths in the range 2 to 3 μm and diameters between 40 and 50 nm. Figure 5.1(b) highlights the uniformity and strong anti-reflection behaviour of the nanostructured Si sample.

5.2.2 Studying the phonon-localization effect :

In this report, phonon localization effect is studied using a WITec alpha 300 micro-Raman system equipped with a 532 nm fibre-coupled laser for excitation. For Raman measurements, the sample is cleaved and mounted vertically to scan the cross-section of the cleaved wafer. The excitation laser power is varied from 1 to 40 ± 1 mW using an external attenuator. This approach is known to allow discriminating laser-induced heating from the phonon-confinement effect (Cloutier, Guico et Xu, 2005). To study how the nanowire's Raman-signal peak position and peak width changes with increasing laser power, a Gaussian curve is fitted onto the silicon Raman peak (*circa* 520 cm^{-1}), providing information about the peak's intensity, position and width.

5.2.3 Studying the chemical composition contamination at the surface :

Finally, X-ray photoelectron spectroscopy (XPS) measurement is performed using VG ESCALAB 3 Mark II XPS machine equipped with Mg κα source to confirm the complete removal of residual Ag by-products from the reaction after cleaning.

5.3 Results and discussion:

With the cleaved sample mounted vertically under the microscope to scan the cross-section as shown in Figure 5.2(a), we have the ability to map the Raman peak's intensity (Fig. 5.2b), the peak width (Fig. 5.2c) and the peak position (Fig. 5.2d), where brighter colours represent higher values for each case. In Figure 5.2(b), we notice that while scanning the sample's cross-section, the Raman peak intensity is significantly stronger at the top of the nanostructured region (tip of the nanowires). This is a first indicator of possible phonon-localization effect (Adu et al., 2006). Most importantly, Figure 5.2(c) also show a significantly wider (brighter) and Figure 5.2(d) shows a significantly downshifted (darker) Raman peak at the tip of the nanowires compared to the bulk silicon substrate, which further suggests phonon-localization (Duan, Kong et Shen, 2012).

To discard other potential causes to explain these observations, it is important to look at the evolution of the Raman peak's downshift and width as the 532 nm excitation laser power is varied (Cloutier et al., 2006). Figure 5.3 shows the evolution of the silicon Raman peak width and position with increasing laser power. Clearly, the Raman signal originating from the nanowire tips is significantly broader (brighter) and down-shifted (darker) as the laser power is increased. A similar phenomenon can be seen for the silicon Raman signal originating from the bulk silicon substrate due to heating effect; however the effect is much less pronounced.

These evolutions are highlighted in Figure 5.4(a, b), comparing the average Raman peak position and FWHM as a function of the excitation power, for both the nanowire tips and the bulk substrate. Here it becomes obvious that the downshifting and broadening of the silicon Raman signal happens at different rates for the silicon nanowire tips and the bulk substrate. The Raman peak position data for the bulk silicon substrate follows a linear relationship consistent with laser-induced heating:

$$\omega_P = -0.014P + 518.9 \tag{5.1}$$

While the data for the silicon nanowire tips showed the following quadratic relationship:

$$\omega_P = -0.0002P^2 - 0.035P + 518.9 \tag{5.2}$$

Where ω_P is the center of the silicon Raman peak position and P is the excitation laser power in mW.

Moreover, the silicon Raman peak FWHM data for the bulk silicon substrate also followed a linear relationship:

$$\Delta\omega = 0.08P + 4.19 \tag{5.3}$$

While the silicon peak FWHM data originating from the silicon nanowire tips follows a significantly different evolution:

$$\Delta\omega = 0.16P + 4.13 \tag{5.4}$$

Where $\Delta\omega$ is the FWHM of the silicon Raman peak and P is the excitation laser power in mW. The nature of the downshift plot (Figure 5.4a) is consistent with phonon localization effects [28, 29]. The spatial mapping of the Raman peak evolution clearly suggests that the phenomenon is limited exclusively to the nanowire tips. This result can eliminate chemically-induced damage as the possible cause for this effect as it would appear everywhere and not exclusively at the tip of the nanowires. Because of the apex-shaped tip of the nanowires, this is indeed the only place where spatial phonon confinement can occur.

The shift-width progressions shown in Figure 5.5 visually highlight the different underlying mechanisms between the nanowire tips and the substrate for increasing laser powers. As such, the phonon peak downshift as a function of its broadening with increasing laser power can be used to confirm phonon localization in the nanowire tips. Indeed, the Raman peak downshifts and broadens at different rates for increasing laser power in the nanowire tips, which is another strong evidence of phonon localization(Fukata et al., 2006; Hayashi et Kanamori, 1982).

Recent development has shown significant downshift in the photoluminescence spectra with decreasing diameter of silicon nanowires (Canham, 1990; Colli et al., 2006). While the Raman signatures are collected directly from the nanowires tip positions in a confocal configuration, any photoluminescence appears to be beyond the range of the CCD camera coupled to the micro-Raman system. As such, we collected photoluminescence spectra from the bulk and nanostructured silicon samples using 532 nm laser excitation and a TRIAX320 spectrometer equipped with a JobinYvon–Symphony InGaAs detector array. However, we did not observe any noticeable difference in the PL spectra between the pristine and nanostructured wafers. This should be expected as the photoluminescence spectrum is

collected from the entire sample including the bulk, while the phonon confinement takes place in the vicinity of the nanowire tips and can be seen only in the confocal configuration. As a result a correlation between Raman measurements and photoluminescence spectra is not possible.

An important factor yet to consider is the possibility of residual surface-enhanced Raman scattering (SERS) effect due to Ag nanoparticle residues from the MAWCE process (Lee et al., 2011; Wang et al., 2011; Xu et al., 2012b). Indeed, the synthesis method uses $AgNO_3$ solution and the presence of some remaining Ag nanoparticles on the silicon nanowires is certainly possible. These excess Ag nanoparticles could be responsible for the contrast figures such as seen in Figures 5.2 and 5.3 due to local metal-enhancement effects (Canham, 1990). Therefore, it is essential to differentiate the contribution of phonon localization from any possible surface enhanced Raman scattering effect. This is why we perform the additional HNO_3cleaning step described in the previous section. The complete removal of the Ag by-products can be directly confirmed using X-ray photoelectron spectroscopy analysis (XPS). The XPS spectrum (Banerjee et al., 2016) has been collected from the entire nanostructured surface after thorough HNO_3cleaning and confirms no measurable Ag residue on the surface. Hence, the contrast images in Figures 5.2 and 5.3 originate purely from phonon localization effects and not from local metal-enhancement artefacts due to Ag residues.

5.4 Conclusions :

In summary, our results confirm phonon-localization in vertically-aligned silicon nanowire arrays produced over large areas using low-cost all solution-based galvanic displacement methods. Phonon confinement effects are localized in the top part of the elongated nanowires, where the feature sizes remain small enough to be consistent with the literature (Adu et al., 2005; Piscanec et al., 2003; Wang et al., 2000). Phonons play an essential role in compensating for the momentum mismatch between carriers in silicon. Band-to-band transitions become more likely when localization occurs. Superior emission and absorption

properties are expected to improve the current generation of nano-engineered silicon-based optoelectronic devices.

Acknowledgment

S.G.C. is most thankful for the financial support from the Canada Research Chairs and the NSERC Discovery programs. The authors thank Josianne Lefebvre from the LASM at Ecole Polytechnique de Montreal for her support with the XPS measurements and their interpretation.

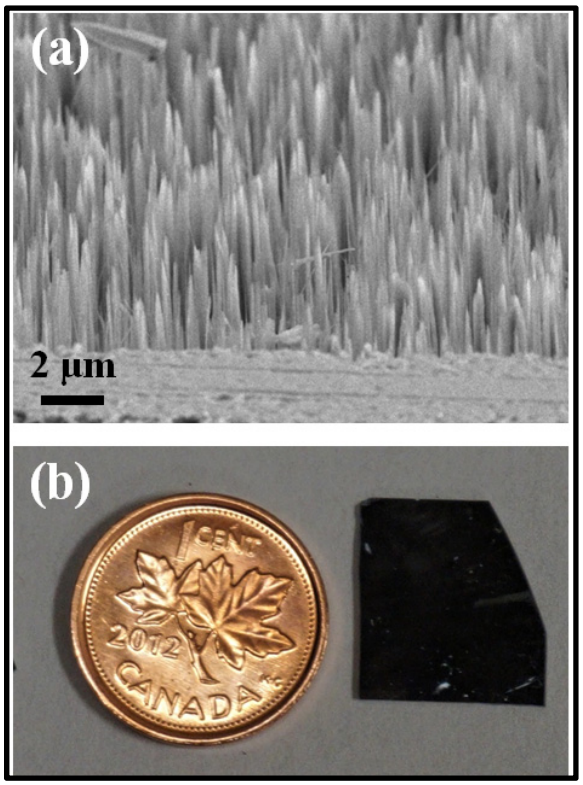

Figure 5.1 (a) SEM micrograph of the silicon nanowire arrays synthesized using GDM (b) Top-view of the nanostructured silicon sample, highlighting the uniformity and the strong anti-reflection behaviour of the nanoengineered surface

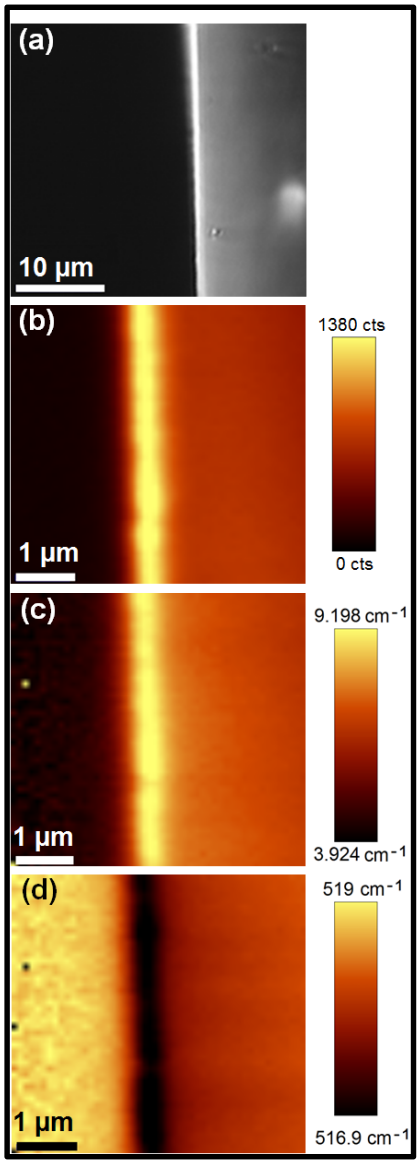

Figure 5.2 (a) Cross-sectional view of the cleaved nanostructured-silicon wafer
(b) Silicon Raman peak intensity distribution using 532 nm excitation laser
The top of the nanostructured area (tips of the nanowires) shows much stronger Raman signal
(c) Silicon Raman peak's width distribution showing larger FWHM at the top of the nanostructured region
(d) Silicon Raman peak's position showing a significantly down-shifted Raman peak at the top of the nanostructured region

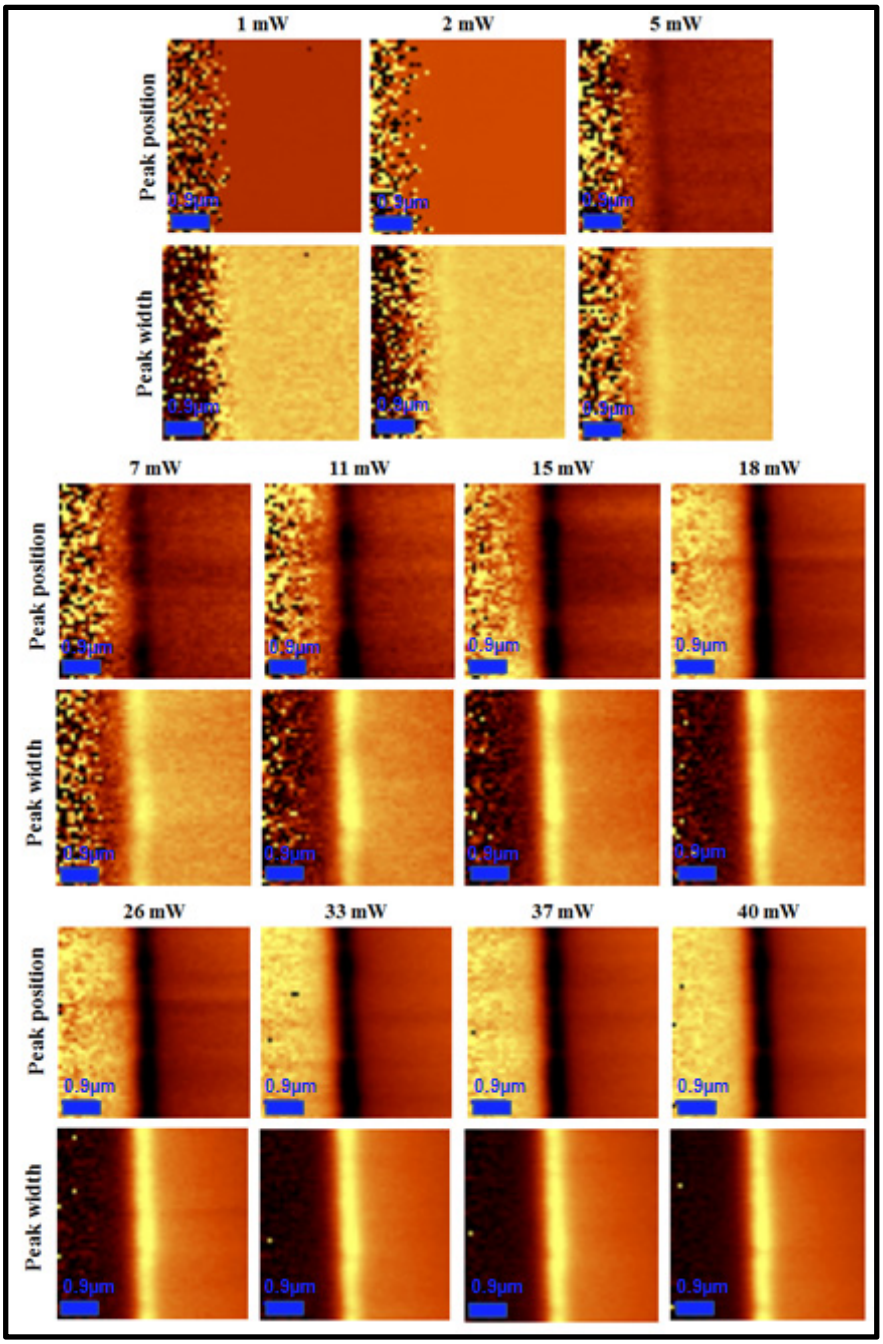

Figure 5.3 Spatial distribution of the nanostructured silicon's Raman peak and width with increasing laser power (left region is air, middle region is the top parts of the nanowires) All the scale bars are 0.9 μm

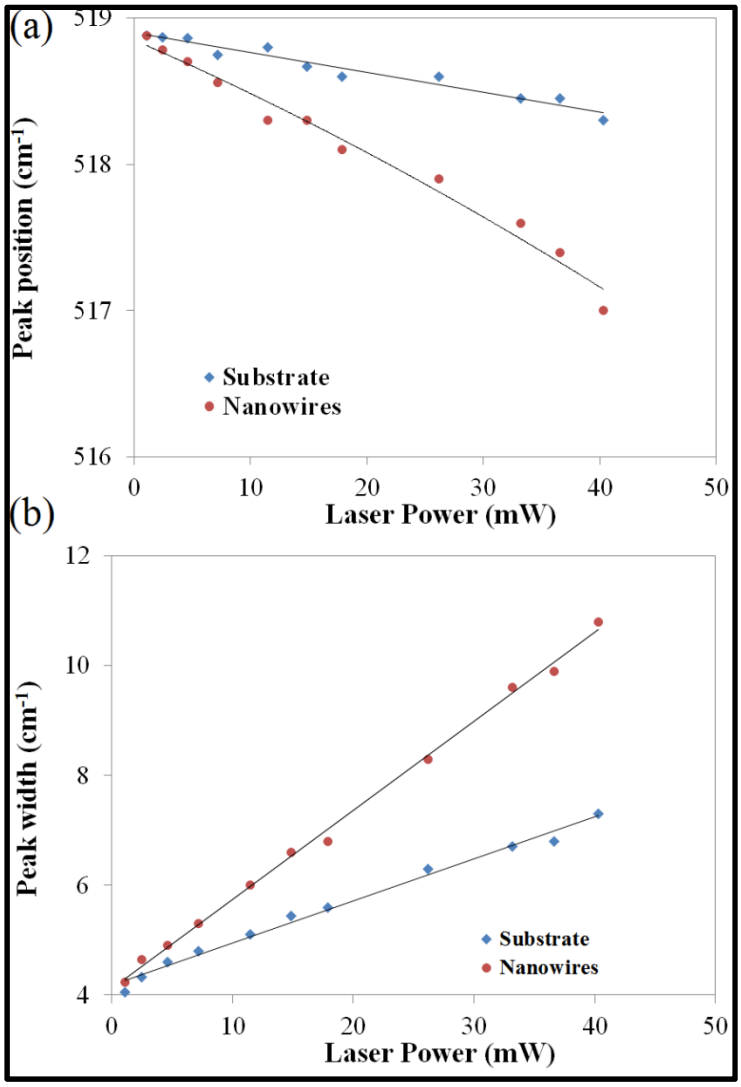

Figure 5.4 (a) Evolution of silicon Raman peak position and
(b) Evolution of silicon Raman peak width with increasing laser power
The blue diamonds (♦) represent the silicon substrate and red dots (●) represent the SiNWs

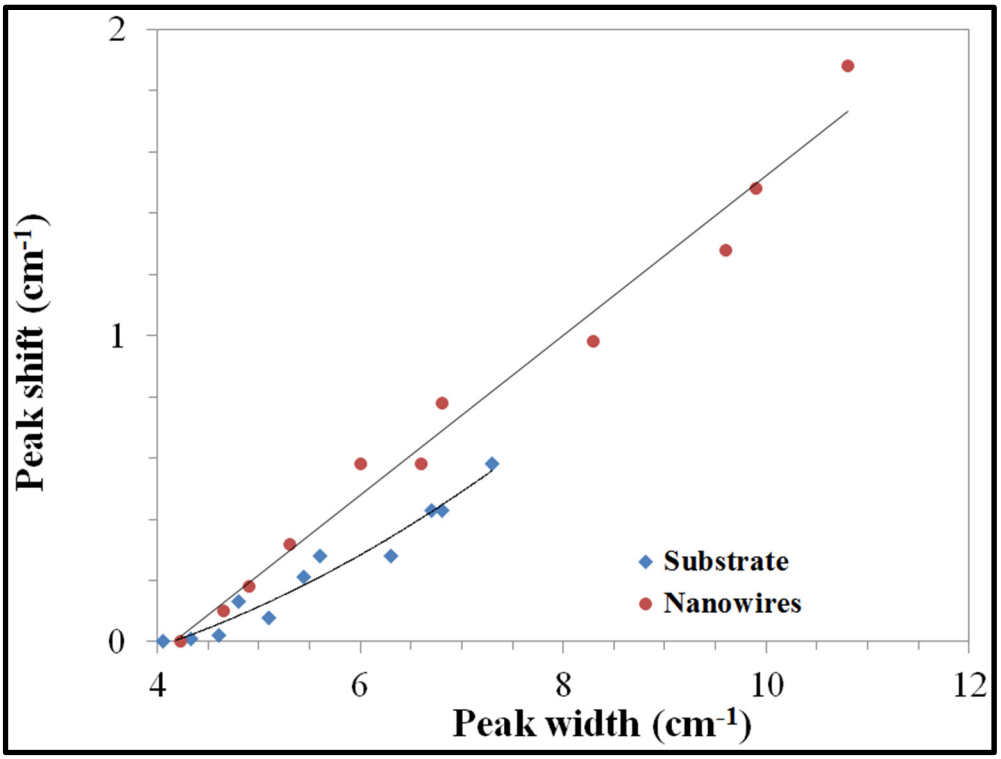

Figure 5.5 Nanostructured silicon's Raman peak shift-width evolution with laser power
The blue diamonds (♦) represent the silicon substrate and red dots (●) represent the SiNWs

CHAPTER 6

TAILORED INTERFACES OF BULK SILICON NANOWIRE/TiO_2 HETEROJUNCTION PROMOTING ENHANCED PHOTOVOLTAIC PERFORMANCES

D. Banerjee [a], S. Cloutier [b], J. Benavides [c] and X. Guo [d],
[a, b, c and d] Department of Electrical Engineering, École de Technologie Supérieure,
1100 Notre-Dame West, Montreal, Quebec, Canada H3C 1K3

Paper published in *ACS Omega*, May 2018

Abstract: We report significantly-improved silicon nanowire / TiO_2 n^+-n heterojunction solar cells prepared by sol-gel synthesis of TiO_2 thin-film atop vertically-aligned silicon nanowires arrays obtained by facile metal-assisted wet electroless chemical etching (MAWCE) of a bulk highly-doped n-type silicon wafer. As we show, chemical treatment of the nanowire arrays prior to depositing the sol-gel precursor has dramatic consequences on the device performance. While hydrofluoric (HF) treatment to remove the native oxide already improves significantly the device performances, hydrobromic (HBr) treatment consistently yields by far the best device performances with power conversion efficiencies (Ƞ) ranging between 4.2% and 6.2% with fill factors up-to 60% under AM 1.5G illumination. In addition to yield high-quality and easy to produce n^+-n solar cell devices, these findings regarding the surface treatment of silicon nanowires with HBr suggest that HBr could contribute to the enhancement of the device performance not only for solar cells but also for other optoelectronics devices based on semiconductor nanostructures.

6.1 Introduction:

In recent years, the fabrication of silicon (Si) hybrid heterojunction solar cells has generated a significant interest since it can promise higher efficiencies at significantly-lower fabrication costs (Huang et al., 2012a; Shen et al., 2011; Yu et al., 2012; Yu et al., 2015). Semiconductor heterojunction can be advantageous since both materials can absorb light from different regions of the solar spectrum (Lin et al., 2013; Patel et Tyagi, 2015). Efforts have also been made to better understand and exploit the unique electrical, mechanical and thermal

properties of nanowires (NWs) for photovoltaic device integration (Cheng et al., 2015; Doganay et al., 2016). Finally, silicon is already well-known to be cheap, non-toxic and abundant (Schmidt et al., 2009; Shimizu et al., 2007). These combined advantages coupled with adequate industrial infrastructure can help produce Si nanowire-based devices at relatively low manufacturing costs. Metal-assisted wet-chemical etching (MAWCE) of bulk silicon wafers can allow useful all solution-based mass-production of ordered vertically-aligned nanowire arrays over large areas because it permits control over the geometry of their diameter, length and spacing, while avoiding high-cost and low-output usual lithographic processes (Banerjee et al., 2016; Peng et al., 2006). MAWCE is based on the principles of galvanic displacement reaction, details of which have been previously discussed (Garnett et Yang, 2010; Hung et al., 2011; Kawasaki et al., 2010).

Meanwhile, anatase TiO_2 is a wide-bandgap, n-type semiconductor (Tang et al., 1994). TiO_2 is already widely used for carrier extraction in dye- and quantum dot-sensitized solar cells (Meen et al., 2009; Mi Yeon et al., 2004) and as a transparent front contact in heterojunction solar cells (Hsu et al., 2015; Yin et al., 2014). However, fewer reports describe how TiO_2 can also be used as the main component for fabricating an efficient heterojunction with Si. This is because previous works mainly focused on fabricating narrow bandgap semiconductors (Lotfi et al., 2013; Shin et al., 2014).

Indeed, n-type silicon nanowires can also be used in conjunction with anatase TiO_2 to form an n^+-n isotype heterojunction with favorable band-alignment to produce good solar cell devices (Fan et al., 2011). However, early efforts to fabricate n-Si/n-TiO_2 isotype heterojunction solar cells have yielded very low efficiencies, to the tune of 0.0005% with a small FF of 21%(Hwang, Boukai et Yang, 2009). Subsequently, researchers fabricated TiO_2 heterojunction in conjunction with silicon nanowires, which seemingly improved both short-circuit current density and open-circuit voltage, essential traits for the fabrication of solar cells (Hwang, Boukai et Yang, 2009; Tang et al., 1994). Meanwhile, p-type silicon coated with anatase TiO_2 is limited by unfavorable band-bending at the heterojunction. In the case of a p-SiNWs and n-TiO_2 heterojunction, the band energies of n-TiO_2 will shift upward while

the band energies of p-SiNWs will shift downward at open circuit under illumination. So, the open circuit voltage (V_{oc}) from the cell will be the V_{oc} of TiO_2/front contact junction minus V_{oc} of SiNWs/TiO_2 junction as shown in Figure 6.1(a). However, photo-generated holes in the Si move towards TiO_2 to recombine with electrons due to a built-in electric field in the space-charge region for n-SiNWs/n-TiO_2 (Hwang, Boukai et Yang, 2009; Meen et al., 2009). Hence, the open circuit voltage (V_{oc}) for n-SiNWs/n-TiO_2 will be the sum of the V_{oc} at the n-TiO_2/front contact junction plus the V_{oc} at n-SiNWs/n-TiO_2 junction because, the Fermi energy (E_F) and band energies of n-SiNWs and n-TiO_2 shift upward at open circuit condition under illumination as shown in Figure 6.1(a).

However, we should also consider several other critical issues to maximize the silicon nanowire/TiO_2 photovoltaic device performances. First, carrier recombination loss (Bartesaghi et al., 2015; Zhao et al., 1995) should be minimized to increase the fill factor (FF), thereby increasing the power conversion efficiency (η) of the devices. Second, carrier diffusion should also be limited to favor carrier extraction (Bozyigit et al., 2015; Piatkowski et al., 2016). Surface recombination is a major concern for nanowire-based devices due to their high surface-to-volume ratio. Presence of dangling bonds at the surface can significantly reduce the photovoltaic performance of nanowire-based devices by trapping the impurities and then electronically-neutralizing them (Dan et al., 2011). It has been shown that, reducing the surface recombination can dramatically increase the photosensitivity of photodetectors by up-to two orders of magnitude (Dan et al., 2011; Mallorquí et al., 2015). As such, reduced surface recombination at the nanowires surface is shown to increase in open-circuit voltage, short-circuit current and overall η of the nanowire based solar cells (Shin et al., 2014). Thermal SiO_2 (Deal et Grove, 1965; Zhao et al., 1998), a-SiNx:H (Ferre et al., 2008; Wolf et al., 2005) or Al_2O_3 (Hoex et al., 2008; Hoex et al., 2006) are some of the materials most widely used for such surface passivation.

In this report, we explore isotype heterojunction devices produced from n-type silicon nanowires covered with anatase TiO_2 produced by sol-gel chemistry and we propose a new pathway towards low cost, all solution based, easily available n-SiNW/n-TiO_2 isotype

photovoltaic device using interface engineering. Indeed, we demonstrate dramatic improvements in the photovoltaic performance of silicon nanowire/TiO_2 n-n isotype heterojunction solar cell devices containing H+ passivated nanowire surfaces obtained through HBr treatment just before fabrications of the heterojunction. Compared with untreated and HF-treated nanowire arrays, the photovoltaic performances of these HBr-treated heterojunction solar cells have improved by two orders of magnitude to consistently achieve power conversion efficiencies (η) ranging between 4.2% and 6.2%. In the future, we believe that such surface modification using solution-based HBr will yield significantly-better heterojunction devices fabricated in an efficient and cost-effective manner.

6.2 Results and discussions:

6.2.1 Structure of the solar cells :

Figure 6.1(b) shows the schematics for the SiNWs/TiO_2 heterojunction solar cell device and its band-alignment (figure 6.1(a)). The heterojunction device observed under SEM after each step is shown in Figure 6.2. Figure 6.2(a,b) shows the scanning electron micrograph of vertically-aligned n-type SiNWs of approximately 800-1000nm in length and 40-50 nm in diameter produced by MAWCE over large area using the protocol fully-described in the experimental section.

The MAWCE-prepared silicon nanowires are then immersed in 20% HBr solution for 2 minutes. Following treatment, the etched substrate is spin-coated with TiO_2 sol-gel precursor solution followed by a thermal conversion at 550^oC for one hour to obtain the anatase crystalline TiO_2 layer. Ideally, this thermal treatment should be performed by rapid thermal annealing (RTA). In contrast, a thermal cycling in a regular furnace consists of few ramps to reach the desired temperature and to cool down to room temperature which takes several hours. This process is harmful for the abruptness of the heterojunction. It can move the junction further away from and more difficult to reach for the photons. Therefore, the device should not stay for long time inside the furnace. Figure 6.2(c) shows the Raman spectra of the converted anatase TiO_2 coated atop the Si nanowire array. We observe the

three peaks at 395, 513 and 634 cm^{-1}, which are characteristic peaks for anatase TiO_2. Figure 6.2 (d) shows the SEM micrographs of the 45° tilted cross-section of the nanowire array after sol-gel precursor deposition and complete conversion to anatase TiO_2.

We have investigated the effectiveness of the native oxide removal by dipping the samples in 2%, 10% and 20% concentrated solutions of HF and HBr for 2 minutes each. Energy dispersive X-ray analysis (EDX) was performed to inspect the atomic percentage of oxygen in these samples. The samples were transferred for EDX measurements within an hour of the surface treatments. The EDX spectra were collected from the nanowire surfaces. Table AIS1 in the supporting information section demonstrates the atomic percentage of oxygen present in the sample surfaces. We have observed that higher concentration of HBr provides an almost oxygen-free silicon surface where in case of HF-treated samples, amount of oxygen remains same as in 2% to 20% concentration. We have found that these results are in good agreement with the literatures(Collins et Holmes, 2011; Kim et al., 2008). Hence, we have used 2% HF and 20% HBr for the surface treatments.

We also have varied the treatment time of HF and HBr from 1 minute to 30 minutes to investigate the atomic percentage of oxygen amount on the surfaces. We have performed EDX analysis to optimize the amounts of oxygen present in the devices. The samples were transferred for EDX measurements within one hour of the surface treatments. The EDX spectra were collected from the nanowire surfaces. The optimized parameters of the atomic percentage of oxygen from all the samples are depicted in table AIS2. We have observed reduced percentage of oxygen after 2 minutes of HF or HBr treatments. The EDX shows the similar amount of oxygen with HF or HBr till 30 minutes of the treatments. Hence, the surface treatment effect gets saturated after 2 minutes immersion in 2% HF or with 20% HBr.

6.2.2 Performance of the solar cells :

The current density-voltage (J-V) characteristics under the air mass (AM) 1.5G condition are plotted in Figure 6.3. In total, we fabricated 24 solar cells with optimized parameters and

investigated the variations in their J-V characteristics. These devices are divided equally in three groups of 8 samples in preparation for surface treatment. Devices from the first group (pristine) did not sustain any chemical treatment prior to the junction fabrication. Samples from the second group are treated with 2% HF for 2 minutes in order to remove the native oxide layer from the SiNWs surface before sol-gel deposition. The last group of samples is treated with 20% HBr for 2 minutes.

Figure 6.3(a,c) shows some photovoltaic behavior from all these 24 solar cell devices. First, Figure 6.3 (a) shows the J-V characteristics for the solar cells without any treatment prior to sol-gel deposition and their device parameters are listed in Table AIS3. For this first group of 8 samples, we measure short-circuit current densities (J_{sc}) between 0.6-1.2 mA, open-circuit voltages (V_{oc}) between 143-224 mV and fill factors (FF) in the range of 20.6-32.5%. Thus, the power-conversion efficiencies measured from these devices are very small (0.03-0.06%). In contrast, Figure 6.3(b) shows the J-V characteristics of all the devices from the samples treated with HF prior to sol-gel deposition and their device parameters are listed in Table AIS4. For this second group of 8 samples, we measure short-circuit current densities (J_{sc}) between 8.4-12.1 mA, open-circuit voltages (V_{oc}) between 421-514 mV and fill-factors (FF) in the range of 26.1-37.7%. As such, the power-conversion efficiencies are between 1.2-2.0% and significantly (30-40×) higher compared to the group 1 (untreated) devices.

Finally, Figure 6.3(c) shows the J-V characteristics of all the devices from the samples treated with HBr prior to sol-gel deposition and their device parameters are listed in Table AIS5. For this third group of 8 samples, we measure short-circuit current densities (J_{sc}) between 15.3-18.4mA, open-circuit voltages (V_{oc}) between 482-553 mV and fill-factors (FF) in the range of 48.1-60.3%. The power-conversion efficiencies are between 4.2-6.15% and again significantly (3-4×) higher compared to the HF-treated devices and close to 100× higher compared to any sample from the first group (untreated). Figure 6.3(d) compared the J-V characteristics for the best device from each group under AM 1.5 G illuminations. Clearly, HBr-treated devices perform way better than the untreated or HF-treated devices.

The logarithmic J-V characteristics in the dark are shown in Figure 6.4. Figure 6.4(a,b,c) show the dark J-V characteristics for the eight (8) devices from groups 1, 2 and 3 respectively. Figure 6.4(d) compares the dark J-V characteristics for the best device from each group. Clearly, the devices treated with HBr show very small reverse leakage current compared to the other devices. This suggests a reduction in the series resistance and increase in the shunt resistance for the solar cells treated with 20% HBr. Also, a significant increase in the dark current is noticed under forward bias condition above 400 mV which indicates a clear improvement in the hole extraction efficiency after the interface treatment with HBr.
Figure 6.5 shows histogram distributions of (a) the power-conversion efficiencies (η), (b) short-circuit current densities (J_{sc}), (c) open-circuit voltages (V_{oc}), and (d) fill-factors (FF) for the 24 devices from the three different groups. The histogram reveals a wide distribution of η between 0.03-6.2%. Similar responses have been found from the FF values distributed between 21-60%. It is shown that J_{sc} and V_{oc} values are also distributed between 0.6-18.4 mA/cm^2 and 143-553mV respectively. The origin of these large variations in all the parameters comes from the interfacial treatment with HBr. This treatment clearly provides significantly-better device characteristics overall by controlling the oxidation of the junction.

6.2.3 Role of surface treatment using HBr and HF in SiNWs/TiO_2 solar cells :

We have observed a dramatic enhancement in the photovoltaic performance in HBr treated solar cells. As predicted elsewhere (Dan et al., 2011; Mallorquí et al., 2015), surface recombination in SiNWs surface has a substantial impact on the short circuit current density and open circuit voltage. Comparing the J-V characteristics of all the 24 devices, it can be clearly observed that the devices treated with HBr before the sol-gel deposition, yielded much higher short circuit current densities and open circuit voltages compared with HF-treated or untreated devices. Thus, we have obtained dramatically-improved fill-factors and power-conversion efficiencies from those devices. This improvement in the device performance can be attributed to the surface passivation effect of HF and HBr on SiNWs surface (Nemanick et al., 2006). To prove this effect, we have performed X-ray photoelectron spectroscopy (XPS) measurements of Si 2p, O 1s and C 1s peak levels from

the pristine, HF-treated and HBr-treated SiNWs surfaces as depicted in figure 6.6 (a,b,c). The XPS spectra have been collected within 2 hours after the surface treatments. The impression of higher binding energy peak in the Si 2p region (figure 6.6a) is an indication of the growth of a surface oxide layer. Also, we have observed the emergence of a peak in the O 1s region (figure 6.6b); provide a clear signature of the formation of a surface oxide layer immediately after the treatment. It is evident from the XPS result that HBr-treated SiNWs sample has a lower rate of surface oxidation compared to the pristine or HF-treated SiNWs samples. One possible hypothesis for this decreased oxidation effect can be ascribed to the fact that HF and HBr treatment results in H-terminated nanowire surface (Nemanick et al., 2006; Rivillon et al., 2005). However, HBr treatment gives better passivation effect than HF (Li et al., 1995). This is because, HF is a weak acid that cannot dissociate completely in the water solution (Odde et al., 2004). Hence, the etching mechanism of the native oxide layer is changeable depending on the nature of the fluorine species that dominates the surface treatment process(Kikuyama et al., 1994). The main elements in the solution for low pH are HF and HF_2, while in case of higher pH HF_2 dominates. Moreover, fluorine has the largest electronegativity of 4.98, where bromine has an electronegativity of 2.96. Hence, the ionic bond is stronger between hydrogen and fluorine as compared to hydrogen and bromine. Thus, HF releases less H^+ ions in the water solution as compared to HBr. Since the H^+ concentration in diluted aqueous HF is low (~pH 3.27), the dissolution into the water solution is not very efficient thus re-oxidizes fast(Choi et al., 2003; Li et al., 1995). On the contrary, HBr is a strong acid (~pH 3.01) that can fully dissociate in the water(Poterya et al., 2007), thus release more H+ ions in the solution and therefore is more efficient to remove the oxide layer from the nanowire surface. Hence, we can notice an increased lifespan of the surface passivation effect on HBr treated sample compared to the HF treated one. We have observed from the XPS measurements that the pristine SiNWs devices contain large amounts of native oxide layers and carbon contaminations. This oxide layer works as a barrier that appears to prevent the tunneling of the photo generated carriers, hence making it difficult for them to reach the contacts. On the other hand, removing the native oxide layer helps to transit the photo generated carriers to the contacts in case of HF and HBr-treated devices. Hence, these

HBr-treated SiNWs/TiO_2 heterojunction are better candidates for photovoltaic devices as compared to the pristine or HF-treated devices.

6.3 Conclusion:

In this work we have investigated the photovoltaic performance of n-SiNWs/TiO_2 based heterojunction solar cells by chemically treating the SiNWs with HBr and HF. We have demonstrated that the chemical treatment of the SiNWs with HBr before the junction fabrication leads to an H-passivation of dangling bonds and suppression of the fixed charges at the interface. The photovoltaic performance of HBr treated n-SiNWs/TiO_2 heterojunction solar cells yields much higher power-conversion efficiencies (up-to 6.2%) compared to other treatments. Our findings reveal the potential use of HBr treatment for improving the performances of Si nanowire-based photovoltaic and optoelectronic devices.

6.4 Experimental methods:

6.4.1 Synthesis of vertically aligned silicon nanowires :

Vertically aligned silicon nanowires were synthesized using metal assisted wet electroless chemical etching (MAWCE) method via galvanic displacement reaction. We have found galvanic displacement method as the most cost effective technique than any other methods used for the synthesis of silicon nanowires. Details of this process have been described elsewhere (Garnett et Yang, 2010; Hung et al., 2011). For our work, we have used n-type silicon wafer with resistivity 1-10 ohm-cm. The etchant composition was 0.02 M silver nitrate solution ($AgNO_3$) with 4.8M hydrogen fluoride acid (HF) mixed with 1:1 ratio. The etching takes place at room temperature for 40 minutes. The residual silver nanoparticles have been removed completely at room temperature using 70% nitric acid (HNO_3) solution and DI water in 1:2 ratio for 1 hour. The diameter of the nanowires varied in the range between 40-50nm and the length was in between 800-1000nm. Figure 6.2 shows the cross sectional morphology of the fabricated silicon nanowires.

6.4.2 Synthesis of TiO_2 sol-gel :

Thin film layer of anatase TiO_2 has been deposited on top of the as prepared silicon nanowires to form the heterojunction. There are several ways to synthesize TiO_2, being sol-gel one of the most popular because it allows easy processing of the material as thin films or even to nanometer scale using common processes such as dip-coating and spin-coating. Most importantly, TiO_2 synthesize through sol-gel method offers advantages such as room temperature reaction, high homogeneity and purity of the final product. In this study, Raman spectroscopy was used to verify the crystalline structure of the obtained TiO_2. Characteristic peaks of the anatase phase were observed at 395cm^{-1}, 513cm^{-1} and 634cm^{-1} as shown in figure 6.2(c). The peak observed for anatase TiO_2 at 513cm^{-1} coincides with SiNWs peak, hence we observed an intense peak at 513cm^{-1}.

The TiO_2 solution has been synthesized using modified sol-gel technique (Xu et al., 2012a). First, 28.8532 grams (Gms) of ethanol mixed with 1.4748 Gms of acetylacetonate (ACAC) in a beaker and covered with parafilm. This mixture has stirred with a magnetic stirrer for 20 minutes. Then 10.8604 Gms of titanium butoxide (TBT) has added to this mixture and covered with parafilm again. Then stirring of this mixture occurs for 40 minutes. Finally 0.84 ml DI water has added to the mixture and covered with parafilm and stirred for 120 minutes. TiO_2 sol gel will be in optimum condition to be used after 24 hours of starting the reaction. The addition of ACAC decreases the hydrolysis velocity of the TBT during the sol-gel reaction, helping to avoid the formation of precipitates and chunks.

6.4.3 Formation of the Heterojunction :

The as prepared nanowires are cleaned using 20% HBr for 2 minutes. Then TiO_2 sol-gel coating has done via spin-coating method. The spin rate was set at 500 r.p.m. for 20 seconds and 2000 r.p.m. for 40 seconds. Then the samples are annealed at 550^0C for 1 hour to get the anatase crystalline structure of the TiO_2.

6.4.4 Contact fabrication :

Silver finger grids have been deposited via sputtering technique to serve as a front contact for the heterojunction solar cells. The thin film layer of Al has been deposited as a back contact via sputtering technique. The thickness of this Al layer was 200nm. After the sputtering process, the sample was annealed at 350 ^{0}C for 10 minutes in a nitrogen environment. After the heat treatment, the solar cells are ready for characterizations.

6.4.5 Device characterization :

The SiNWs samples were characterized using Hitachi SU-8230 field emission scanning electron microscope (SEM). Anatase nature of TiO_2 has seen using WI Tec alpha 300 micro-Raman system equipped with a 532 nm fiber-coupled laser for excitation. The surface passivation effect was investigated using X-ray photoelectron spectroscopy (XPS) measurement using VG ESCALAB 3 Mark II XPS machine equipped with Mg κα source. The reflectance measurement was carried out by Perkin Elmer LAMBDA 750 UV/VIS system. The solar cells were characterized using a solar panel test bench equipped with Keithley 2400 source meter under 1.5G air mass condition.

Acknowledgment:
S.G.C. is most thankful for the financial support from the Canada Research Chairs and the NSERC Discovery programs.

Author contributions:
D.B. and S.G.C. have developed the concept of the devices. D.B. and J.B. have carried out the chemical synthesis part. Device characterizations have done by D.B. and X.G. Data analysis was discussed between D.B. and S.G.C. The manuscript is written by D.B. and corrected by S.G.C. All authors have approved the manuscript before submission.
Competing interests: The authors declare no competing financial interests.

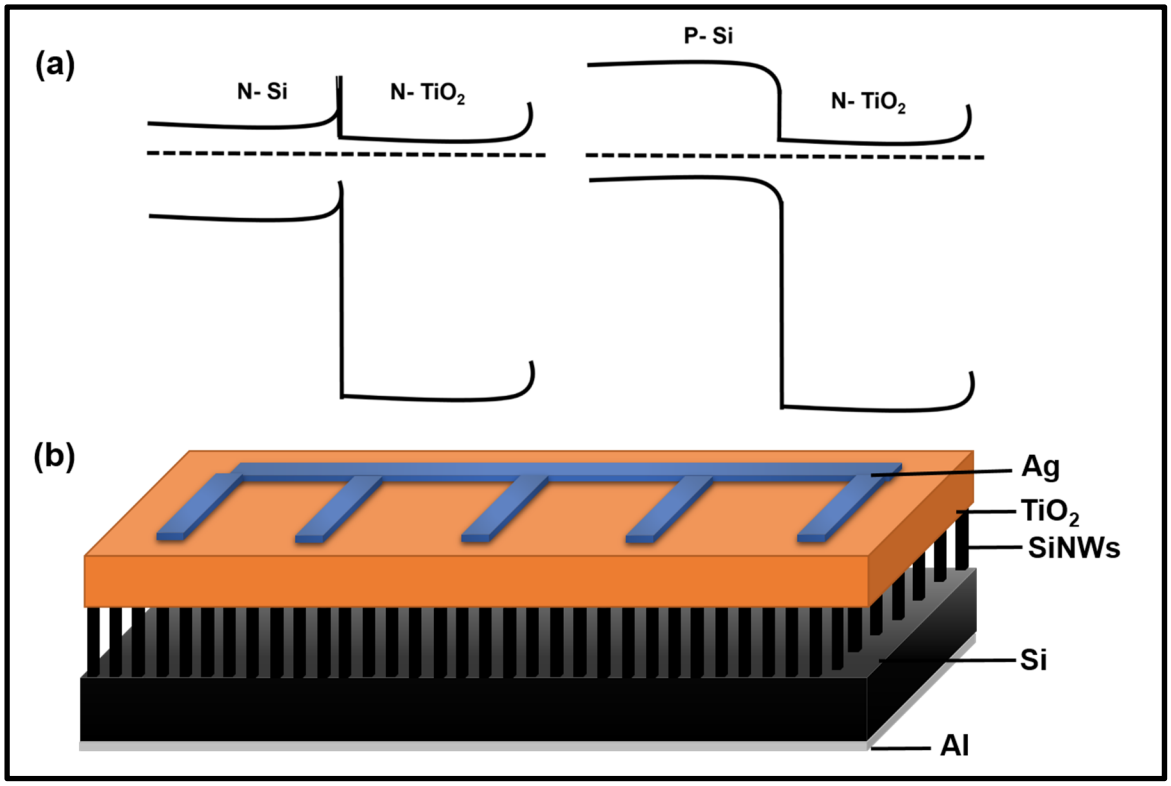

Figure 6.1 (a) Band diagram of n-n isotype heterojunction (left) and band diagram of p-n heterojunction (right)
(b) Schematic of n SiNWs/TiO_2 heterojunction solar cell

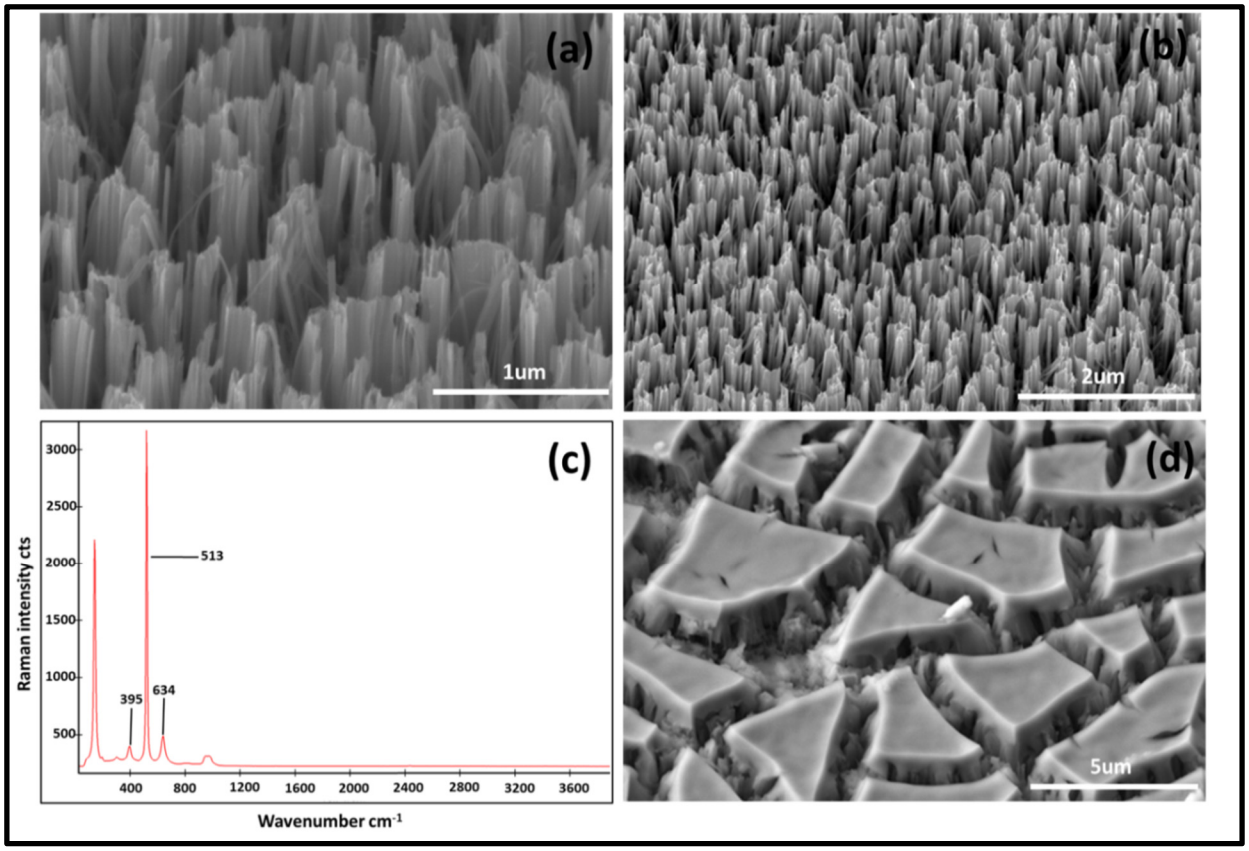

Figure 6.2 (a) SEM micrograph of the silicon nanowire array structure synthesized by GDM
(b) Raman peaks for anatase TiO_2 on SiNWs
(c) and (d) SEM micrographs of the SiNWs/TiO_2 bulk heterojunction

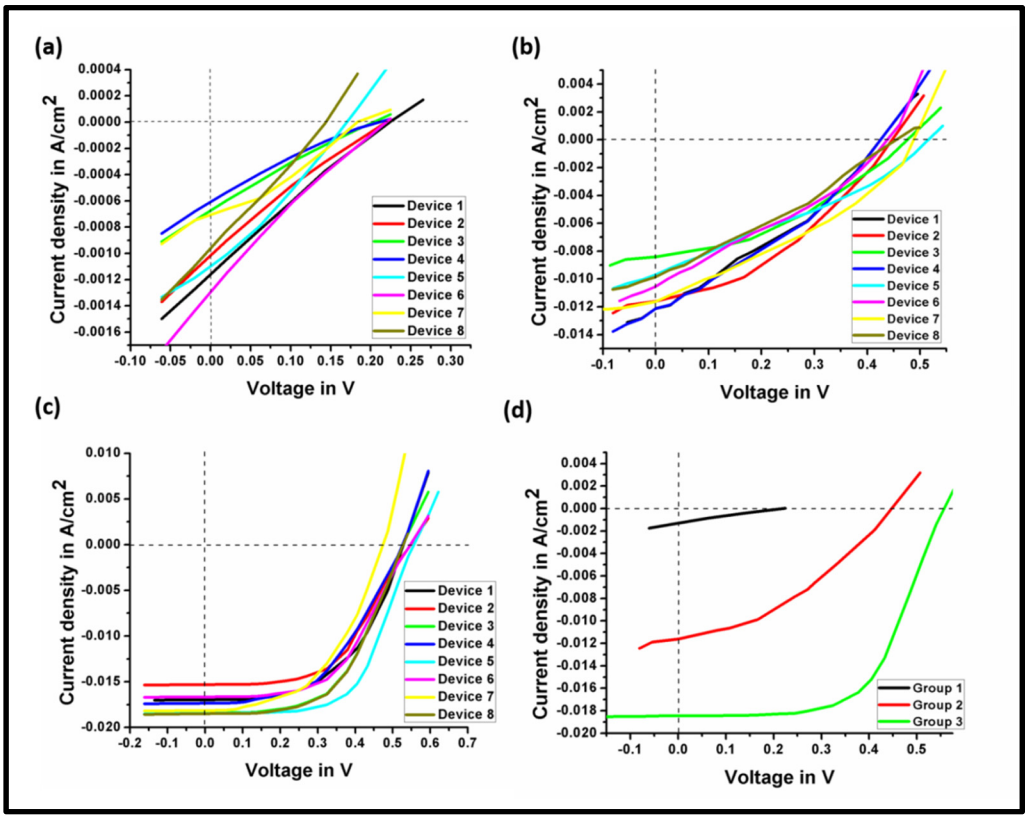

Figure 6.3 (a) J-V curve of the heterojunction solar cells under AM 1.5G from group 1
(b) and (c) J-V curve from group 2 and group 3 devices
(d) J-V curve of best performing devices from each group

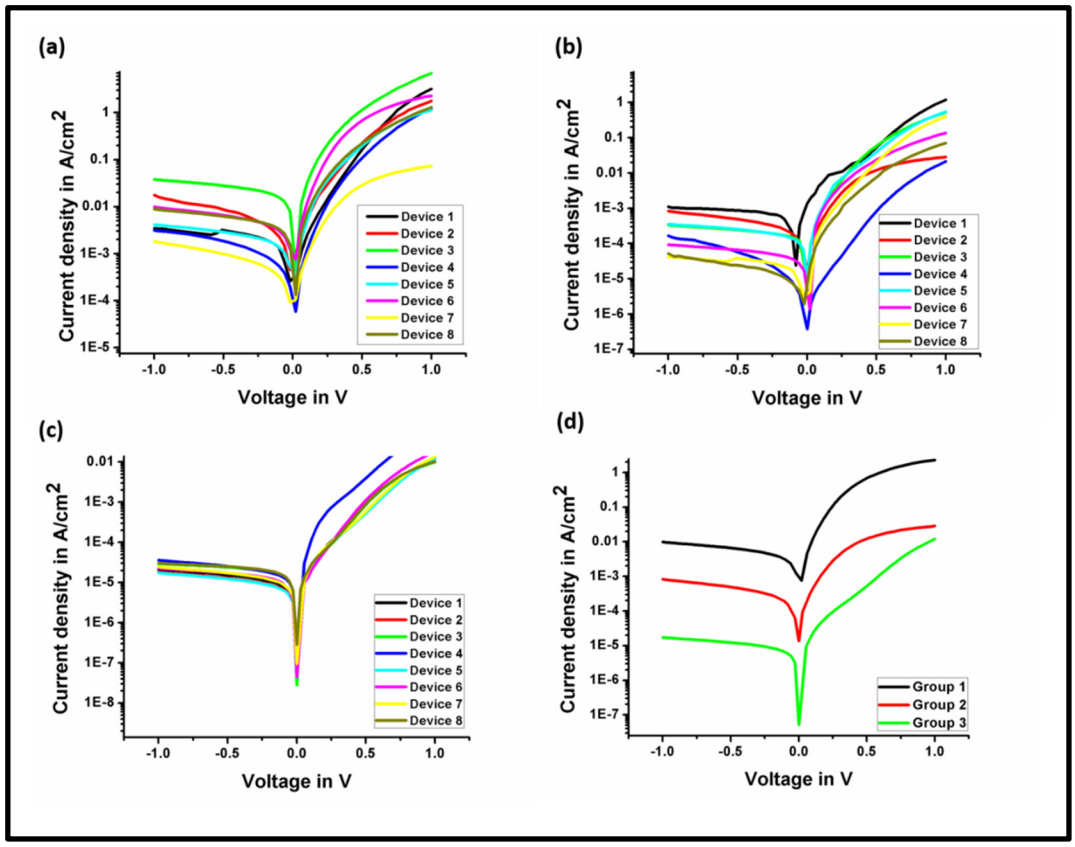

Figure 6.4 (a) Log-plot of the dark current of group 1 devices
(b) and (c) Log-plot of the dark current of group 2 and group 3 devices
(d) Log-plot of the dark current of best performing devices from each group

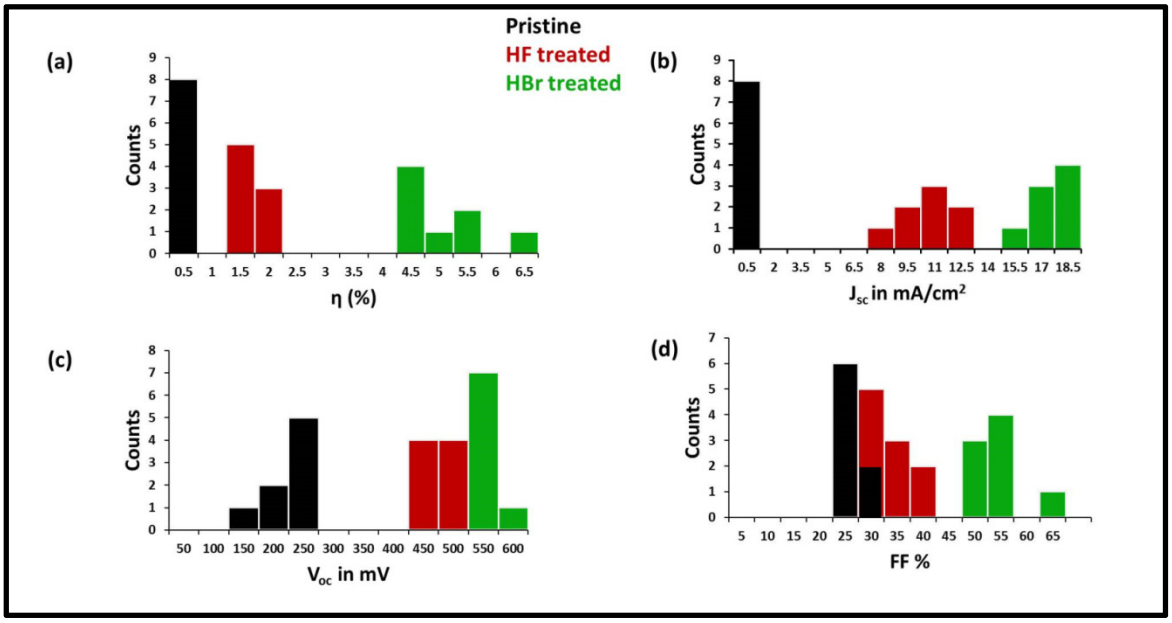

Figure 6.5 Histogram plots of the solar cell parameters
(a) Power conversion efficiency (η), (b) Short circuit current density (J_{sc})
(c) Open circuit voltage (V_{oc}) and (d) Fill factor (FF) of the 24 devices from 3 groups

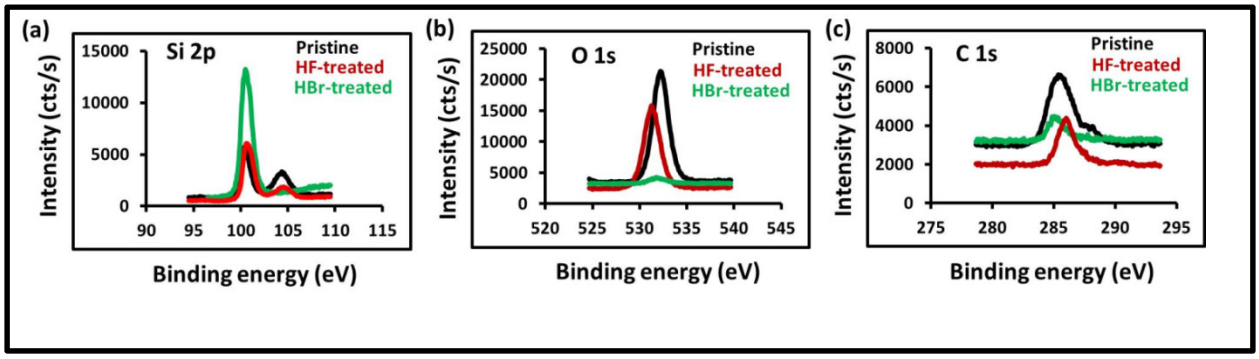

Figure 6.6 XPS spectra of (a) Si 2p, (b) O 1s, (c) C 1s peaks from the pristine (non-treated) (black), HF treated (red) and HBr treated (green) SiNWs samples

CHAPTER 7

PLASMON-ENHANCED SILICON NANOWIRE ARRAY-BASED HYBRID HETEROJUNCTION SOLAR CELLS

D. Banerjee [a], S. Cloutier [b] and X. Guo [c],
[a, b and c] Department of Electrical Engineering, École de Technologie Supérieure,
1100 Notre-Dame West, Montreal, Quebec, Canada H3C 1K3

Paper published in *Solar RRL,* April 2018

Abstract: In the last decade, freestanding, single crystal silicon nanowires (SiNWs) have attracted significant attention as a potential material for low-cost optoelectronic devices. In this paper, we demonstrate how strong localized surface plasmon modes induced using silver nanoparticles can be used to achieve significant improvement in a simple hybrid organic-inorganic photovoltaic device between n-type silicon nanowires and poly(3,4-ethylenedioxythiophene):poly-(styrenesulfonate) (PEDOT:PSS). At photon energies above plasmon resonance, metallic nanoparticle-induced absorption leads to a dramatic reduction of the reflectivity and we report a significant improvement in both the short circuit current density (J_{sc}) and the open circuit voltage (V_{oc}). This leads to an overall 52% increase in the power conversion efficiencies (PCEs) of the photovoltaic devices when decorating the SiNWs with silver nanoparticles prior to PEDOT:PSS deposition.

7.1 Introduction:

About 70% of the energy consumption of the world comes from fossil fuels (Chow, Kopp et Portney, 2003; Shafiee et Topal, 2009), which not only pollutes the environment but also depletes our natural resources. Renewable energy sources provide an ideal solution to these problems as it generates energy in a sustainable way (Lund, 2007; Sims, Rogner et Gregory, 2003). However, much more research is required to dramatically reduce the cost of solar cells while significantly increasing their efficiencies (Garnett et Yang, 2010; Pillai et al., 2007). Crystalline silicon (Si) solar cells play an important role in the photovoltaic (PV) market due to their relatively high power conversion efficiencies achieved at moderate cost (Dimitrov et

Du, 2013). But, the fabrication process of these devices still requires costly endeavor like high-temperature diffusion or implantation techniques to form the p-n junction (Aberle, 2001; Green, 1987). An economical substitute to this problem is to switch to hybrid silicon-based heterojunction solar cells which will not only reduce the processing cost by using cheap materials in combination with Si, but also enhance the power conversion efficiencies of these devices (He et al., 2015; Huang et al., 2012b; Shen et al., 2011). Recently, profoundly-efficient organic-inorganic hybrid solar cells using poly (3,4-ethelenedioxythiophene): poly (styrenesulfonate) (PEDOT:PSS) and n-type Si have generated a lot of attention due to their high PV potential and low processing costs (Syu, Shiu et Lin, 2012). The PEDOT:PSS layer works as a hole-transporting material when combined with electron-transporting n-type Si. In order to increase the light trapping efficiency (Avasthi et al., 2011), Si nanostructures such as nanowires, nanorods, nanograss etc. have been shown to increase the short-circuit current density (J_{sc}) (He et al., 2015; Huang et al., 2012a). Considerable improvement of the power-conversion efficiency (PCE) has also been achieved for Si nanowires/PEDOT:PSS hybrid heterojunction solar cells (Lai et al., 2016; Wang et al., 2015). Recently it has been reported that efficiencies as high as 16% can be obtained for Si nanowires/PEDOT:PSS hybrid heterojunction solar cells using embedded metal micro grid electrode (Um et al., 2017). Other reports mention using different materials like DMSO, IPA, SDS mixed in various conditions (for example molecular weights and ratios, temperature, sonication, stirring etc.) with PEDOT:PSS to increase the conductivity of the PEDOT:PSS layer (Funda et al., 2016; Wang et al., 2015). Finally, researchers have also explored the introduction of some interfacial layers like Al_2O_3 or SiO_2, thus significantly increasing the performance of these devices (Pudasaini et al., 2013; Richter et al., 2011).

Enhanced light detection and photocurrent generation from the excitation of localized surface plasmons on around metallic nanoparticles is another possible pathway towards better low-cost optoelectronic devices (Kossyrev et al., 2005; Wang et Vial, 2013). Indeed, metallic nanoparticles exhibit localized surface plasmon resonance by the interaction of photons with the free valence electrons available at the metal surface (Haes et al., 2004; Hu et al., 2008). Due to their large scattering cross section and plasma resonance frequencies in the visible,

AgNP are appealing candidates for plasmon-enhanced photovoltaic devices (Catchpole et Polman, 2008; Liu et al., 2013; Temple et al., 2009). Recently, Sharma *et al*. (Sharma et al., 2014) demonstrated a 10% increase in the PCE of solar cells by incorporating AgNPs on the back surface of the device. Ouyang *et al*. (Ouyang et al., 2011) also reported a 27% enhancement of the short-circuit current density of silicon solar cells by depositing self-assembled AgNPs on the back surface of the solar cells. Finally, Yenchalwar *et al*. (Yenchalwar, Azhagan et Shelke, 2014) described a significant increase of photocurrent for SiNWs/Titanium dioxide (TiO_2) heterostructures by depositing gold (Au) NPs on the top surface of the heterojunction.

In this work, we explore the optical behavior of Ag nanoparticle-decorated SiNW arrays and their application in PEDOT:PSS hybrid heterojunction solar cells. The SiNW arrays are fabricated using all solution based galvanic displacement method (GDM) (Banerjee et al., 2016; Carraro, Maboudian et Magagnin, 2007; Kawasaki et al., 2010) and small quantities of Ag nanoparticles are introduced into the SiNW arrays by controlling the cleaning after the GDM. The hybrid heterojunction solar cells are then produced by simply spin-coating PEDOT:PSS atop of the nanoparticle-decorated SiNW arrays. Introduction of the Ag nanoparticles contributes to suppressed reflection at wavelengths below 600 nm due to metal-enhanced absorption. This simple device structure is promising for the realization of effective low-cost solar cells, especially considering the 52% increase in PCE compared to identical devices without Ag nanoparticles. As such, PCEs up-to 8.4% are demonstrated in these low-cost hybrid solar cell devices.

7.2 **Results** and **discussions:**

7.2.1 **Plasmonic response of SiNWs :**

The key concept underlying this work entails the plasmonic enhancement effect on hybrid heterojunction photovoltaic cells using vertically-aligned silicon nanowire arrays embedded in PEDOT:PSS. The vertically-aligned nanowire arrays are fabricated using all-solution

based GDM (Banerjee et al., 2016; Carraro, Maboudian et Magagnin, 2007). Figure 7.1(a) shows the resulting SiNWs covered with residual Ag dendrites. Plasmon-sensitized SiNWs are obtained by controlling the cleaning protocol following GDM processing as shown in Figure 7.1(b). As such, some Ag nanoparticles remain on the sidewalls of the SiNWs after cleaning the Ag dendrites. We performed X-ray photoelectron spectroscopy (XPS) as shown in Figure 7.2 to evaluate he amount of residual Ag for the SiNWs samples just after GDM processing (Fig. 7.2a) and after cleaning-away the Ag dendrites (Fig. 7.2b). Ag survey of SiNW arrays with and without the Ag dendrites are shown in Figure 7.2(c, d). From the literature, the Auger parameter obtained from the XPS indicates the presence of metallic Ag (Ferraria, Carapeto et Botelho do Rego, 2012; Smekal, Werner et Powell, 2005). The kinetic energy of the Auger electron peak (357.5eV) and the binding energy of the photoelectron peak of Ag3d5/2 (368.7eV) are employed to determine the Auger parameter. We have confirmed the presence of metallic Ag at 45.6% (atomic) using the SiNWs with the dendrites. After removing the Ag dendrites, we find the presence of residual metallic Ag nanoparticles at 1.1% (atomic). The identification and quantification of elements identified from the XPS survey scan are depicted in Table AIIS1.

To observe the plasmonic resonance due to the silver nanoparticles, we have studied the optical reflectivity spectra of these SiNW arrays with and without the Ag nanoparticles as shown in Figure 7.3. We observe a strong plasmon-induced attenuation at wavelengths below 600 nm for silicon nanowires decorated with Ag nanoparticles. This effect is a direct consequence of the oscillation of the conduction electrons of the metal under the excitation increasing their absorption cross-section(Pillai et al., 2007).

7.2.2 The hybrid organic-inorganic heterojunction solar cells :

Figure 7.4(a) shows the schematic of the plasmon-sensitized n-type SiNWs and PEDOT: PSS hybrid heterojunction solar cell. To fabricate the heterojunction, Ag nanoparticle-decorated SiNWs are spin-coated with PEDOT:PSS followed by a thermal annealing at 150 ^{0}C for 15 minutes inside a tube furnace. It has been previously reported that the conductivity of

PEDOT:PSS can be boosted by solvent treatment (Kim et al., 2011; Yeon et al., 2017). As such, we have tried treating our PEDOT:PSS with either isopropyl alcohol (IPA) or Sodium dodecyl sulfate (SDS) solution to increase its conductivity. Groups of identical devices are fabricated using IPA- and SDS-treated PEDOT:PSS with either IPA or SDS. For treatment, we have mixed IPA with PEDOT: PSS solution at 3:1 volume ratio followed by ultra-sonication for 15 minutes. The mixture is then filtered using a 0.2 um filter and spin-coated at 3000 rpm directly atop the SiNW arrays to form the heterojunction. SDS treatment has also been already proven capable to significantly increase conductivity of PEDOT:PSS films. For SDS treatment, we have mixed 0.4mM (i.e. 0.115mg) concentrated SDS solution with 10 ml of PEDOT: PSS solution. This mixture is stirred at 85 ^{0}C for 2 hours, then filtered using a 0.2 um filter and spin-coated atop the SiNW arrays. After the formation of the hybrid heterojunction by thermal annealing of the PEDOT:PSS, a 70nm- thick Ag front contact is thermally-evaporated using a shadow mask and a 150 nm-thick Al back contact is deposited by thermal evaporation.

The energy band diagram of the hybrid heterojunction is shown in Figure 7.4(b). The work function of Ag is 4.64 eV and the electron affinity of the silicon is 4.05 eV. Hence, the electrons have to overcome a barrier potential of 0.59 eV between the SiNWs and the Ag nanoparticles in order to contribute to the current.

7.2.3 Performance of the solar cells :

Figure 7.5 demonstrates the current-density vs. voltage (J-V) characteristics of the hybrid heterojunction solar cells under air mass (AM) 1.5G illumination. We have fabricated 24 devices using optimal experimental parameters to probe the variations in their J-V characteristics. We have distributed these devices equally in to three groups of 8 devices with different fabrication/treatment conditions. The devices from Group 1 (G1) do not contain any Si nanowire structures or Ag nanoparticles. As such, these G1 devices consist of a bulk n-type Si wafer coated with IPA-treated or SDS-treated PEDOT:PSS. In contrast, Group 2 (G2) devices consist of n-type SiNW arrays coated with IPA-treated and SDS-treated

PEDOT:PSS. Finally, Group 3 (G3) devices use Ag nanoparticle-decorated n-type SiNWs coated with IPA-treated and SDS-treated PEDOT:PSS.

The J-V characteristics of all the G1 devices (planar n-type silicon wafer with solvent-treated PEDOT:PSS) are shown in Figure 7.5(a). Short circuit current densities (J_{sc}) range between 4.5-7.8 mA/cm^2 for IPA-treated devices and 7.0-9.3 mA/cm^2 for SDS-treated devices. The open-circuit voltages (V_{oc}) of these devices vary between 422-470 mV for IPA-treated devices and 465-488 mV for SDS-treated devices. The fill-factors (FF) of these solar cells range between 25-32% for IPA-treated and 33-39% for SDS-treated devices. As such, the extracted power conversion efficiencies are ranging from 0.5-1.1% for the IPA-treated devices and 1.1-1.8% for the SDS-treated devices. The numerical values for each device parameters for group G1 are listed in Table AIIS2.

Similarly, the J-V characteristics of all the G2 devices (n-type silicon nanowire arrays coated with solvent-treated PEDOT:PSS) are shown in Figure 7.5(b). Short circuit current densities (J_{sc}) range between 13.0-15.4 mA/cm^2 for IPA-treated devices and 17.0-18.4 mA/cm^2 for SDS-treated devices. The open-circuit voltages (V_{oc}) of these devices vary between 566-578 mV for IPA-treated devices and 570-580 mV for SDS-treated devices. The fill-factors (FF) of these solar cells range between 52-55% for IPA-treated and 52-53% for SDS-treated devices. As such, the extracted power conversion efficiencies are ranging from 4.1-4.6% for the IPA-treated devices and 5.2-5.5% for the SDS-treated devices. The numerical values for each device parameters for group G2 are listed in Table AIIS3.

Finally, the J-V characteristics of all the G3 devices (n-type silicon nanowire arrays decorated with Ag nanoparticles and coated with solvent-treated PEDOT:PSS) are shown in Figure 7.5(c). Short circuit current densities (J_{sc}) range between 20.0-21.7 mA/cm^2 for IPA-treated devices and 22.0-24.2 mA/cm^2 for SDS-treated devices. The open-circuit voltages (V_{oc}) of these devices vary between 580-588 mV for IPA-treated devices and 578-592 mV for SDS-treated devices. The fill-factors (FF) of these solar cells range between 61-63% for IPA-treated and 60-62% for SDS-treated devices. As such, the extracted power conversion

efficiencies are ranging from 7.3-7.9% for the IPA-treated devices and 7.9-8.4% for the SDS-treated devices. The numerical values for each device parameters for group G3 are listed in Table AIIS4. Figure 7.5(d) compares the J-V characteristics of the best SDS-treated device from each group under AM 1.5G illumination.

For our devices, we observe considerably improved V_{oc} for the G2 and G3 silicon nanowire-based devices as compared to the planar silicon-based G1 devices. To reach a better understanding, we have evaluated the wetting of the solvent-treated PEDOT:PSS solution for the different silicon substrates. To do so, a 20 µl droplet of the solvent-treated PEDOT:PSS solution is released on the silicon substrates using a micro syringe. The images of the PEDOT:PSS droplets are taken from the side using a high resolution camera and their contact angles are estimated using the Image J freeware with the low bond axisymmetric drop shape analysis (LBADSA) package. The LBADSA package uses the fitting of the Young-Laplace equation to the image data (Kwok et al., 1997; Stalder et al., 2010) . We have shown the schematic and images of the SDS-treated PEDOT:PSS droplets atop the different silicon substrates in Figure AIIS2 of the supporting information section. We observe 62.2º, 40.5º and 38.4º contact angles for pristine, SiNWs and plasmon enhanced SiNWs substrates respectively. Images of the IPA-treated PEDOT:PSS droplets atop the different silicon substrates are shown in Figure AIIS3 of the supporting information section. We observe 67.5º, 42.3º and 39.8º contact angles for pristine, SiNWs and plasmon enhanced SiNWs samples respectively. Based on significantly lower contact angles, the SiNWs and plasmon enhanced SiNWs devices clearly allow a better wetting of PEDOT:PSS solution to provide a more uniform interface, which in turn affects the active layer of the device and thus results in larger V_{oc} and FF. In all cases, we observe slightly lower contact angles for the SDS treated PEDOT:PSS, suggesting a better wetting of the silicon substrate.

Figure 7.6 shows histogram distributions of (a) the power conversion efficiency (PCE), (b) short circuit current density (J_{sc}), (c) open circuit voltage (V_{oc}), and (d) fill factor (FF) for the 24 solar cells from G1 (black), G2 (red) and G3 (green). The histogram exhibits a large distribution of PCE between 0.5-8.4%. The J_{sc} and V_{oc} have been distributed between 4.5-

24.2 mA/cm^2 and 422-592mV respectively. The FF values have distributed between 25-63%. The root of these wide distribution in all the parameters comes from plasmonic response of SiNW arrays.

Figure 7.7(a) shows the EQE spectra for each group of devices (G1, G2 and G3). A significant EQE increase is observed in the UV region for the G3 devices, which can be directly attributed to the plasmonic enhancement by the Ag nanoparticles. We also find that EQE of G2 and G3 nanowire-based devices are also both higher than that of G1 devices above 425 nm. This can be attributed to the enhanced surface-to-volume ratio for SiNWs samples as compared to the bare Si, resulting in higher light trapping capability. In Figure 7.7(b), we have calculated the IQE for the G1, G2 and G3 cells from the EQE and the reflectance (R) data of these devices by employing the relation IQE = EQE / (1-R)(Law et al., 2008). We observe higher IQEs for G1 devices as compared to G2 and G3 devices. These results suggest an increase in the series resistance and recombination from the metal nanoparticles and the texturing of the devices. Yet, we observe higher J_{sc} and V_{oc} for G2 and G3 devices compared to the G1 devices due to the larger surface area for the textured silicon. For the J-V measurements, we have cleaved the samples into 1 cm^2 pieces and illuminate the whole area under a solar simulator. For the EQE measurements, the spot size of the light is limited to 0.76mm × 1mm by an aperture, which is much smaller than the overall devices. Since the interface for the G1 devices are less uniform (contact angle between ~ 62º-67º) than the G2 and G3 devices (contact angle between ~38º-42º), G1 devices show lower J_{sc}, V_{oc}, FF and during the J-V measurements, resulting in lower efficiencies.

First, these data clearly show that, SDS-treated devices consistently outperform the IPA-treated devices, especially in J_{sc} and PCE for all groups. In addition to a slightly better wetting described earlier, SDS is an anionic surfactant containing 12-carbon tails attached to its sulfate group. SDS treatment helps reducing the insulating PSS domains, which in turn enhances the inter-chain correlation between PEDOT cores(Yeon et al., 2017). Conductivity is a function of ion concentration and adding SDS provides extra ions in the PEDOT:PSS solution. Hence we observe improved short circuit current density from the SDS treated

devices. The schematic representation of pristine and SDS-treated PEDOT:PSS are shown in Figure AIIS4 of the supporting information section. Clearly, Ag nanoparticle-decorated SiNWs devices show a significant localized surface plasmon-induced enhancement in their J_{sc} and V_{oc}. As such, this leads to a 52% overall improvement in PCE for the SDS-treated SiNW devices decorated with minute amounts of Ag nanoparticles. The significant increase in the J_{sc} also suggests that Ag nanoparticles help carriers overcome the polymer semiconductor junction barrier to contribute to the current.

7.3 Conclusion:

In summary, we have demonstrated significant plasmon-induced enhancement to achieve better ultra-low-cost solar cell devices. Their fabrication relies on all solution-based galvanic displacement method to produce arrays of vertically-aligned silicon nanowires at the surface of commercial n-type silicon wafers. After cleaning these nanostructured silicon wafers, the nanowire arrays are covered with solvent-treated PEDOT:PSS. Our study shows that SDS-treated devices consistently outperform IPA-treated devices. Most importantly, we show that controlling the cleaning protocol to leave minute amounts of Ag nanoparticles attached to the silicon nanowires before coating with solvent-treated PEDOT:PSS leads to a significant improvement in J_{sc} and V_{oc}, resulting in a 52% overall improvement in PCE for the SDS-treated SiNW devices decorated with minute amounts of Ag nanoparticles. The devices produced show a PCE up-to 8.4% under AM 1.5G illumination, compared to 5.5% without Ag nanoparticles.

7.4 Methods :

7.4.1 Synthesis of plasmon sensitized silicon nanowires :

Plasmon sensitized SiNWs are fabricated by employing all solution based GDM. Details of the GDM have been described elsewhere (Banerjee et al., 2016; Carraro, Maboudian et Magagnin, 2007).

For our study, we have used low doped n type Si wafer with the resistivity of 1-10 ohm-cm. The etchant solution contains 0.02M silver nitrate ($AgNO_3$) solution and 4.6M hydrogen fluoride (HF) solution mixed in 1:1 ratio. The Si substrates have cleaved into 1 cm^2 pieces and cleaned using ultra sonication with acetone and IPA for 15 minutes each. Then the Si pieces have rinsed with deionized (DI) water and dried using nitrogen (N_2) flow. The cleaned samples are transferred immediately into the etching bath at room temperature for 40 minutes. After the etching, vertically aligned SiNWs have been formed covered with Ag dendrites layers. These Ag dendrites layers are removed using diluted nitric acid (HNO_3) solution (1:5 of 70% HNO_3 and DI water) for 30 minutes at room temperature. Vertically aligned SiNWs with Ag nanoparticles on the sidewalls of the nanowires are found after the cleaning. Pure SiNWs have found without any Ag contamination when the cleaning has been done using concentrated (70%) HNO_3 at room temperature for 1 hour. Hence, the post cleaning protocol after the fabrication of the nanowires plays the key role to achieve plasmon sensitized SiNWs. These nanowires vary from 800-1000nm in length and 40-50 nm in diameter.

7.4.2 Formation of the hybrid heterojunction :

The as prepared SiNWs are treated with 2% HF for 1 minute to remove the native oxide layer from the nanowire surface. The IPA and SDS treated PEDOT: PSS is deposited using spin coating technique. The spinning rate is set at 3000 r.p.m. for 1 minute to achieve a uniform thin film layer of PEDOT:PSS. The thickness of the PEDOT:PSS layer is ~130 nm. Finally the samples are annealed at 150 ^{0}C for 15 minutes in air.

7.4.3 Contact structure :

Ag fingers and bus bar have deposited via thermal evaporation technique to serve as front contact of the solar cells. The thin film layer of Al has deposited as the back contact using thermal evaporation method. Both thermal evaporations are performed with a speed of 0.5 Angstrom/s.

7.4.4 Materials and device characterization :

The scanning electron micrographic characterizations have done using Hitachi SU-8230 field emission scanning electron microscope. The chemical composition is investigated using X-ray photoelectron spectroscopy (XPS) measurement by VG ESCALAB 3 Mark II XPS machine equipped with Mg κα source. The reflectance measurement has performed using Perkin Elmer LAMBDA 750 UV/VIS system. Then, solar cells are characterized using a solar panel test bench equipped with Keithley 2400 source meter under air mass 1.5G condition.

Acknowledgement. S.G.C. is most thankful for the financial support from the Canada Research Chairs and the NSERC Discovery programs.

Author contributions. D.B. and S.G.C. have developed the concept of the paper. D.B. and X.G. have carried out the device fabrication part. Device characterization has done by D.B. Data analysis has discussed between D.B, X.G. and S.G.C. D.B. has written the manuscript and S.G.C. has corrected it. All authors have approved the manuscript before submission.

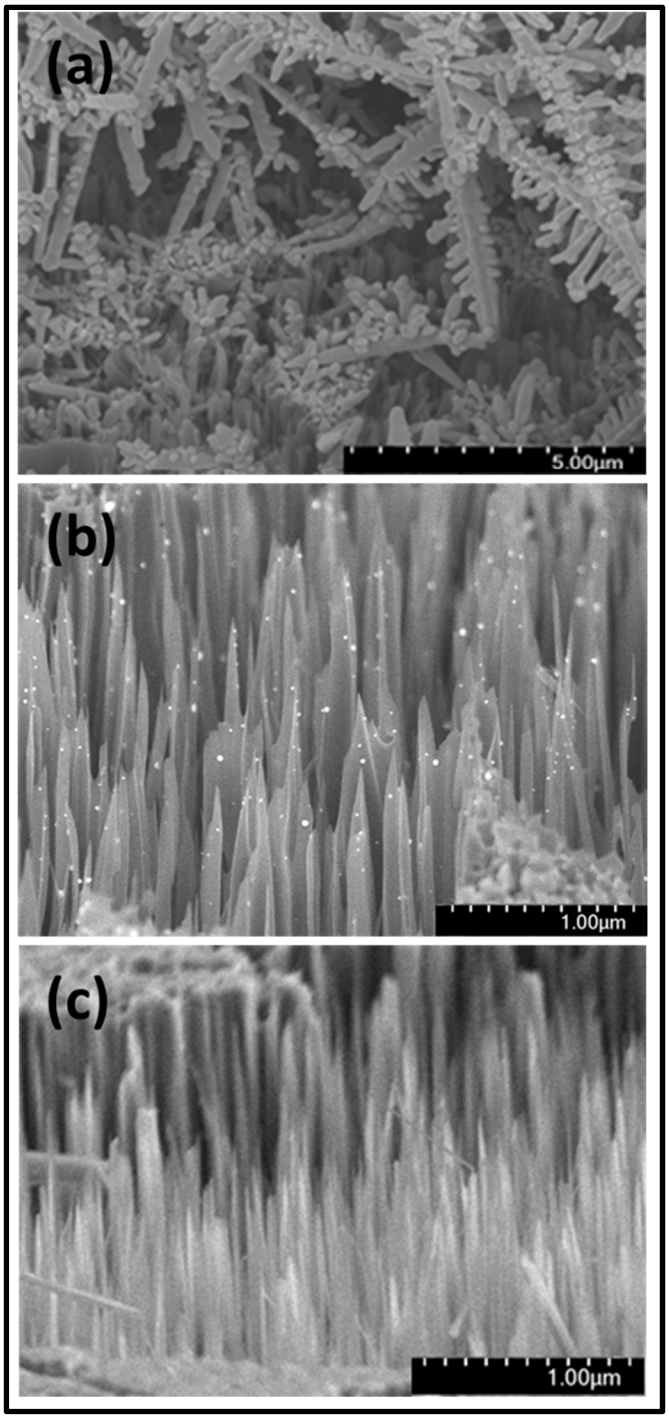

Figure 7.1 (a) Si nanowires covered with Ag dendrites after GDM, (b) Ag nanoparticle-decorated Si nanowires after removal of the Ag dendrites only, (c) Si nanowires after complete removal of the Ag

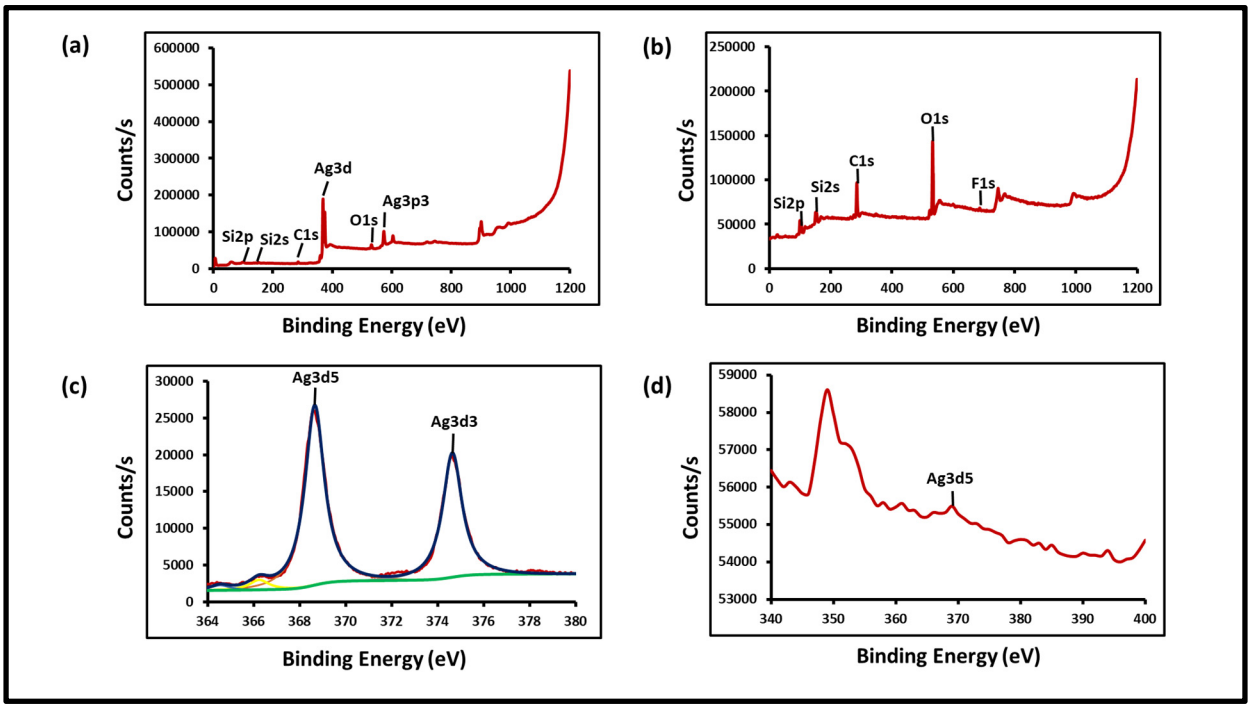

Figure 7.2 (a) XPS spectra of Si nanowires with Ag dendrites, (b) XPS spectra of Si nanowires decorated with Ag nanoparticles, (c) Ag survey of Si nanowires with Ag dendrites, (d) Ag survey of Si nanowires decorated with Ag nanoparticles

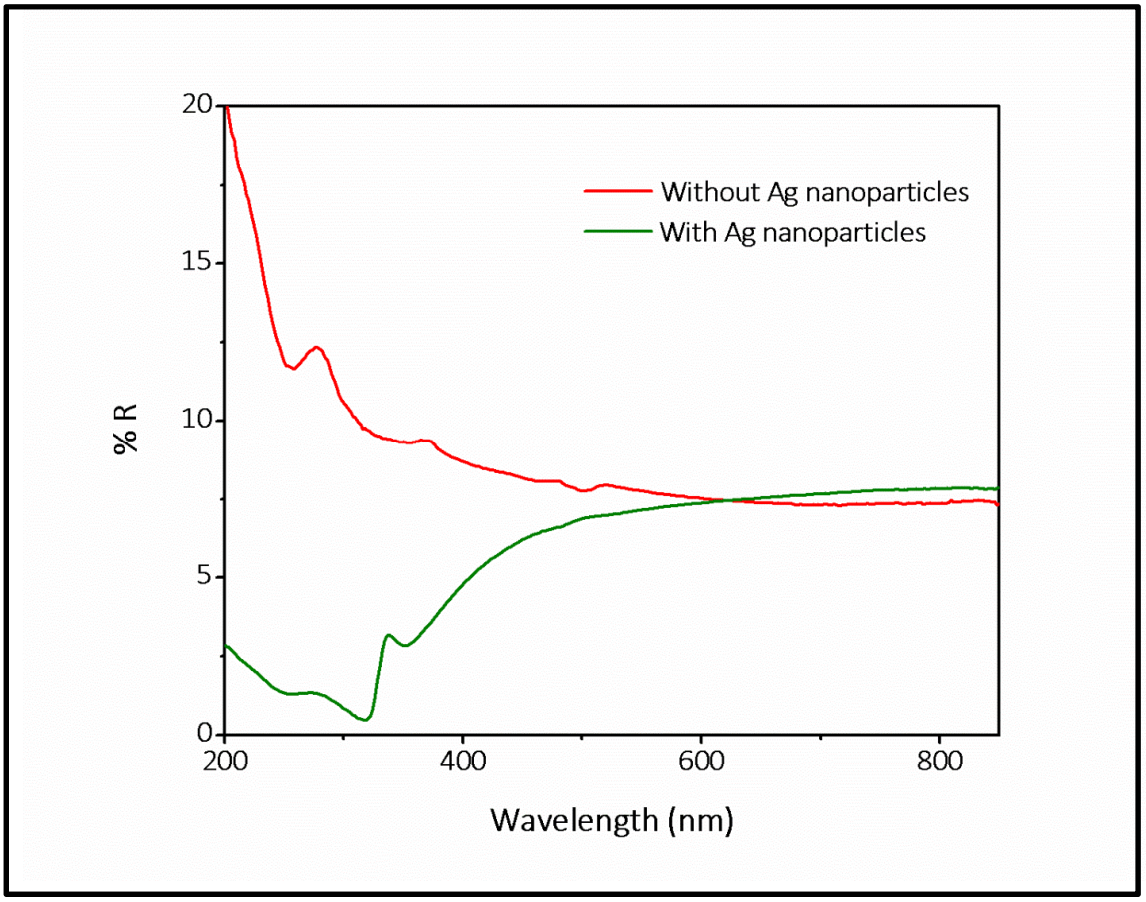

Figure 7.3 Optical reflectance (% R) of Si nanowires arrays with and without minute amounts of Ag nanoparticles

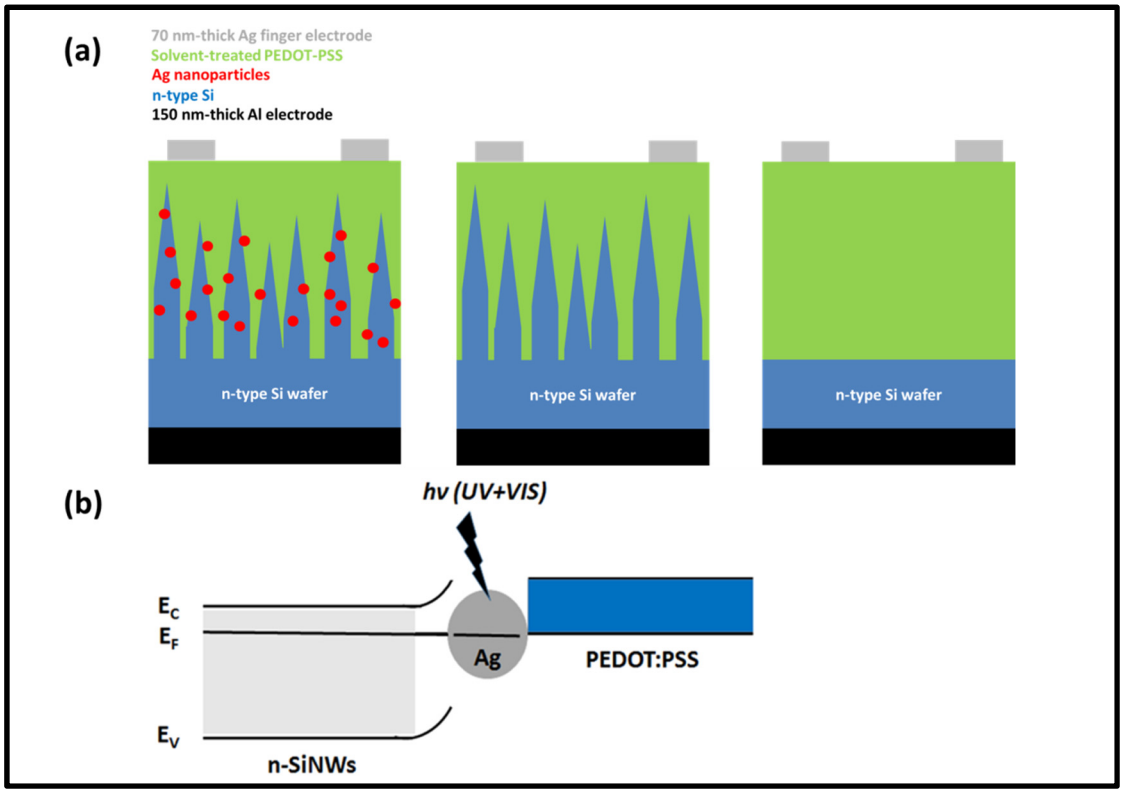

Figure 7.4 (a) Schematic of the hybrid heterojunction solar cells, (b) energy band diagram of the hybrid heterostructure

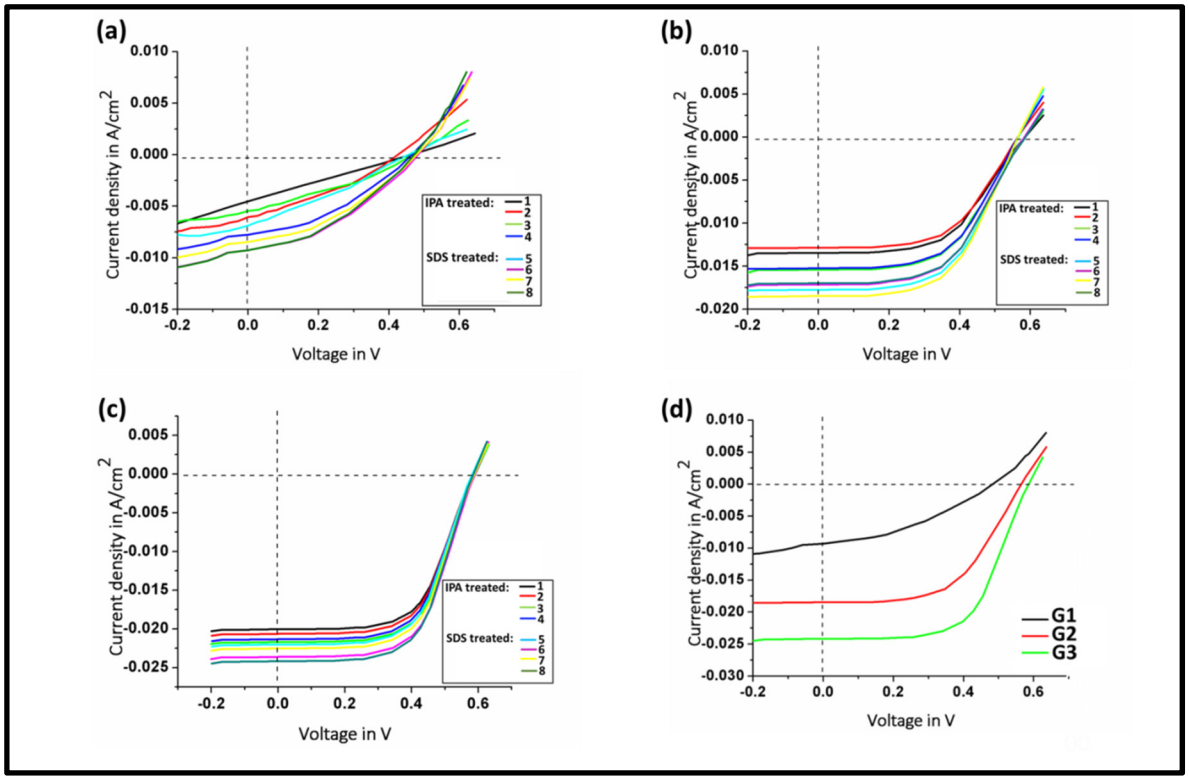

Figure 7.5 J-V characteristics of the solar cells under illumination. (a) Si/PEDOT:PSS (device 1-4 treated with IPA and device 5-8 treated with SDS), (b) SiNWs/PEDOT:PSS (device 1-4 treated with IPA and device 5-8 treated with SDS), (c) plasmonic SiNWs/PEDOT:PSS (device 1-4 treated with IPA and device 5-8 treated with SDS), (d) best devices from a,b and c

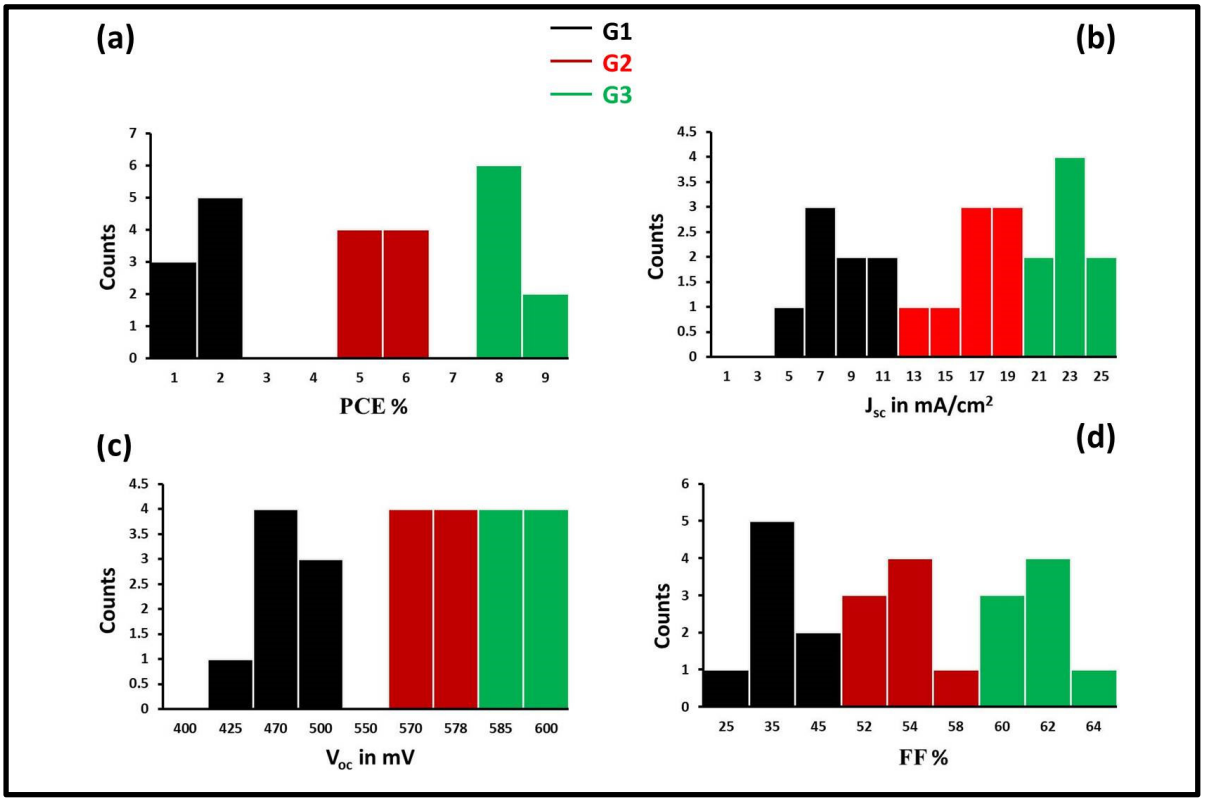

Figure 7.6 Histogram plots of the solar cell parameters of the 24 devices from 3 different groups: (a) Power conversion efficiency (PCE), (b) Short circuit current density (J_{sc}) (c) and (d) Open circuit voltage (Voc) and fill factor (FF)

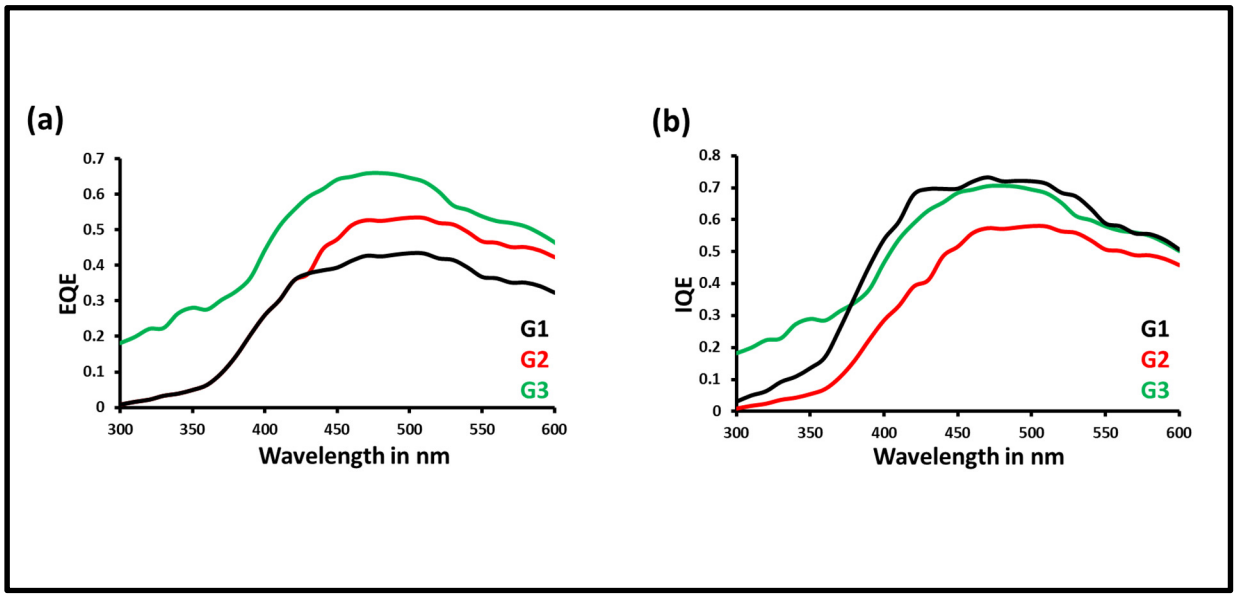

Figure 7.7 (a) EQE and (b) IQE of the samples from each groups

CHAPTER 8

CONCLUSIONS

In this thesis, various aspects of SiNWs based heterojunction solar cells are demonstrated, including the effect of HF and HBr treatments on the passivation of SiNWs surface, phonon confinement mechanisms on the apex of the SiNWs, and plasmonic effect on the SiNWs based hybrid heterojunction.

Phonon processes in vertically aligned SiNWs are analyzed in this thesis. We have shown that phonon confinement takes place exclusively in the apex of the vertically aligned SiNWs since the diameters of the nanowires are relatively large. Since, phonon helps to recompense the momentum mismatch between carriers in Si, probability of band to band transitions is increased when phonon confinement takes place which is beneficial for optoelectronic devices.

The influence of the HF and HBr treatments on the electrical performances (I_{sc}, V_{oc}) of SiNWs/TiO_2 bulk heterojunction solar cell devices are also explored. Our investigation shows that HBr treated solar cells outperform the pristine or HF treated devices. We conclude that pristine devices have large amounts of carbon contamination and a native oxide layer that works as a barrier to prevent the tunneling of the photo generated carriers. Hence, we have noticed very small I_{sc} and V_{oc} for these devices. HF and HBr treatments are helpful to remove the native oxide layer and reduce the carbon contamination from the SiNWs surface. Thus we have observed improved I_{sc} and V_{oc} from the devices treated with HF and HBr. However, HF treated SiNWs surface re-oxidizes faster than the HBr treated ones since; HBr is a strong acid as compared to HF. Hence, HBr treated devices offer more enhanced photovoltaic performance than HF treated devices. A maximum PCE of 6.2% has observed for HBr treated solar cells which is the highest reported efficiency for SiNWs/TiO_2 solar cells till date.

The impact of plasmonic response of SiNWs and its application in hybrid heterojunction solar cells have studied in this thesis. At photon energies above plasmon resonance, metallic

nanoparticle-induced absorption leads to a dramatic reduction of the reflectivity resulting significant enhancement of the PCE of the photovoltaic devices. We show that controlling the cleaning protocol to leave minute amounts of Ag nanoparticles attached to the silicon nanowires before coating with solvent treated PEDOT:PSS leads to a significant improvement in I_{sc} and V_{oc} resulting in 52% overall improvement in the PCE of the photovoltaic devices. The devices produced show a PCE up to 8.4% under AM 1.5G illumination, compared to 5.5% without Ag nanoparticles.

CHAPTER 9

STATEMENT OF ORIGINAL CONTRIBUTIONS AND FUTURE WORKS

9.1 Statement of original contributions:

Using HBr for interface modification of SiNWs surface is one of the key contribution from this thesis. Surface passivation using HBr is a novel chemical method that could prove potential for pohotovoltaic devices. Another key contribution is emplyoing plasmonic effect in the SiNWs based hybrid heterojunction solar cells to enhance its efficiency.

All the original contributions contained in this thesis are listed as follows.

1. Characterization of phonon confinement effect in silicon nanowires to enhance the photovoltaic efficiency;
2. Develop new device architecture to fabricate SiNWs/TiO_2 bulk heterojunction solar cells;
3. Develop new route for surface passivation of SiNWs;
4. Improve the optoelectronic properties of SiNWs fabricated by all solution based GDM method by carefully controlling the etching kinetics and cleaning protocol after etching;
5. Develop new pathway to fabricate hybrid heterojunction solar cells and increase its efficiency by incorporating plasmonic effect;
6. Establish new route for increasing the efficiency of cost-effective solar cells fabricated using all solution based synthesis.

9.2 Future works :

This study can be extended in any of the following areas:

9.2.1 Room temperature fabrication of silicon hybrid photovoltaics using amorphous TiO_2 :

We have fabricated SiNWs/ TiO_2 bulk heterojunction solar cells where TiO_2 has been used to fabricate the heterojunction with SiNWs. We annealed the device at 550 ^oC for the formation of anatase crystalline TiO_2. The same structure can be used to fabricate photovoltaic device

at room temperature using amorphous TiO_2. In this way, we can omit the need for the high-temperature fabrication process. The PCE will be less than anatase TiO_2 but the synthesis process will be more cost-effective. Interface modification of the amorphous TiO_2 layer can prove to be beneficial to increase the PCE of the solar cells.

9.2.2 Fabrication of plasmon sensitized SiNWs/TiO_2 heterojunction for photovoltaic application

Vertically aligned SiNWs are potential candidates for low-cost solar cells since past decade. Ag plasmon sensitized free-standing n-type SiNWs and anatase TiO_2 heterojunction can be formed. The optical properties of the heterostructure should be significantly influenced by the surface plasmons of Ag nanoparticles. A promising light trapping mechanism for these plasmon sensitized SiNWs/TiO_2 heterojunction can be explored.

9.2.3 Characterization of plasmonic response in nanowire solar cells by controlling the plasmons size distribution

Surface plasmons play a crucial role in the enhancement of the electronic and optical properties of the plasmon sensitized solar cells. We have observed plasmonic response of vertically aligned SiNWs by carefully controlling the cleaning mechanism after the GDM. More control over the cleaning protocol can be effective to change the size distribution of the Ag plasmons. We can probe the optical response of these plasmonic nanowires by varying the plasmon sizes. Efficient solar cells can be fabricated with the optimum size of the surface plasmons.

LIST OF PUBLICATIONS

1. **Banerjee, D.**, Trudeau, C., Gerlein, L. F. & Cloutier, S. G. Phonon processes in vertically aligned silicon nanowire arrays produced by low-cost all-solution galvanic displacement method. *Applied Physics Letters* **108**, 113109, doi:10.1063/1.4944334 (2016).

2. **Banerjee, D.**, Benavides, J., Guo, X. & Cloutier, S.G. Tailored interfaces of bulk silicon nanowire/TiO_2 heterojunction promoting enhanced photovoltaic performances. *ACS Omega* **3(5)**, 5064-5070, doi :10.1021/acsomega.8b00522 (2018).

3. **Banerjee, D.**, Guo, X. & Cloutier, S.G. Plasmon-enhanced silicon nanowire array-based hybrid heterojunction solar cells. *Solar RRL*, doi :10.1002/solr.201800007 (2018).

4. **Banerjee, D.** & Cloutier, S.G. Approaching to the S-Q limit by calculating the loss mechanisms of light using RCWA for silicon nanowires. *To be submitted*.

5. **Banerjee, D.**, Asuo, I.M. & Cloutier, S.G. Robust broad spectral photodetection from plasmon-sensitized silicon nanowires and amorphous TiO_2 heterostructure. *To be submitted*.

6. Chaabane, I., **Banerjee, D.**, Touayar, O. & Cloutier, S.G. Shallow V-shape nanostructured pit arrays in germanium using aqua regia electroless chemical etching. *Materials* **10(8)**, 854, doi: 10.3390/ma10080854 (2017).

7. Guo, X., Benavides, J., **Banerjee, D.**, Moisan, F.R. & Cloutier, S.G. Color tunable polymer light emitting diodes by electrospraying techniques. *To be submitted.*

8. Asuo, I. M., **Banerjee, D.**, Nechache, R. & Cloutier, S.G. Synthesis of high performance hybrid perovskites on silicon nanowires for fast and ultra-broadband photodetector. *To be submitted.*

LIST OF REFERENCES

Aberle, Armin G. 2000. « Surface passivation of crystalline silicon solar cells: a review ». *Progress in Photovoltaics: Research and Applications,* vol. 8, nº 5, p. 473-487.

Aberle, Armin G. 2001. « Overview on SiN surface passivation of crystalline silicon solar cells ». *Solar Energy Materials and Solar Cells,* vol. 65, nº 1, p. 239-248.

Adu, K. W., H. R. Gutiérrez, U. J. Kim, G. U. Sumanasekera et P. C. Eklund. 2005. «Confined Phonons in Si Nanowires ». *Nano Letters,* vol. 5, nº 3, p. 409-414.

Adu, K. W., Q. Xiong, H. R. Gutierrez, G. Chen et P. C. Eklund. 2006. « Raman scattering as a probe of phonon confinement and surface optical modes in semiconducting nanowires ». *Applied Physics A,* vol. 85, nº 3, p. 287.

Alfaro, P., A. Miranda, A.E. Ramos et M. Cruz-Irisson. 2006. « Hydrogenated Ge nanocrystals: band gap evolution with increasing size ». *Brazilian Journal of Physics,* vol. 36, p. 375-378.

Anatoly, V. Zayats, et I. Smolyaninov Igor. 2003. « Near-field photonics: surface plasmon polaritons and localized surface plasmons ». *Journal of Optics A: Pure and Applied Optics,* vol. 5, nº 4, p. S16.

Antonelli, David M., et Jackie Y. Ying. 1995. « Synthesis of Hexagonally Packed Mesoporous TiO2 by a Modified Sol–Gel Method ». *Angewandte Chemie International Edition in English,* vol. 34, nº 18, p. 2014-2017.

Avasthi, Sushobhan, Stephanie Lee, Yueh-Lin Loo et James C. Sturm. 2011. « Role of Majority and Minority Carrier Barriers Silicon/Organic Hybrid Heterojunction Solar Cells ». *Advanced Materials,* vol. 23, nº 48, p. 5762-5766.

Banerjee, Debika, Charles Trudeau, Luis Felipe Gerlein et Sylvain G. Cloutier. 2016. «Phonon processes in vertically aligned silicon nanowire arrays produced by low-cost all-solution galvanic displacement method ». *Applied Physics Letters,* vol. 108, nº 11, p. 113109.

Barbagiovanni, Eric G., David J. Lockwood, Peter J. Simpson et Lyudmila V. Goncharova. 2014. « Quantum confinement in Si and Ge nanostructures: Theory and experiment ». *Applied Physics Reviews,* vol. 1, nº 1, p. 011302.

Bartesaghi, Davide, Irene del Carmen Pérez, Juliane Kniepert, Steffen Roland, Mathieu Turbiez, Dieter Neher et L. Jan Anton Koster. 2015. « Competition between recombination and extraction of free charges determines the fill factor of organic solar cells ». *Nature Communications,* vol. 6, p. 7083.

Bozyigit, Deniz, Weyde M. M. Lin, Nuri Yazdani, Olesya Yarema et Vanessa Wood. 2015. «A quantitative model for charge carrier transport, trapping and recombination in nanocrystal-based solar cells ». *Nature Communications,* vol. 6, p. 6180.

Campbell, I. H., et P. M. Fauchet. 1986. « The effects of microcrystal size and shape on the one phonon Raman spectra of crystalline semiconductors ». *Solid State Communications,* vol. 58, nº 10, p. 739-741.

Campostrini, R., G. Carturan, L. Palmisano, M. Schiavello et A. Sclafani. 1994. « Sol-gel derived anatase TiO2: morphology and photoactivity ». *Materials Chemistry and Physics,* vol. 38, nº 3, p. 277-283.

Canham, L. T. 1990. « Silicon quantum wire array fabrication by electrochemical and chemical dissolution of wafers ». *Applied Physics Letters,* vol. 57, nº 10, p. 1046-1048.

Carraro, Carlo, Roya Maboudian et Luca Magagnin. 2007. « Metallization and nanostructuring of semiconductor surfaces by galvanic displacement processes ». *Surface Science Reports,* vol. 62, nº 12, p. 499-525.

Catchpole, K. R., et A. Polman. 2008. « Plasmonic solar cells ». *Optics Express,* vol. 16, nº 26, p. 21793-21800.

Cheng, Zhe, Longju Liu, Shen Xu, Meng Lu et Xinwei Wang. 2015. « Temperature Dependence of Electrical and Thermal Conduction in Single Silver Nanowire ». *Scientific Reports,* vol. 5, p. 10718.

Choi, K., H. Harris, S. Gangopadhyay et H. Temkin. 2003. « Cleaning of Si and properties of the HfO2–Si interface ». *Journal of Vacuum Science & Technology A: Vacuum, Surfaces, and Films,* vol. 21, nº 3, p. 718-722.

Chow, Jeffrey, Raymond J. Kopp et Paul R. Portney. 2003. « Energy Resources and Global Development ». *Science,* vol. 302, nº 5650, p. 1528-1531.

Cloutier, S. G, C. H. Hsu, P. A Kossyrev et J. Xu. 2006. « Enhancement of Radiative Recombination in Silicon via Phonon Localization and Selection-Rule Breaking ». *Advanced Materials,* vol. 18, nº 7, p. 841-844.

Cloutier, Sylvain G., Rodney S. Guico et Jimmy M. Xu. 2005. « Phonon localization in periodic uniaxially nanostructured silicon ». *Applied Physics Letters,* vol. 87, nº 22, p. 222104.

Colli, A., S. Hofmann, A. Fasoli, A. C. Ferrari, C. Ducati, R. E. Dunin-Borkowski et J. Robertson. 2006. « Synthesis and optical properties of silicon nanowires grown by different methods ». *Applied Physics A,* vol. 85, nº 3, p. 247-253.

Collins, Gillian, et Justin D. Holmes. 2011. « Chemical functionalisation of silicon and germanium nanowires ». *Journal of Materials Chemistry,* vol. 21, nº 30, p. 11052-11069.

Conibeer, Gavin, Martin Green, Richard Corkish, Young Cho, Eun-Chel Cho, Chu-Wei Jiang, Thipwan Fangsuwannarak, Edwin Pink, Yidan Huang, Tom Puzzer, Thorsten Trupke, Bryce Richards, Avi Shalav et Kuo-lung Lin. 2006. « Silicon nanostructures for third generation photovoltaic solar cells ». *Thin Solid Films,* vol. 511-512, nº Supplement C, p. 654-662.

Dan, Yaping, Kwanyong Seo, Kuniharu Takei, Jhim H. Meza, Ali Javey et Kenneth B. Crozier. 2011. « Dramatic Reduction of Surface Recombination by in Situ Surface Passivation of Silicon Nanowires ». *Nano Letters,* vol. 11, nº 6, p. 2527-2532.

Deal, B. E., et A. S. Grove. 1965. « General Relationship for the Thermal Oxidation of Silicon ». *Journal of Applied Physics,* vol. 36, nº 12, p. 3770-3778.

Dimitrov, Dimitre Z., et Chen-Hsun Du. 2013. « Crystalline silicon solar cells with micro/nano texture ». *Applied Surface Science,* vol. 266, p. 1-4.

Dincer, Ibrahim. 2000. « Renewable energy and sustainable development: a crucial review ». *Renewable and Sustainable Energy Reviews,* vol. 4, nº 2, p. 157-175.

Doganay, Doga, Sahin Coskun, Cevdet Kaynak et Husnu Emrah Unalan. 2016. « Electrical, mechanical and thermal properties of aligned silver nanowire/polylactide nanocomposite films ». *Composites Part B: Engineering,* vol. 99, p. 288-296.

Duan, Y., J. F. Kong et W. Z. Shen. 2012. « Raman investigation of silicon nanocrystals: quantum confinement and laser-induced thermal effects ». *Journal of Raman Spectroscopy,* vol. 43, nº 6, p. 756-760.

Ellingson, Randy J., Matthew C. Beard, Justin C. Johnson, Pingrong Yu, Olga I. Micic, Arthur J. Nozik, Andrew Shabaev et Alexander L. Efros. 2005. « Highly Efficient Multiple Exciton Generation in Colloidal PbSe and PbS Quantum Dots ». *Nano Letters,* vol. 5, nº 5, p. 865-871.

Fan, Hui-Jie, Hui-Qiang Zhang, Jing-Jing Wu, Zheng-Fang Wen et Feng-Ying Ma. 2011. «Photovoltaic Behaviors in an Isotype n-TiO 2 /n-Si Heterojunction ». *Chinese Physics Letters,* vol. 28, nº 12, p. 127305.

Fan, Zhiyong, Haleh Razavi, Jae-won Do, Aimee Moriwaki, Onur Ergen, Yu-Lun Chueh, Paul W. Leu, Johnny C. Ho, Toshitake Takahashi, Lothar A. Reichertz, Steven Neale, Kyoungsik Yu, Ming Wu, Joel W. Ager et Ali Javey. 2009. « Three-dimensional nanopillar-array photovoltaics on low-cost and flexible substrates ». *Nature Materials,* vol. 8, p. 648.

Fang, Xing, C. Y. Zhao et Hua Bao. 2014. « Radiative behaviors of crystalline silicon nanowire and nanohole arrays for photovoltaic applications ». *Journal of Quantitative Spectroscopy and Radiative Transfer,* vol. 133, p. 579-588.

Ferraria, Ana Maria, Ana Patrícia Carapeto et Ana Maria Botelho do Rego. 2012. « X-ray photoelectron spectroscopy: Silver salts revisited ». *Vacuum,* vol. 86, nº 12, p. 1988-1991.

Ferre, R., A. Orpella, D. Munoz, I. Martín, F. Recart, C. Voz, J. Puigdollers, P. Roca i Cabarrocas et R. Alcubilla. 2008. « Very low surface recombination velocity of crystalline silicon passivated by phosphorus-doped a-SicxNy:H(n) alloys ». *Progress in Photovoltaics: Research and Applications,* vol. 16, nº 2, p. 123-127.

Forro, L., O. Chauvet, D. Emin, L. Zuppiroli, H. Berger et F. Lévy. 1994. « High mobility n- type charge carriers in large single crystals of anatase (TiO2) ». *Journal of Applied Physics,* vol. 75, nº 1, p. 633-635.

Fuhrmann, Bodo, Hartmut S. Leipner, Hans-Reiner Höche, Luise Schubert, Peter Werner et Ulrich Gösele. 2005. « Ordered Arrays of Silicon Nanowires Produced by Nanosphere Lithography and Molecular Beam Epitaxy ». *Nano Letters,* vol. 5, nº 12, p. 2524-2527.

Fukata, N., T. Oshima, N. Okada, K. Murakami, T. Kizuka, T. Tsurui et S. Ito. 2006. «Phonon confinement and self-limiting oxidation effect of silicon nanowires synthesized by laser ablation ». *Journal of Applied Physics,* vol. 100, nº 2, p. 024311.

Funda, Shuji, Tatsuya Ohki, Qiming Liu, Jaker Hossain, Yoshihiro Ishimaru, Keiji Ueno et Hajime Shirai. 2016. « Correlation between the fine structure of spin-coated PEDOT:PSS and the photovoltaic performance of organic/crystalline-silicon heterojunction solar cells ». *Journal of Applied Physics,* vol. 120, nº 3, p. 033103.

Gao, Wei, Shouwen Yu et Ganyun Huang. 2006. « Finite element characterization of the size-dependent mechanical behaviour in nanosystems ». *Nanotechnology,* vol. 17, nº 4, p. 1118.

Garnett, Erik C., Mark L. Brongersma, Yi Cui et Michael D. McGehee. 2011. « Nanowire Solar Cells ». *Annual Review of Materials Research,* vol. 41, nº 1, p. 269-295.

Garnett, Erik C., et Peidong Yang. 2008. «Silicon Nanowire Radial p−n Junction Solar Cells». *Journal of the American Chemical Society,* vol. 130, nº 29, p. 9224-9225.

Garnett, Erik, et Peidong Yang. 2010. « Light Trapping in Silicon Nanowire Solar Cells ». *Nano Letters,* vol. 10, nº 3, p. 1082-1087.

Goldberger, Josh, Allon I. Hochbaum, Rong Fan et Peidong Yang. 2006. « Silicon Vertically Integrated Nanowire Field Effect Transistors ». *Nano Letters,* vol. 6, nº 5, p. 973-977.

Grann, Eric B., M. G. Moharam et Drew A. Pommet. 1994. « Artificial uniaxial and biaxial dielectrics with use of two-dimensional subwavelength binary gratings ». *Journal of the Optical Society of America A,* vol. 11, nº 10, p. 2695-2703.

Green, M. A. 1987. « High Efficiency Silicon Solar Cells ». In *Seventh E.C. Photovoltaic Solar Energy Conference: Proceedings of the International Conference, held at Sevilla, Spain, 27–31 October 1986*, sous la dir. de Goetzberger, A., W. Palz et G. Willeke. Green1987. p. 681-687. Dordrecht: Springer Netherlands. https://doi.org/10.1007/978-94-009-3817-5_121

Green, Martin A. 2001. « Third generation photovoltaics: Ultra-high conversion efficiency at low cost ». *Progress in Photovoltaics: Research and Applications,* vol. 9, nº 2, p. 123-135.

Green, Martin A. 2002. « Third generation photovoltaics: solar cells for 2020 and beyond ». *Physica E: Low-dimensional Systems and Nanostructures,* vol. 14, nº 1, p. 65-70.

Hadiseh, Alaeian, C. Atre Ashwin et A. Dionne Jennifer. 2012. « Optimized light absorption in Si wire array solar cells ». *Journal of Optics,* vol. 14, nº 2, p. 024006.

Haes, Amanda J., Shengli Zou, George C. Schatz et Richard P. Van Duyne. 2004. «Nanoscale Optical Biosensor: Short Range Distance Dependence of the Localized Surface Plasmon Resonance of Noble Metal Nanoparticles ». *The Journal of Physical Chemistry B,* vol. 108, nº 22, p. 6961-6968.

Hayashi, S., et H. Kanamori. 1982. « Raman scattering from the surface phonon mode in GaP microcrystals ». *Physical Review B,* vol. 26, nº 12, p. 7079-7082.

He, J., P. Gao, M. Liao, X. Yang, Z. Ying, S. Zhou, J. Ye et Y. Cui. 2015. « Realization of 13.6% Efficiency on 20 mum Thick Si/Organic Hybrid Heterojunction Solar Cells via Advanced Nanotexturing and Surface Recombination Suppression ». *ACS Nano,* vol. 9, nº 6, p. 6522-31.

He, Zhicai, Chengmei Zhong, Shijian Su, Miao Xu, Hongbin Wu et Yong Cao. 2012. «Enhanced power-conversion efficiency in polymer solar cells using an inverted device structure ». *Nature Photonics,* vol. 6, p. 591.

Heeger, Alan J. 2014. « 25th Anniversary Article: Bulk Heterojunction Solar Cells: Understanding the Mechanism of Operation ». *Advanced Materials,* vol. 26, nº 1, p. 10-28.

Hochbaum, Allon I., Renkun Chen, Raul Diaz Delgado, Wenjie Liang, Erik C. Garnett, Mark Najarian, Arun Majumdar et Peidong Yang. 2008. « Enhanced thermoelectric performance of rough silicon nanowires ». *Nature,* vol. 451, p. 163.

Hoex, B., J. J. H. Gielis, M. C. M. van de Sanden et W. M. M. Kessels. 2008. « On the c-Si surface passivation mechanism by the negative-charge-dielectric Al2O3 ». *Journal of Applied Physics,* vol. 104, nº 11, p. 113703.

Hoex, B., S. B. S. Heil, E. Langereis, M. C. M. van de Sanden et W. M. M. Kessels. 2006. «Ultralow surface recombination of c-Si substrates passivated by plasma-assisted atomic layer deposited Al2O3 ». *Applied Physics Letters,* vol. 89, nº 4, p. 042112.

Hofmann, S., C. Ducati, R. J. Neill, S. Piscanec, A. C. Ferrari, J. Geng, R. E. Dunin-Borkowski et J. Robertson. 2003. « Gold catalyzed growth of silicon nanowires by plasma enhanced chemical vapor deposition ». *Journal of Applied Physics,* vol. 94, nº 9, p. 6005-6012.

Holmes, Justin D., Keith P. Johnston, R. Christopher Doty et Brian A. Korgel. 2000. «Control of Thickness and Orientation of Solution-Grown Silicon Nanowires ». *Science,* vol. 287, nº 5457, p. 1471.

Höök, Mikael, et Xu Tang. 2013. « Depletion of fossil fuels and anthropogenic climate change—A review ». *Energy Policy,* vol. 52, nº Supplement C, p. 797-809.

Hsu, Weitse, Carolin M. Sutter-Fella, Mark Hettick, Lungteng Cheng, Shengwen Chan, Yunfeng Chen, Yuping Zeng, Maxwell Zheng, Hsin-Ping Wang, Chien-Chih Chiang et Ali Javey. 2015. « Electron-Selective TiO(2) Contact for Cu(In,Ga)Se(2) Solar Cells ». *Scientific Reports,* vol. 5, p. 16028.

Hu, Min, Carolina Novo, Alison Funston, Haining Wang, Hristina Staleva, Shengli Zou, Paul Mulvaney, Younan Xia et Gregory V. Hartland. 2008. « Dark-field microscopy studies of single metal nanoparticles: understanding the factors that influence the linewidth of the localized surface plasmon resonance ». *Journal of Materials Chemistry,* vol. 18, nº 17, p. 1949-1960.

Huang, B. Y., H. W. Liu, T. G. Chen, E. C. Chen, B. h. Chen, T. Y. Liu, P. Yu et H. F. Meng. 2012a. « Solution-processed silicon hybrid heterojunction photovoltaics with silver nanowires ». In *2012 38th IEEE Photovoltaic Specialists Conference*. (3-8 June 2012), p. 002537-002539.

Huang, Bohr-Ran, Ying-Kan Yang, Tzu-Ching Lin et Wen-Luh Yang. 2012b. « A simple and low-cost technique for silicon nanowire arrays based solar cells ». *Solar Energy Materials and Solar Cells,* vol. 98, nº Supplement C, p. 357-362.

Huang, Zhipeng, Nadine Geyer, Peter Werner, Johannes de Boor et Ulrich Gösele. 2011. «Metal-Assisted Chemical Etching of Silicon: A Review ». *Advanced Materials,* vol. 23, nº 2, p. 285-308.

Hung, Yung, Jr., San-Liang Lee, Kai-Chung Wu, Yian Tai et Yen-Ting Pan. 2011. «Antireflective silicon surface with vertical-aligned silicon nanowires realized by simple wet chemical etching processes ». *Optics Express,* vol. 19, nº 17, p. 15792-15802.

Hwang, Yun Jeong, Akram Boukai et Peidong Yang. 2009. « High Density n-Si/n-TiO_2 Core/Shell Nanowire Arrays with Enhanced Photoactivity ». *Nano Letters,* vol. 9, nº 1, p. 410-415.

Hybertsen, Mark S. 1994. « Absorption and emission of light in nanoscale silicon structures ». *Physical Review Letters,* vol. 72, nº 10, p. 1514-1517.

Ingale, Alka, et K. C. Rustagi. 1998. « Raman spectra of semiconductor nanoparticles: Disorder-activated phonons ». *Physical Review B,* vol. 58, nº 11, p. 7197-7204.

Jan, Schmidt, Kerr Mark et Cuevas Andrés. 2001. « Surface passivation of silicon solar cells using plasma-enhanced chemical-vapour-deposited SiN films and thin thermal SiO_2 /plasma SiN stacks ». *Semiconductor Science and Technology,* vol. 16, nº 3, p. 164.

Kaushika, N. D., et Anil K. Rai. 2007. « An investigation of mismatch losses in solar photovoltaic cell networks ». *Energy,* vol. 32, nº 5, p. 755-759.

Kawasaki, H., T. Yao, T. Suganuma, K. Okumura, Y. Iwaki, T. Yonezawa, T. Kikuchi et R. Arakawa. 2010. « Platinum nanoflowers on scratched silicon by galvanic displacement for an effective SALDI substrate ». *Chemistry,* vol. 16, nº 35, p. 10832-43.

Kelzenberg, M. D., M. C. Putnam, D. B. Turner-Evans, N. S. Lewis et H. A. Atwater. 2009. « Predicted efficiency of Si wire array solar cells ». In *2009 34th IEEE Photovoltaic Specialists Conference (PVSC)*. (7-12 June 2009), p. 001948-001953.

Kikuyama, H., M. Waki, M. Miyashita, T. Yabune, N. Miki, J. Takano et T. Ohmi. 1994. « A Study of the Dissociation State and the SiO2 Etching Reaction for HF Solutions of Extremely Low Concentration ». *Journal of The Electrochemical Society,* vol. 141, nº 2, p. 366-374.

Kim, Hui-Seon, Ivan Mora-Sero, Victoria Gonzalez-Pedro, Francisco Fabregat-Santiago, Emilio J. Juarez-Perez, Nam-Gyu Park et Juan Bisquert. 2013. « Mechanism of carrier accumulation in perovskite thin-absorber solar cells ». *Nature Communications,* vol. 4, p. 2242.

Kim, Jung Yup, Jim McVittie, Krishna Saraswat et Yoshio Nishi. 2008. « Passivation Studies of Germanium Surfaces ». *Solid State Phenomena,* vol. 134, p. 33-36.

Kim, Yong Hyun, Christoph Sachse, Michael L. Machala, Christian May, Lars Müller-Meskamp et Karl Leo. 2011. « Highly Conductive PEDOT:PSS Electrode with Optimized Solvent and Thermal Post-Treatment for ITO-Free Organic Solar Cells ». *Advanced Functional Materials,* vol. 21, nº 6, p. 1076-1081.

Kluth, O., B. Rech, L. Houben, S. Wieder, G. Schöpe, C. Beneking, H. Wagner, A. Löffl et H. W. Schock. 1999. « Texture etched ZnO:Al coated glass substrates for silicon based thin film solar cells ». *Thin Solid Films,* vol. 351, nº 1, p. 247-253.

Knupfer, M. 2003. « Exciton binding energies in organic semiconductors ». *Applied Physics A,* vol. 77, nº 5, p. 623-626.

Kossyrev, Pavel A., Aijun Yin, Sylvain G. Cloutier, David A. Cardimona, Danhong Huang, Paul M. Alsing et Jimmy M. Xu. 2005. « Electric Field Tuning of Plasmonic Response of Nanodot Array in Liquid Crystal Matrix ». *Nano Letters,* vol. 5, nº 10, p. 1978-1981.

Kwok, D. Y., T. Gietzelt, K. Grundke, H. J. Jacobasch et A. W. Neumann. 1997. « Contact Angle Measurements and Contact Angle Interpretation. 1. Contact Angle Measurements by Axisymmetric Drop Shape Analysis and a Goniometer Sessile Drop Technique ». *Langmuir,* vol. 13, nº 10, p. 2880-2894.

L., Huldt. 1971. « Band-to-band auger recombination in indirect gap semiconductors ». *physica status solidi (a),* vol. 8, nº 1, p. 173-187.

Lai, Yi-Chun, Yu-Fan Chang, Pei-Ting Tsai, Jan-kai Chang, Wei-Hsuan Tseng, Yi-Cheng Lin, Chu-Yen Hsiao, Hsiao-Wen Zan, Chih- I. Wu, Gou-Chung Chi, Hsin-Fei Meng et Peichen Yu. 2016. « Rear interface engineering of hybrid organic-silicon nanowire solar cells via blade coating ». *Optics Express,* vol. 24, nº 2, p. A414-A423.

Landsberg, P. T. 1967. « Radiative decay in compound semiconductors ». *Solid-State Electronics,* vol. 10, nº 6, p. 513-537.

Lauhon, Lincoln J., Mark S. Gudiksen, Deli Wang et Charles M. Lieber. 2002. « Epitaxial core–shell and core–multishell nanowire heterostructures ». *Nature,* vol. 420, p. 57.

Law, Matt, Matthew C. Beard, Sukgeun Choi, Joseph M. Luther, Mark C. Hanna et Arthur J. Nozik. 2008. « Determining the Internal Quantum Efficiency of PbSe Nanocrystal Solar Cells with the Aid of an Optical Model ». *Nano Letters,* vol. 8, nº 11, p. 3904-3910.

Law, Matt, Lori E. Greene, Justin C. Johnson, Richard Saykally et Peidong Yang. 2005. «Nanowire dye-sensitized solar cells ». *Nature Materials,* vol. 4, p. 455.

Law, Matt, Lori E. Greene, Aleksandra Radenovic, Tevye Kuykendall, Jan Liphardt et Peidong Yang. 2006. « ZnO−Al2O3 and ZnO−TiO2 Core−Shell Nanowire Dye-Sensitized Solar Cells ». *The Journal of Physical Chemistry B,* vol. 110, nº 45, p. 22652-22663.

Lee, Chang H., Mikella E. Hankus, Limei Tian, Paul M. Pellegrino et Srikanth Singamaneni. 2011. « Highly Sensitive Surface Enhanced Raman Scattering Substrates Based on Filter Paper Loaded with Plasmonic Nanostructures ». *Analytical Chemistry,* vol. 83, nº 23, p. 8953-8958.

Lee, S. T., N. Wang, Y. F. Zhang et Y. H. Tang. 2013. « Oxide-Assisted Semiconductor Nanowire Growth ». *MRS Bulletin,* vol. 24, nº 8, p. 36-42.

Li, L., H. Bender, T. Trenkler, P. W. Mertens, M. Meuris, W. Vandervorst et M. M. Heyns. 1995. « Surface passivation and microroughness of (100) silicon etched in aqueous hydrogen halide (HF, HCl, HBr, HI) solutions ». *Journal of Applied Physics,* vol. 77, nº 3, p. 1323-1325.

Li, Xinming, Hongwei Zhu, Kunlin Wang, Anyuan Cao, Jinquan Wei, Chunyan Li, Yi Jia, Zhen Li, Xiao Li et Dehai Wu. 2010. « Graphene-On-Silicon Schottky Junction Solar Cells ». *Advanced Materials,* vol. 22, nº 25, p. 2743-2748.

Lin, Yuxuan, Xinming Li, Dan Xie, Tingting Feng, Yu Chen, Rui Song, He Tian, Tianling Ren, Minlin Zhong, Kunlin Wang et Hongwei Zhu. 2013. « Graphene/semiconductor heterojunction solar cells with modulated antireflection and graphene work function ». *Energy & Environmental Science,* vol. 6, nº 1, p. 108-115.

Liu, Kong, Shengchun Qu, Xinhui Zhang, Furui Tan et Zhanguo Wang. 2013. « Improved photovoltaic performance of silicon nanowire/organic hybrid solar cells by incorporating silver nanoparticles ». *Nanoscale Research Letters,* vol. 8, nº 1, p. 88.

Lotfi, Hossein, Robert T. Hinkey, Lu Li, Rui Q. Yang, John F. Klem et Matthew B. Johnson. 2013. « Narrow-bandgap photovoltaic devices operating at room temperature and above with high open-circuit voltage ». *Applied Physics Letters,* vol. 102, nº 21, p. 211103.

Lu, Yuerui, et Amit Lal. 2010. « High-Efficiency Ordered Silicon Nano-Conical-Frustum Array Solar Cells by Self-Powered Parallel Electron Lithography ». *Nano Letters,* vol. 10, nº 11, p. 4651-4656.

Lund, Henrik. 2007. « Renewable energy strategies for sustainable development ». *Energy,* vol. 32, nº 6, p. 912-919.

Ma, D. D. D., C. S. Lee, F. C. K. Au, S. Y. Tong et S. T. Lee. 2003. « Small-Diameter Silicon Nanowire Surfaces ». *Science,* vol. 299, nº 5614, p. 1874.

Mallorquí, Anna Dalmau, Esther Alarcón-Lladó, Ignasi Canales Mundet, Amirreza Kiani, Bénédicte Demaurex, Stefaan De Wolf, Andreas Menzel, Margrit Zacharias et Anna Fontcuberta i Morral. 2015. « Field-effect passivation on silicon nanowire solar cells ». *Nano Research,* vol. 8, nº 2, p. 673-681.

McAlpine, Michael C., Habib Ahmad, Dunwei Wang et James R. Heath. 2007. « Highly ordered nanowire arrays on plastic substrates for ultrasensitive flexible chemical sensors ». *Nature Materials,* vol. 6, p. 379.

Meen, T. H., W. Water, W. R. Chen, S. M. Chao, L. W. Ji et C. J. Huang. 2009. «Application of TiO_2 nano-particles on the electrode of dye-sensitized solar cells ». *Journal of Physics and Chemistry of Solids,* vol. 70, nº 2, p. 472-476.

Mi Yeon, Song, Kim Do Kyun, Ihn Kyo Jin, Jo Seong Mu et Kim Dong Young. 2004. «Electrospun TiO_2 electrodes for dye-sensitized solar cells ». *Nanotechnology,* vol. 15, nº 12, p. 1861.

Moharam, M. G., Eric B. Grann, Drew A. Pommet et T. K. Gaylord. 1995. « Formulation for stable and efficient implementation of the rigorous coupled-wave analysis of binary gratings ». *Journal of the Optical Society of America A,* vol. 12, nº 5, p. 1068-1076.

Morales, Alfredo M., et Charles M. Lieber. 1998. « A Laser Ablation Method for the Synthesis of Crystalline Semiconductor Nanowires ». *Science,* vol. 279, nº 5348, p. 208.

Moulé, Adam J., Jörg B. Bonekamp et Klaus Meerholz. 2006. « The effect of active layer thickness and composition on the performance of bulk-heterojunction solar cells ». *Journal of Applied Physics,* vol. 100, nº 9, p. 094503.

Nemanick, E. Joseph, Patrick T. Hurley, Lauren J. Webb, David W. Knapp, David J. Michalak, Bruce S. Brunschwig et Nathan S. Lewis. 2006. « Chemical and Electrical Passivation of Single-Crystal Silicon(100) Surfaces through a Two-Step Chlorination/Alkylation Process ». *The Journal of Physical Chemistry B,* vol. 110, nº 30, p. 14770-14778.

Ng, I. K., K. Y. Kok, S. S. Zainal Abidin, N. U. Saidin et T. F. Choo. 2011. « Aqueous Synthesis of Silicon Nanowire Arrays and Core-shell Structures via Electroless Nanoelectrochemical Process ». *AIP Conference Proceedings,* vol. 1341, nº 1, p. 315-319.

Niu, Junjie, Jian Sha et Deren Yang. 2004. « Silicon nanowires fabricated by thermal evaporation of silicon monoxide ». *Physica E: Low-dimensional Systems and Nanostructures,* vol. 23, nº 1, p. 131-134.

Noh, Jun Hong, Sang Hyuk Im, Jin Hyuck Heo, Tarak N. Mandal et Sang Il Seok. 2013. «Chemical Management for Colorful, Efficient, and Stable Inorganic–Organic Hybrid Nanostructured Solar Cells ». *Nano Letters,* vol. 13, nº 4, p. 1764-1769.

Odde, Srinivas, Byung Jin Mhin, Sik Lee, Han Myoung Lee et Kwang S. Kim. 2004. «Dissociation chemistry of hydrogen halides in water ». *The Journal of Chemical Physics,* vol. 120, nº 20, p. 9524-9535.

Ouyang, Zi, Xiang Zhao, Sergey Varlamov, Yuguo Tao, Johnson Wong et Supriya Pillai. 2011. « Nanoparticle-enhanced light trapping in thin-film silicon solar cells ». *Progress in Photovoltaics: Research and Applications,* vol. 19, nº 8, p. 917-926.

Pan, Z. W., Z. R. Dai, L. Xu, S. T. Lee et Z. L. Wang. 2001. « Temperature-Controlled Growth of Silicon-Based Nanostructures by Thermal Evaporation of SiO Powders ». *The Journal of Physical Chemistry B,* vol. 105, nº 13, p. 2507-2514.

Patel, Kamlesh, et Pawan K. Tyagi. 2015. « Multilayer graphene as a transparent conducting electrode in silicon heterojunction solar cells ». *AIP Advances,* vol. 5, nº 7, p. 077165.

Peng, K. Q., Y. J. Yan, S. P. Gao et J. Zhu. 2002. « Synthesis of Large-Area Silicon Nanowire Arrays via Self-Assembling Nanoelectrochemistry ». *Advanced Materials,* vol. 14, nº 16, p. 1164-1167.

Peng, K., Y. Yan, S. Gao et J. Zhu. 2003. « Dendrite-Assisted Growth of Silicon Nanowires in Electroless Metal Deposition ». *Advanced Functional Materials,* vol. 13, nº 2, p. 127-132.

Peng, Kuiqing, Hui Fang, Juejun Hu, Yin Wu, Jing Zhu, Yunjie Yan et ShuitTong Lee. 2006. « Metal-Particle-Induced, Highly Localized Site-Specific Etching of Si and Formation of Single-Crystalline Si Nanowires in Aqueous Fluoride Solution ». *Chemistry – A European Journal,* vol. 12, nº 30, p. 7942-7947.

Peng, Kuiqing, Jiansheng Jie, Wenjun Zhang et Shuit-Tong Lee. 2008. « Silicon nanowires for rechargeable lithium-ion battery anodes ». *Applied Physics Letters,* vol. 93, nº 3, p. 033105.

Peng, Kuiqing, Yin Wu, Hui Fang, Xiaoyan Zhong, Ying Xu et Jing Zhu. 2005. « Uniform, Axial-Orientation Alignment of One-Dimensional Single-Crystal Silicon Nanostructure Arrays ». *Angewandte Chemie International Edition,* vol. 44, nº 18, p. 2737-2742.

Peng, Song, et G. Michael Morris. 1995. « Efficient implementation of rigorous coupled-wave analysis for surface-relief gratings ». *Journal of the Optical Society of America A,* vol. 12, nº 5, p. 1087-1096.

Piatkowski, Piotr, Boiko Cohen, Carlito S. Ponseca, Manuel Salado, Samrana Kazim, Shahzada Ahmad, Villy Sundström et Abderrazzak Douhal. 2016. « Unraveling Charge Carriers Generation, Diffusion, and Recombination in Formamidinium Lead Triiodide Perovskite Polycrystalline Thin Film ». *The Journal of Physical Chemistry Letters,* vol. 7, nº 1, p. 204-210.

Pillai, S., K. R. Catchpole, T. Trupke et M. A. Green. 2007. « Surface plasmon enhanced silicon solar cells ». *Journal of Applied Physics,* vol. 101, nº 9, p. 093105.

Piscanec, S., M. Cantoro, A. C. Ferrari, J. A. Zapien, Y. Lifshitz, S. T. Lee, S. Hofmann et J. Robertson. 2003. « Raman spectroscopy of silicon nanowires ». *Physical Review B,* vol. 68, nº 24, p. 241312.

Poterya, Viktoriya, Michal Fárník, Petr Slavíček, Udo Buck et Vitaly V. Kresin. 2007. «Photodissociation of hydrogen halide molecules on free ice nanoparticles ». *The Journal of Chemical Physics,* vol. 126, nº 7, p. 071101.

Pudasaini, Pushpa Raj, Francisco Ruiz-Zepeda, Manisha Sharma, David Elam, Arturo Ponce et Arturo A. Ayon. 2013. « High Efficiency Hybrid Silicon Nanopillar–Polymer Solar Cells ». *ACS Applied Materials & Interfaces,* vol. 5, nº 19, p. 9620-9627.

Q. Peng, K., Z. P. Huang et J. Zhu. 2004. « Fabrication of Large-Area Silicon Nanowire p–n Junction Diode Arrays ». *Advanced Materials,* vol. 16, nº 1, p. 73-76.

Qu, Yongquan, Lei Liao, Yujing Li, Hua Zhang, Yu Huang et Xiangfeng Duan. 2009. «Electrically Conductive and Optically Active Porous Silicon Nanowires ». *Nano Letters,* vol. 9, nº 12, p. 4539-4543.

Rao, A. M., E. Richter, S. Bandow, B. Chase, P. C. Eklund, K. A. Williams, S. Fang, K. R. Subbaswamy, M. Menon, A. Thess, R. E. Smalley, G. Dresselhaus et M. S. Dresselhaus. 1997. « Diameter-Selective Raman Scattering from Vibrational Modes in Carbon Nanotubes ». *Science,* vol. 275, nº 5297, p. 187-91.

Richards, B. S. 2006. « Enhancing the performance of silicon solar cells via the application of passive luminescence conversion layers ». *Solar Energy Materials and Solar Cells,* vol. 90, nº 15, p. 2329-2337.

Richter, Armin, Jan Benick, Martin Hermle et Stefan W. Glunz. 2011. « Excellent silicon surface passivation with 5 Å thin ALD Al2O3 layers: Influence of different thermal post-deposition treatments ». *physica status solidi (RRL) – Rapid Research Letters,* vol. 5, nº 5-6, p. 202-204.

Richter, H., Z. P. Wang et L. Ley. 1981. « The one phonon Raman spectrum in microcrystalline silicon ». *Solid State Communications,* vol. 39, nº 5, p. 625-629.

Rivillon, Sandrine, Yves J. Chabal, Fabrice Amy et Antoine Kahn. 2005. « Hydrogen passivation of germanium (100) surface using wet chemical preparation ». *Applied Physics Letters,* vol. 87, nº 25, p. 253101.

Samuel, C. Barden, A. Arns James, S. Colburn Willis et B. Williams Joel. 2000. « Volume-Phase Holographic Gratings and the Efficiency of Three Simple Volume-Phase Holographic Gratings ». *Publications of the Astronomical Society of the Pacific,* vol. 112, nº 772, p. 809.

Schmidt, J., A. Merkle, R. Brendel, B. Hoex, M. C. M. van de Sanden et W. M. M. Kessels. 2008. « Surface passivation of high-efficiency silicon solar cells by atomic-layer-deposited Al2O3 ». *Progress in Photovoltaics: Research and Applications,* vol. 16, nº 6, p. 461-466.

Schmidt, Volker, Joerg V. Wittemann, Stephan Senz et Ulrich Gösele. 2009. « Silicon Nanowires: A Review on Aspects of their Growth and their Electrical Properties ». *Advanced Materials,* vol. 21, nº 25-26, p. 2681-2702.

Schubert, L., P. Werner, N. D. Zakharov, G. Gerth, F. M. Kolb, L. Long, U. Gösele et T. Y. Tan. 2004. « Silicon nanowhiskers grown on 〈111〉 Si substrates by molecular-beam epitaxy ». *Applied Physics Letters,* vol. 84, nº 24, p. 4968-4970.

Shafiee, Shahriar, et Erkan Topal. 2009. « When will fossil fuel reserves be diminished? ». *Energy Policy,* vol. 37, nº 1, p. 181-189.

Shah, A., P. Torres, R. Tscharner, N. Wyrsch et H. Keppner. 1999. « Photovoltaic Technology: The Case for Thin-Film Solar Cells ». *Science,* vol. 285, nº 5428, p. 692.

Shah, A. V., H. Schade, M. Vanecek, J. Meier, E. Vallat-Sauvain, N. Wyrsch, U. Kroll, C. Droz et J. Bailat. 2004. « Thin-film silicon solar cell technology ». *Progress in Photovoltaics: Research and Applications,* vol. 12, nº 2-3, p. 113-142.

Sharma, Manisha, Pushpa Raj Pudasaini, Francisco Ruiz-Zepeda, David Elam et Arturo A. Ayon. 2014. « Ultrathin, Flexible Organic–Inorganic Hybrid Solar Cells Based on Silicon Nanowires and PEDOT:PSS ». *ACS Applied Materials & Interfaces,* vol. 6, nº 6, p. 4356-4363.

Shen, Xiaojuan, Baoquan Sun, Dong Liu et Shuit-Tong Lee. 2011. « Hybrid Heterojunction Solar Cell Based on Organic–Inorganic Silicon Nanowire Array Architecture ». *Journal of the American Chemical Society,* vol. 133, nº 48, p. 19408-19415.

Sheng, Jiang, Dan Wang, Sudong Wu, Xi Yang, Li Ding, Juye Zhu, Junfeng Fang, Pingqi Gao et Jichun Ye. 2016. « Ideal rear contact formed via employing a conjugated polymer for Si/PEDOT:PSS hybrid solar cells ». *RSC Advances,* vol. 6, nº 19, p. 16010-16017.

Shimizu, T., T. Xie, J. Nishikawa, S. Shingubara, S. Senz et U. Gösele. 2007. « Synthesis of Vertical High-Density Epitaxial Si(100) Nanowire Arrays on a Si(100) Substrate Using an Anodic Aluminum Oxide Template ». *Advanced Materials,* vol. 19, nº 7, p. 917-920.

Shin, Woong, Takuma Yasuda, Yu Hidaka, Go Watanabe, Ryota Arai, Keiro Nasu, Takahiro Yamaguchi, Wakako Murakami, Kengo Makita et Chihaya Adachi. 2014. « Solar Cells: π-Extended Narrow-Bandgap Diketopyrrolopyrrole-Based Oligomers for Solution-Processed Inverted Organic Solar Cells (Adv. Energy Mater. 17/2014) ». *Advanced Energy Materials,* vol. 4, nº 17, p. n/a-n/a.

Shockley, William, et Hans J. Queisser. 1961. « Detailed Balance Limit of Efficiency of p- n Junction Solar Cells ». *Journal of Applied Physics,* vol. 32, nº 3, p. 510-519.

Sims, Ralph E. H., Hans-Holger Rogner et Ken Gregory. 2003. « Carbon emission and mitigation cost comparisons between fossil fuel, nuclear and renewable energy resources for electricity generation ». *Energy Policy,* vol. 31, nº 13, p. 1315-1326.

Smekal, Werner, Wolfgang S. M. Werner et Cedric J. Powell. 2005. « Simulation of electron spectra for surface analysis (SESSA): a novel software tool for quantitative Auger-electron spectroscopy and X-ray photoelectron spectroscopy ». *Surface and Interface Analysis,* vol. 37, nº 11, p. 1059-1067.

Stalder, Aurélien F., Tobias Melchior, Michael Müller, Daniel Sage, Thierry Blu et Michael Unser. 2010. « Low-bond axisymmetric drop shape analysis for surface tension and contact angle measurements of sessile drops ». *Colloids and Surfaces A: Physicochemical and Engineering Aspects,* vol. 364, nº 1, p. 72-81.

Subramani, Thiyagu, Chen-Chih Hsueh, Hong-Jhang Syu, Chien-Ting Liu, Song-Ting Yang et Ching-Fuh Lin. 2016. « Interface modification for efficiency enhancement in silicon nanohole hybrid solar cells ». *RSC Advances,* vol. 6, nº 15, p. 12374-12381.

Syu, Hong-Jhang, Shu-Chia Shiu et Ching-Fuh Lin. 2012. « Silicon nanowire/organic hybrid solar cell with efficiency of 8.40% ». *Solar Energy Materials and Solar Cells,* vol. 98, p. 267-272.

Takagahara, Toshihide, et Kyozaburo Takeda. 1992. « Theory of the quantum confinement effect on excitons in quantum dots of indirect-gap materials ». *Physical Review B,* vol. 46, nº 23, p. 15578-15581.

Tang, H., H. Berger, P. E. Schmid et F. Lévy. 1994. « Optical properties of anatase (TiO2) ». *Solid State Communications,* vol. 92, nº 3, p. 267-271.

Tawada, Y., H. Okamoto et Y. Hamakawa. 1981. « a- SiC:H/a- Si:H heterojunction solar cell having more than 7.1% conversion efficiency ». *Applied Physics Letters,* vol. 39, nº 3, p. 237-239.

Temple, T. L., G. D. K. Mahanama, H. S. Reehal et D. M. Bagnall. 2009. « Influence of localized surface plasmon excitation in silver nanoparticles on the performance of silicon solar cells ». *Solar Energy Materials and Solar Cells,* vol. 93, nº 11, p. 1978-1985.

Thelander, C., P. Agarwal, S. Brongersma, J. Eymery, L. F. Feiner, A. Forchel, M. Scheffler, W. Riess, B. J. Ohlsson, U. Gösele et L. Samuelson. 2006. « Nanowire-based one-dimensional electronics ». *Materials Today,* vol. 9, nº 10, p. 28-35.

Tian, Bozhi, Xiaolin Zheng, Thomas J. Kempa, Ying Fang, Nanfang Yu, Guihua Yu, Jinlin Huang et Charles M. Lieber. 2007. « Coaxial silicon nanowires as solar cells and nanoelectronic power sources ». *Nature,* vol. 449, p. 885.

Tiedje, T., E. Yablonovitch, G. D. Cody et B. G. Brooks. 1984. « Limiting efficiency of silicon solar cells ». *IEEE Transactions on Electron Devices,* vol. 31, nº 5, p. 711-716.

Tress, Wolfgang, Annette Petrich, Markus Hummert, Moritz Hein, Karl Leo et Moritz Riede. 2011. « Imbalanced mobilities causing S-shaped IV curves in planar heterojunction organic solar cells ». *Applied Physics Letters,* vol. 98, nº 6, p. 063301.

Trupke, T., M. A. Green et P. Würfel. 2002a. « Improving solar cell efficiencies by down-conversion of high-energy photons ». *Journal of Applied Physics,* vol. 92, nº 3, p. 1668-1674.

Trupke, T., M. A. Green et P. Würfel. 2002b. « Improving solar cell efficiencies by up-conversion of sub-band-gap light ». *Journal of Applied Physics,* vol. 92, nº 7, p. 4117-4122.

Tsakalakos, L., J. Balch, J. Fronheiser, B. A. Korevaar, O. Sulima et J. Rand. 2007. « Silicon nanowire solar cells ». *Applied Physics Letters,* vol. 91, nº 23, p. 233117.

Um, Han-Don, Deokjae Choi, Ahreum Choi, Ji Hoon Seo et Kwanyong Seo. 2017. «Embedded Metal Electrode for Organic–Inorganic Hybrid Nanowire Solar Cells ». *ACS Nano,* vol. 11, nº 6, p. 6218-6224.

Wang, Huan, et Alexandre Vial. 2013. « Plasmonic Resonance Tunability and Surface-Enhanced Raman Scattering Gain of Metallic Nanoparticles Embedded in a Liquid Crystal Cell ». *The Journal of Physical Chemistry C,* vol. 117, nº 46, p. 24537-24542.

Wang, Jianxiong, Hao Wang, Ari Bimo Prakoso, Alienor Svietlana Togonal, Lei Hong, Changyun Jiang et Rusli. 2015. « High efficiency silicon nanowire/organic hybrid solar cells with two-step surface treatment ». *Nanoscale,* vol. 7, nº 10, p. 4559-4565.

Wang, Peng, Baibiao Huang, Xiaoyang Zhang, Xiaoyan Qin, Hao Jin, Ying Dai, Zeyan Wang, Jiyong Wei, Jie Zhan, Shaoying Wang, Junpeng Wang et Myung-Hwan Whangbo. 2009. « Highly Efficient Visible-Light Plasmonic Photocatalyst Ag@AgBr ». *Chemistry – A European Journal,* vol. 15, nº 8, p. 1821-1824.

Wang, Rong-ping, Guang-wen Zhou, Yu-long Liu, Shao-hua Pan, Hong-zhou Zhang, Da-peng Yu et Ze Zhang. 2000. « Raman spectral study of silicon nanowires: High-order scattering and phonon confinement effects ». *Physical Review B,* vol. 61, nº 24, p. 16827-16832.

Wang, Xiaotian, Wensheng Shi, Guangwei She et Lixuan Mu. 2011. « Using Si and Ge Nanostructures as Substrates for Surface-Enhanced Raman Scattering Based on Photoinduced Charge Transfer Mechanism ». *Journal of the American Chemical Society,* vol. 133, nº 41, p. 16518-16523.

Wang, Zhongchun, Ulf Helmersson et Per-Olov Käll. 2002. « Optical properties of anatase TiO2 thin films prepared by aqueous sol–gel process at low temperature ». *Thin Solid Films,* vol. 405, nº 1, p. 50-54.

Wenham, S. R., et M. A. Green. 1996. « Silicon solar cells ». *Progress in Photovoltaics: Research and Applications,* vol. 4, nº 1, p. 3-33.

Westwater, J., D. P. Gosain, S. Tomiya, S. Usui et H. Ruda. 1997. « Growth of silicon nanowires via gold/silane vapor–liquid–solid reaction ». *Journal of Vacuum Science & Technology B: Microelectronics and Nanometer Structures Processing, Measurement, and Phenomena,* vol. 15, nº 3, p. 554-557.

Wolf, Stefaan De, Guido Agostinelli, Guy Beaucarne et Petko Vitanov. 2005. « Influence of stoichiometry of direct plasma-enhanced chemical vapor deposited SiNx films and silicon substrate surface roughness on surface passivation ». *Journal of Applied Physics,* vol. 97, nº 6, p. 063303.

Wu, Shun-Der, Thomas K. Gaylord, Elias N. Glytsis et Yu-Ming Wu. 2005. « Angular sensitivities of volume gratings for substrate-mode optical interconnects ». *Applied Optics,* vol. 44, nº 21, p. 4447-4453.

Xia, Y., P. Yang, Y. Sun, Y. Wu, B. Mayers, B. Gates, Y. Yin, F. Kim et H. Yan. 2003. «One-Dimensional Nanostructures: Synthesis, Characterization, and Applications ». *Advanced Materials,* vol. 15, nº 5, p. 353-389.

Xie, W. Q., J. I. Oh et W. Z. Shen. 2011. « Realization of effective light trapping and omnidirectional antireflection in smooth surface silicon nanowire arrays ». *Nanotechnology,* vol. 22, nº 6, p. 065704.

Xu, Fan, Jaime Benavides, Xin Ma et Sylvain G. Cloutier. 2012a. « Interconnected TiO_2 Nanowire Networks for PbS Quantum Dot Solar Cell Applications ». *Journal of Nanotechnology,* vol. 2012, p. 6.

Xu, Zhida, Jing Jiang, Manas Ranjan Gartia et Gang Logan Liu. 2012b. « Monolithic Integrations of Slanted Silicon Nanostructures on 3D Microstructures and Their Application to Surface-Enhanced Raman Spectroscopy ». *The Journal of Physical Chemistry C,* vol. 116, nº 45, p. 24161-24170.

Yenchalwar, Sandeep G., Vedi Kuyil Azhagan et Manjusha V. Shelke. 2014. « Enhanced photoluminescence and photoactivity of plasmon sensitized nSiNWs/TiO_2 heterostructures ». *Physical Chemistry Chemical Physics,* vol. 16, nº 33, p. 17786-17791.

Yeon, C., G. Kim, J. W. Lim et S. J. Yun. 2017. « Highly conductive PEDOT:PSS treated by sodium dodecyl sulfate for stretchable fabric heaters ». *RSC Advances,* vol. 7, nº 10, p. 5888-5897.

Yin, Xingtian, Corsin Battaglia, Yongjing Lin, Kevin Chen, Mark Hettick, Maxwell Zheng, Cheng-Ying Chen, Daisuke Kiriya et Ali Javey. 2014. « 19.2% Efficient InP Heterojunction Solar Cell with Electron-Selective TiO(2) Contact ». *ACS Photonics,* vol. 1, nº 12, p. 1245-1250.

Yu, Miao, Yun-Ze Long, Bin Sun et Zhiyong Fan. 2012. « Recent advances in solar cells based on one-dimensional nanostructure arrays ». *Nanoscale,* vol. 4, nº 9, p. 2783-2796.

Yu, Xuegong, Xinlei Shen, Xinhui Mu, Jie Zhang, Baoquan Sun, Lingsheng Zeng, Lifei Yang, Yichao Wu, Hang He et Deren Yang. 2015. « High Efficiency Organic/Silicon-Nanowire Hybrid Solar Cells: Significance of Strong Inversion Layer ». *Scientific Reports,* vol. 5, p. 17371.

Zhang, Ming-Liang, Kui-Qing Peng, Xia Fan, Jian-Sheng Jie, Rui-Qin Zhang, Shuit-Tong Lee et Ning-Bew Wong. 2008. « Preparation of Large-Area Uniform Silicon Nanowires Arrays through Metal-Assisted Chemical Etching ». *The Journal of Physical Chemistry C,* vol. 112, nº 12, p. 4444-4450.

Zhang, Y. F., Y. H. Tang, N. Wang, D. P. Yu, C. S. Lee, I. Bello et S. T. Lee. 1998. « Silicon nanowires prepared by laser ablation at high temperature ». *Applied Physics Letters,* vol. 72, nº 15, p. 1835-1837.

Zhao, J., et M. A. Green. 1991. « Optimized antireflection coatings for high-efficiency silicon solar cells ». *IEEE Transactions on Electron Devices,* vol. 38, nº 8, p. 1925-1934.

Zhao, J., A. Wang, P. Altermatt et M. A. Green. 1995. « Twenty-four percent efficient silicon solar cells with double layer antireflection coatings and reduced resistance loss ». *Applied Physics Letters,* vol. 66, nº 26, p. 3636-3638.

Zhao, Jianhua, Aihua Wang, Martin A. Green et Francesca Ferrazza. 1998. « 19.8% efficient "honeycomb" textured multicrystalline and 24.4% monocrystalline silicon solar cells ». *Applied Physics Letters,* vol. 73, nº 14, p. 1991-1993.

Zheng, Gengfeng, Fernando Patolsky, Yi Cui, Wayne U. Wang et Charles M. Lieber. 2005. «Multiplexed electrical detection of cancer markers with nanowire sensor arrays ». *Nature Biotechnology,* vol. 23, p. 1294.

ANNEX I

SUPPORTING INFORMATION
TAILORED INTERFACES OF BULK SILICON NANOWIRE/TIO_2 HETEROJUNCTION PROMOTING ENHANCED PHOTOVOLTAIC PERFORMANCES

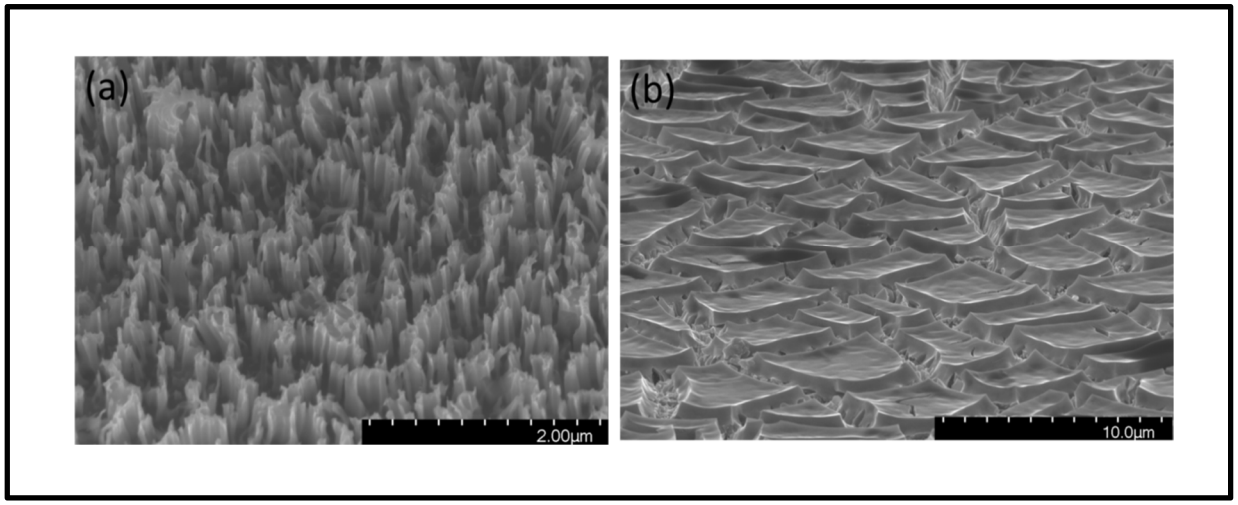

Figure AIS1 SEM micrographs of (a) silicon nanowire array structure synthesized using GDM, (b) SiNWs/TiO_2 bulk heterojunction

Table AIS1 EDX analysis of the atomic percentage of oxygen present in the nanowire samples treated with different concentrations of acids

Acid concentration (%)	**Atomic % of O_2 in HF-treated nanowire samples**	**Atomic % of O_2 in HBr-treated nanowire samples**
2	6.35	12.33
10	6.32	7.28
20	6.28	2.35

Table AIS2 EDX analysis of the atomic percentage of oxygen present in the nanowire samples for different treatment time

Treatment time (minute)	**Atomic % of O_2 in 2% HF-treated nanowire samples**	**Atomic % of O_2 in 20% HBr-treated nanowire samples**
1	10.47	3.48
2	6.33	2.32
5	6.31	2.30
10	6.25	2.28
20	6.22	2.28
30	6.12	2.25

Table AIS3 Photovoltaic characteristics of group 1 solar cells

Samples	**Isc (mA)**	**Voc (mV)**	**FF (%)**	**η (%)**
Device 1	1.18	224	23.15	0.06
Device 2	1.01	224	21.6	0.05
Device 3	0.7	210	20.9	0.03
Device 4	0.6	215	20.56	0.03
Device 5	1.12	165	26.41	0.05
Device 6	1.3	224	21.37	0.06
Device 7	0.7	184	32.47	0.04
Device 8	1	143	24.87	0.04

Table AIS4 Photovoltaic characteristics of group 2 solar cells

Samples	**Isc (mA)**	**Voc (mV)**	**FF (%)**	**η (%)**
Device 1	12.12	421	28.67	1.46
Device 2	11.6	445	37.74	1.95
Device 3	8.41	478	36.73	1.48
Device 4	12.1	422	26.14	1.33
Device 5	9.7	514	30.56	1.52
Device 6	10.52	436	26.88	1.23
Device 7	11.61	488	33.42	1.89
Device 8	9.84	452	30	1.34

Table AIS5 Photovoltaic characteristics of group 3 solar cells

Samples	**Isc (mA)**	**Voc (mV)**	**FF (%)**	**η (%)**
Device 1	16.9	533	49.69	4.48
Device 2	15.3	545	53.05	4.42
Device 3	18.38	535	53.75	5.29
Device 4	17.34	527	48.66	4.45
Device 5	18.44	553	60.32	6.15
Device 6	16.65	541	53.09	4.78
Device 7	18.1	482	48.08	4.2
Device 8	18.5	525	54.38	5.2

ANNEX II

SUPPORTING INFORMATION
PLASMON-ENHANCED SILICON NANOWIRE ARRAY-BASED HYBRID HETEROJUNCTION SOLAR CELLS

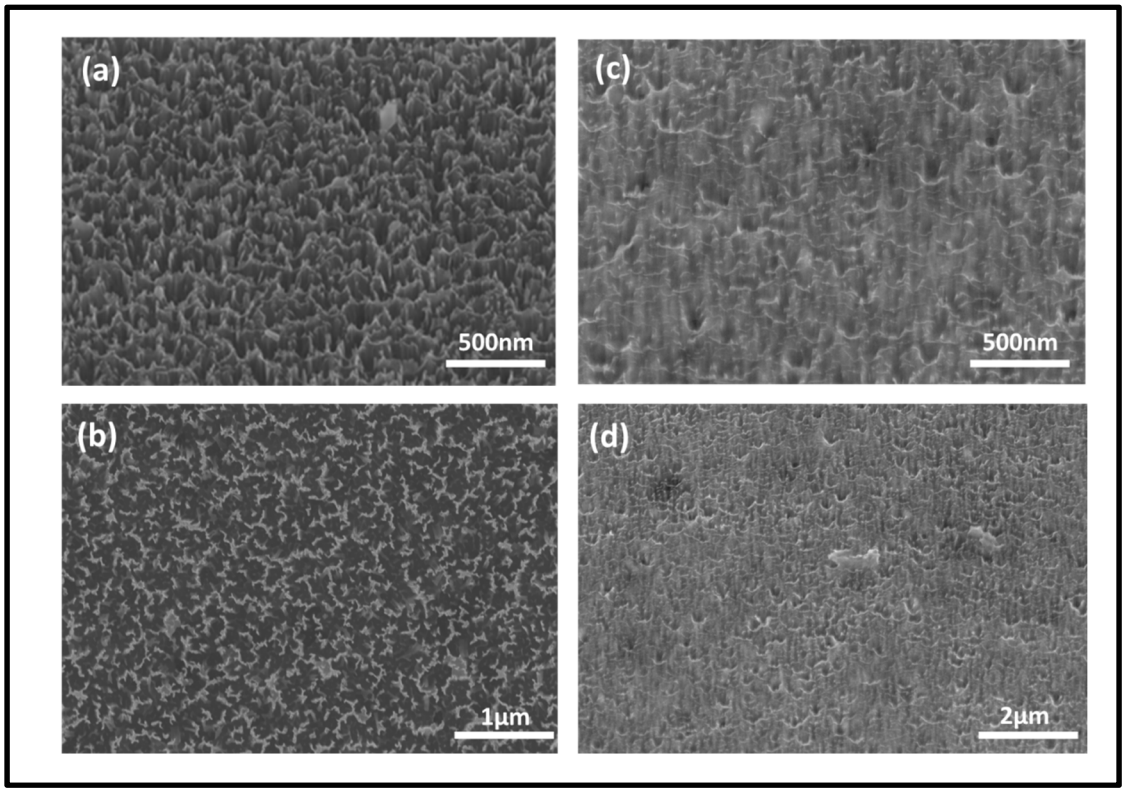

Figure AIIS1 SEM images of (a) SiNWs/PEDOT:PSS heterojunction at 40º tilted condition, (b) Top view of SiNWs/PEDOT:PSS heterojunction, (c) and (d) Plasmonic SiNWs/PEDOT:PSS heterojunction at 40º tilted condition

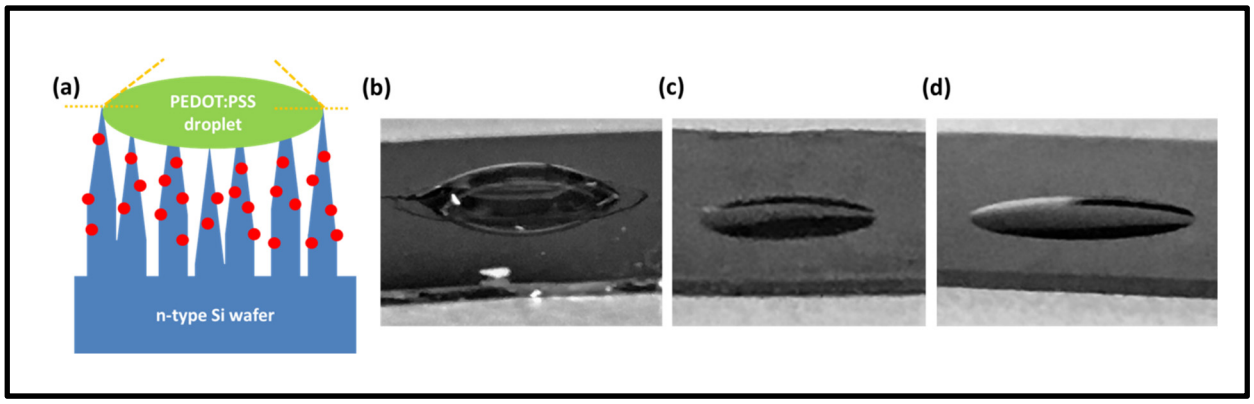

Figure AIIS2 (a) Schematic of solvent-treated PEDOT:PSS droplet on plasmonic nanowire surface for measuring the contact angle, (b) SDS-treated PEDOT:PSS droplet on pristine Si, (c) SDS-treated PEDOT:PSS droplet on SiNWs and (d) SDS-treated PEDOT:PSS droplet on plasmonic SiNWs samples

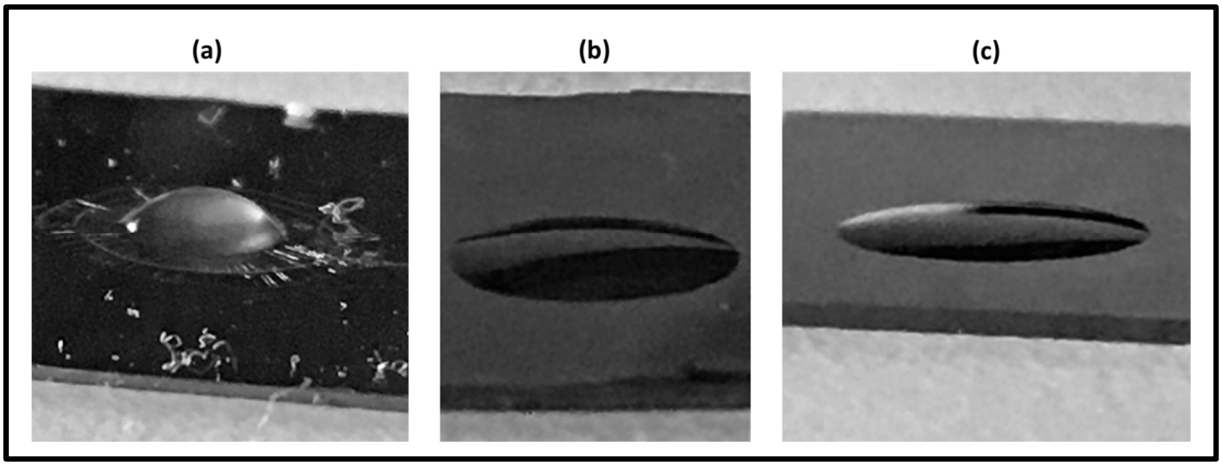

Figure AIIS3 IPA-treated PEDOT:PSS droplet on (a) Pristine Si, (b) SiNWs and (c) Plasmonic SiNWs samples

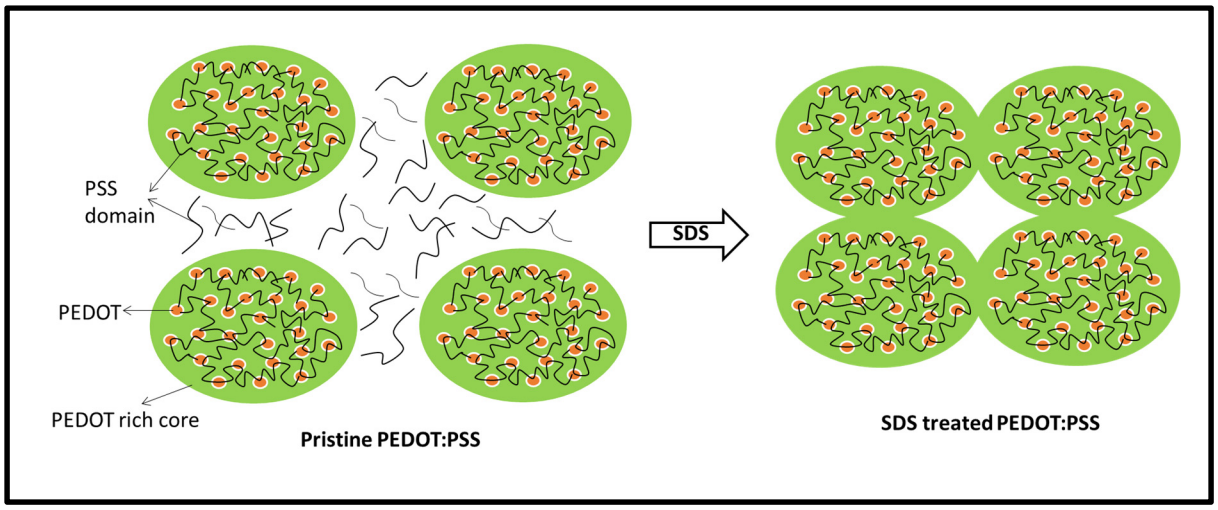

Figure AIIS4 Schematic of the pristine and SDS-treated PEDOT:PSS

Table AIIS1 Identification and quantification of elements from the XPS survey scan

Name	Binding energy	Atomic % of SiNWs with Ag dendrites	Atomic % of SiNWs with Ag plasmons only
Si2p	99.3	9.6	20.7
C1s	285.0	20.9	40.8
Ag3d	368.7	45.6	1.1
O1s	532.2	23.8	36.8
F1s	686.2	….	0.5

Table AIIS2 Photovoltaic characteristics of all solar cells from group 1

Samples	Isc (mA)	Voc (mV)	FF (%)	PCE(%)
Device 1	4.5	466	25	0.5
Device 2	6	422	32	0.8
Device 3	5.4	470	31	0.8
Device 4	7.8	468	31	1.1
Device 5	7	465	33	1.1
Device 6	9.3	488	39	1.8
Device 7	8.4	476	38	1.5
Device 8	9.2	484	35	1.6

Table AIIS3 Photovoltaic characteristics of all solar cells from group 2

Samples	Isc (mA)	Voc (mV)	FF (%)	PCE (%)
Device 1	13.5	578	52	4.1
Device 2	13	570	55	4.1
Device 3	15.4	571	52	4.5
Device 4	15.2	566	54	4.6
Device 5	17.7	570	52	5.2
Device 6	17.1	576	53	5.2
Device 7	18.4	570	53	5.5
Device 8	17	580	53	5.2

Table AIIS4 Photovoltaic characteristics of all solar cells from group 3

Samples	Isc (mA)	Voc (mV)	FF (%)	PCE (%)
Device 1	20	585	62	7.3
Device 2	20.6	580	61	7.3
Device 3	21.7	588	61	7.8
Device 4	21.3	588	63	7.9
Device 5	22	578	62	7.9
Device 6	23.6	590	60	8.3
Device 7	22.5	592	60	8
Device 8	24.2	580	60	8.4